INFORMATION TO USERS

This was produced from a copy of a document sent to us for microfilming. While the most advanced technological means to photograph and reproduce this document have been used, the quality is heavily dependent upon the quality of the material submitted.

The following explanation of techniques is provided to help you understand markings or notations which may appear on this reproduction.

1. The sign or "target" for pages apparently lacking from the document photographed is "Missing Page(s)". If it was possible to obtain the missing page(s) or section, they are spliced into the film along with adjacent pages. This may have necessitated cutting through an image and duplicating adjacent pages to assure you of complete continuity.

2. When an image on the film is obliterated with a round black mark it is an indication that the film inspector noticed either blurred copy because of movement during exposure, or duplicate copy. Unless we meant to delete copyrighted materials that should not have been filmed, you will find a good image of the page in the adjacent frame.

3. When a map, drawing or chart, etc., is part of the material being photographed the photographer has followed a definite method in "sectioning" the material. It is customary to begin filming at the upper left hand corner of a large sheet and to continue from left to right in equal sections with small overlaps. If necessary, sectioning is continued again—beginning below the first row and continuing on until complete.

4. For any illustrations that cannot be reproduced satisfactorily by xerography, photographic prints can be purchased at additional cost and tipped into your xerographic copy. Requests can be made to our Dissertations Customer Services Department.

5. Some pages in any document may have indistinct print. In all cases we have filmed the best available copy.

University
Microfilms
International

300 N. ZEEB ROAD, ANN ARBOR, MI 48106
18 BEDFORD ROW, LONDON WC1R 4EJ, ENGLAND

YEH, TAUN-RAN

PHOTOFISSION AND PHOTOEXCITATION STUDIES

City University of New York PH.D. 1980

PHOTOFISSION AND PHOTOEXCITATION STUDIES

by

TAUN-RAN YEH

A dissertation submitted to the Graduate Faculty in Physics in partial fulfillment of the requirements for the degree of Doctor of Philosophy, The City University of New York.

1979

This manuscript has been read and accepted for the Graduate Faculty in Engineering in satisfaction of the dissertation requirement for the degree of Doctor of Philosophy.

Jan 4, 1980
date

Chairman of Examining Committee

Jan. 8, 1980
date

Executive Officer

Professor Peter Lesser

Professor Carl Shakin

Professor Ambuj Mukerji

Professor Edward Melkonian
Supervisory Committee

The City University of New York

Abstract

PHOTOFISSION AND PHOTOEXCITATION STUDIES

by

TAUN-RAN YEH

Advisor: Professor Henry Lancman

The high proton beam current available from the Brooklyn College Dynamitron Accelerator have been used to generate beams of gamma-rays of well defined and variable energy from the (p, γ) reaction on various targets. Eleven such gamma-rays in the energy range from 5.8 to 11.5 MeV have been used to induce photofission in the even-even nuclei of ^{238}U and ^{232}Th. Spectra of photofission fragments have been measured with a photon energy resolution of several hundred eV. Polycarbonate films have been used as fission track detectors. The absolute efficiency of these films for counting fission fragments from thick uranium and thorium foils has been determined experimentally. Evidence of structure resulting from class II states was observed in ^{232}Th.

The average photofission cross sections for each (p, γ) resonance have been compared with published values. The results of our measurements are in good agreement with those of Caldwell et al[9] at energies above 7 MeV for both ^{238}U and ^{232}Th. At lower energies our value are higher than Caldwell's in the case of ^{238}U but agree well for ^{232}Th. The fission probability obtained from the average photofission cross section was compared with the theoretical predictions of the statistical model of Back et al[20] to extract the barrier parameters of ^{238}U and ^{232}Th.

In the course of the photofission work a nuclear resonance fluorescence experiment was carried out on ^{208}Pb and the widths of the 7.06 and

7.08 MeV states were determined to be $\Gamma_o = 29 \pm 3$ eV and $\Gamma_o = 16 \pm 3$ eV respectively. The $^{19}F(p, \alpha\gamma)^{16}O$ reaction was used to produce the incident gamma-rays.

ACKNOWLEDGEMENTS

I would like to express my deep appreciation to my research advisor, Professor Henry Lancman, for suggesting the idea and for continuous counsel, advice, and assistance during the course of this work.

I am indebted to Dr. Richard Yen for his patient help in taking data at the early stage of this work and also his vigorous help in maintaining the Dynamitron accelerator. I also wish to thank Professor Peter Lesser, director of this laboratory, for many suggestions and encouragement at the time when these were desperately needed.

I would like to express my appreciation to Dr. B.B. Back at Argonne National Laboratory for providing me with the computer code for calculating the fission probability and many helpful discussions. I am grateful also to Dr. B. Chrien at Brookhaven National Laboratory who kindly lent to us several pieces of ^{238}U and ^{232}Th foil for some of the preliminary runs.

Many members of the laboratory staff have contributed their effort to this experiment. Among them, Sol Coltun and Martine Berman in the machine shop, and Ira Senzon in electronics shop deserve particular credit for their useful advice and helpful assistance.

I am also grateful to Larry Burke for his help in building the multi-electrode sparking device. Special thanks are due to Chang-Chin Kwan of his help in preparing some of the chemical solutions.

Finally, I would like to thank my wife Chimei, for her patience and encouragement, which was vital to the completion of this work.

TABLE OF CONTENTS

	Page
I. INTRODUCTION	1
II. THEORETICAL AND EXPERIMENTAL BACKGROUND	5
(A). Fission theory	5
(B). Fission experiments	33
III. THE EXPERIMENT	39
(A). Introduction	39
(B). The gamma-ray source	40
(1). Gamma-rays from the (p,γ) reaction	40
(2). The accelerator	42
(3). Proton targets	44
(4). The gamma-ray energy resolution	47
(C). Detection of fission fragments	57
(1). Introduction	57
(2). Film processing	57
(3). Absolute fission rate measurements	64
(D). Fission foils	80
(E). Experimental set-up and procedures use in data acquisition	81
(F). Data analysis	82
(1). Efficiency of the Ge(Li) detector	82
(2). Fission counts	84
(3). Determination of the cross sections	87
IV. RESULTS AND CONCLUSIONS	94
(A). Introduction	94
(B). Photofission in ^{238}U and ^{232}Th	96
(1). Cross sections	96
(2). Fission probability	109
(3). Suggestions for further work	115
(C). Photo-excitation of the 7.06 and 7.08 MeV dipole states in ^{208}Pb	130
BIBLIOGRAPHY	

(I) INTRODUCTION

Our present understanding of the mechanism of fission at low excitation energies is based on ideas forwarded by A. Bohr[1] who pointed out that near the fission threshold most of the energy of the fissioning nucleus as it passes through the saddle point is concentrated in the deformation energy. In such a cold nucleus the transition states near the saddle point represent quite simple collective excitations similar to the low lying states at ground state deformation. These transition states are the fission exit channels. The measurements of fission induced by gamma rays is particularly useful for studying these states since photons are absorbed predominantly with E1, and with a considerably smaller probability, E2 multipolarities. This selective absorption results in excited states of a very limited range of angular momenta. For example, in even-even nuclei such as ^{238}U or ^{232}Th the states excited in this way may be expected to have spins and parities of 1^- and 2^+, corresponding to quadrupole and octupole vibrations and rotations associated with them.

Measurements of the energy dependence of the photofission cross section near the fission barrier and of angular distributions of the fission fragments can provide information on the barrier parameters for the various fission channels. This is in contrast to measurements of fission induced in particle reactions in which parameters averaged over many angular momentum states are determined.

Measurements of photofission cross sections have been carried out using a number of methods. Bremsstrahlung has been used for the determination of the energy dependence of the cross section[2] and the angular distribution of the fission fragments. Such measurements are difficult, since the bremsstrahlung spectrum is very broad with rapidly falling intensity toward

the end of the spectrum. The method relies on an unfolding procedure and detailed structure within energy intervals of less than about 200 keV is very difficult to study.

Photofission cross sections have been measured also using monoenergetic gamma rays. Khan and Knowles[3] used variable-in-energy compton scattered gamma rays from the Ni(n, γ) reaction to study the photofission of ^{232}Th, ^{235}U and ^{238}U. The gamma rays in this experiment had an energy resolution (relative energy spread) of 4 to 5%. Their energy was variable from 5 to 8.3 MeV. This method also requires an unfolding procedure. It has the advantage over the bremsstrahlung method in that the intensity of the scattered beam is peaked at the maximum energy. Similar measurements have been done by Yester[4] for ^{232}Th and ^{236}U. Monoenergetic photons derived from bremsstrahlung by means of the tagging technique were also used by Dickey and Axel[5] to measure the photofission cross section for ^{238}U and ^{232}Th with an energy resolution of $\sim$ 100 keV.

Neutron capture gamma rays in the energy range from 5 to 9 MeV have been used by a number of investigators for photofission studies[6-7]. This method provides excellent resolution (determined by the Doppler broadening of the line — typically a few eV) and intensity on target of the order of 10^4 photons/cm^{2}sec. The method has severe limitations, however following from the fixed energy and restricted number of suitable lines. In the experiments mentioned above about 10 lines were used. In addition the analysis is complicated by the fact that usually several lines contribute to the photofission yield.

The cross section determined by Khan and Knowles exhibits a considerable amount of broad structure. In the case of ^{238}U, for example, broad peaks

were observed at 5.2; 5.7; 6.2; 7.1 and 7.8 MeV. Many of these peaks were also observed by Dickey and Axel. The bremsstrahlung measurements do not resolve these peaks but indicate a hump slightly above 6 MeV. The hump which may correspond to the 6.2 MeV peak observed by Khan and Knowles was interpreted as a photofission resonance. However, Huizenga and Britt[8], and Dickey and Axel presented evidence that it may be due to the onset of neutron competition. Considerable structure in the photofission cross section near threshold has been reported by Caldwell et al[9].

The photofission measurements observed using the sharp gamma lines from thermal neutron capture show large fluctuations about the results of Khan and Knowles, which may be due to the fact that individual levels are excited. (the average level spacing of states is $\sim$10 eV at an excitation energy of 6 MeV).

Although the method of Khan and Knowles and Dickey and Axel provides a photon beam of variable energy their resolution is low. To study the details of the observed structure in the photofission cross section, photon beams of variable energy and high resolution are necessary. In this thesis, we describe a simultaneous measurement of the photofission cross section for ^{238}U and ^{232}Th nuclei between 5.8 and 11.5 MeV, using photons produced from resonances in (p, γ) reactions on various targets. The typical energy resolution of such photons is of the order of several hundred eV. With this resolution one may expect to observe structure due to the states in the second well of the double-humped potential barrier.

Chapter II contains a review of the theoretical and the experimental aspects of photofission with emphasis on the effects of the double-humped fission barrier. The details of our experiments are described in chapter III.

The results are presented in chapter IV and followed by a discussion. In the last section of chapter IV, we describe a photo-excitation experiment on ^{208}Pb.

(II) THEORETICAL AND EXPERIMENTAL BACKGROUND

(A) Fission theory

Nuclear fission was discovered in 1938 by Hahn and Strassman[10,11]. It was observed when uranium was bombarded with neutrons. Since then a very large number of articles has been published on various aspects of fission, and the subject is still receiving a considerable amount of attention.

The particle induced fission process is usually described as taking place in two different phases. A compound nucleus is formed which undergoes a series of collective oscillations and intrinsic excitations until it fissions by passing through the saddle point. To describe the fission process a sophisticated model of the nucleus is needed. Among existing models, the liquid drop model (LDM) of Bohr and Wheeler[12] has played a very important role in our understanding of fission.

In the liquid drop model, the nucleus is represented by a uniformly charged drop of incompressible nuclear matter having a definite surface. The total potential energy of the drop includes two constituents, the electrostatic Coulomb energy which acts to pull the drop apart, and the surface tension energy which acts to hold it together. As a result, the total potential energy of actinide nuclei as a function of deformation exhibits a barrier. Spontaneous fission is the result of penetration through this barrier

To describe the deformation of a nucleus, the radius vector of the charged drop is frequently expanded in terms of the Legendre polynomials[13]

$$R(\theta) = R_0 \left(1 + \sum_{l=1}^{N} \epsilon_l P_l (\cos\theta)\right) \qquad (1)$$

The drop is presumed to have axial symmetry with a radius R_o. The even numbered terms in the sum preserve reflection symmetry at a plane perpendicular to the symmetry axis, whereas the odd numbered terms destroy this symmetry.

Calculations of the potential energy of the drop in terms of even terms have been done up to $\ell = 18$. For an actinide nucleus, a simplified contour map of the potential energy as a function of ϵ_2 and ϵ_4 is sketched in Fig. 1. The minimum potential is represented by the dot on the ϵ_2 axis. At small value of ϵ the nucleus has essentially a quadrupole deformation. The dashed line, drawn from the minimum potential through a saddle point x, shows the prefered route to fission and is used to defined a generalized deformation coordinate β .

Strutinsky[14,15] pointed out that nuclear shells should modulate the liquid drop potential energy as a function of deformation, since the shells produce a non-uniformity in the distribution of single particle states. At a given deformation, this non-uniformity provides a negative correction to the total ground state energy when the single particle state density is low at the Fermi energy (the nucleus is more bound than in the LDM). On the other hand, when the single particle state density is high at the Fermi energy, the correction will be zero or positive (the nucleon is less bound than in the LDM or equally bound).

Detailed calculations show that in the region of actinide nuclei, shell corrections oscillate as a function of deformation and can affect the LDM potential by as much as $\pm$ 8 MeV. These calculations predict that as a result, the potential energy curve should exhibit a double-humped barrier as a function of the deformation. Calculations of Nilsson et al[16] indicate that the barrier heights of the two humps are about the same for the

Fig. 1: Simplified representation of the contour map of the potential energy as a function of two deformation coordinates ϵ_2 and ϵ_4.

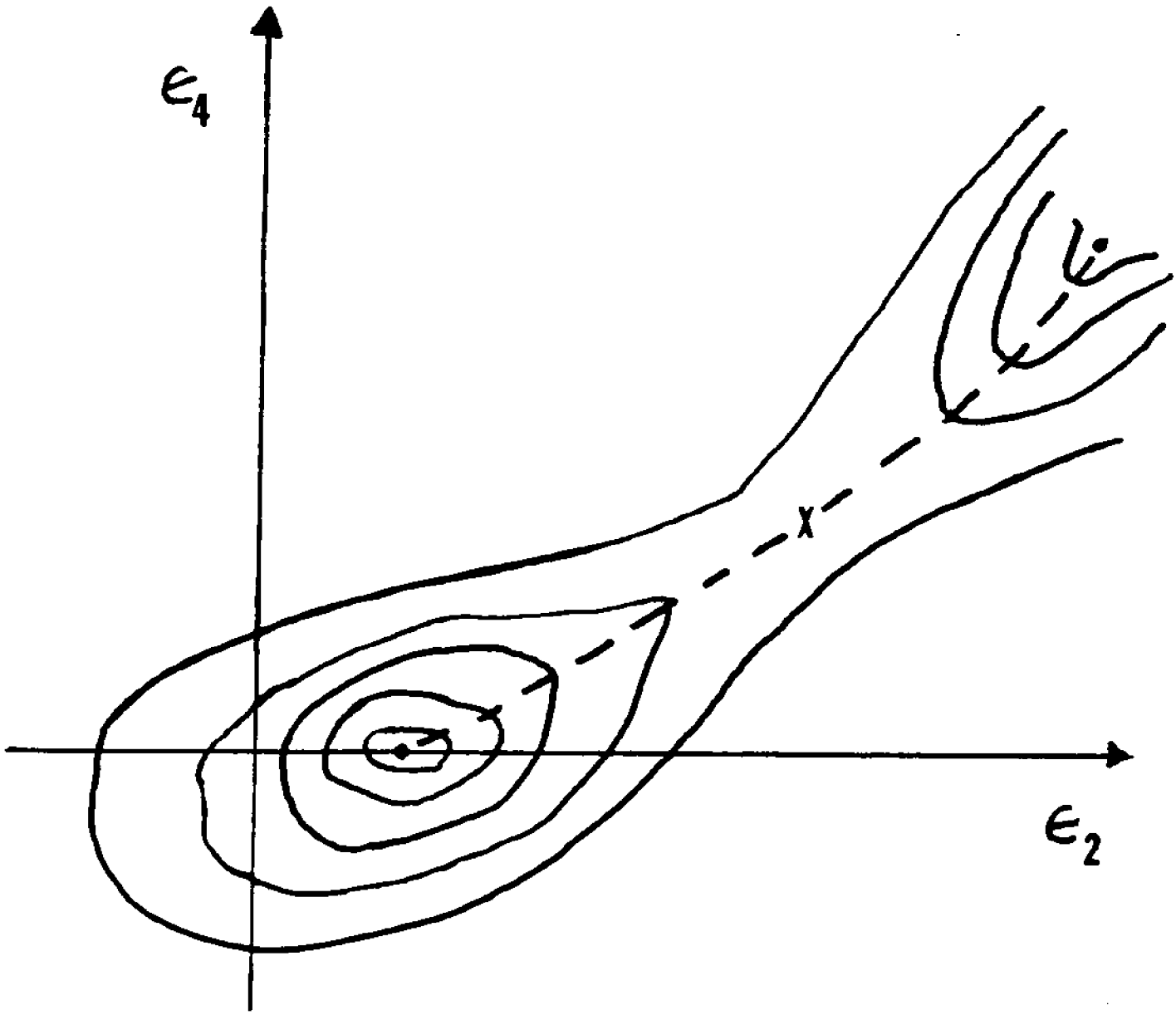
ϵ_4
ϵ_2

atomic number Z = 94. As Z increases the outer barrier becomes lower than the inner one, and vice versa. A typical double-humped fission barrier is schematically shown in Fig. 2. The inner and outer barriers are designated A and B respectively. The barrier heights E_A, E_B and the energy of the second well E_{II} are measured above the ground state, which is at bottom of the first well. The parameters $\hbar\omega$ indicate the barrier/well curvature. The smaller $\hbar\omega$, the broader the barrier/well.

For actinide nuclei the observed values of E_A and E_{II} are well reproduced by the Strutinsky-type calculations in which only quadrupole, P_2, and hexadecapole, P_4, deformations are included. The calculated outer barrier E_B, however, is usually higher by several MeV than the measured one. Some early calculations[17,18] carried out without employing the Strutinsky method, indicated that the inclusion of P_3 lowers the potential energy surface. This fact and the observed asymmetric fission of the actinide nuclei seem to show that the odd-numbered deformation parameters which lead to asymmetric shape distortion are important. Moller[19] did calculations with the inclusion of the P_3, P_5 and P_1 terms. His results for ^{238}U and ^{232}Th are listed in Table 1. Experimental results taken from Back et al[20] are included for comparsion.

The inclusion of axially asymmetric[45], γ-angle deformation, can lower the inner barrier and keep, the outer barrier unchanged for most actinide nuclei. The effect of non-istropic quadrupole pairing[46] can bring up the inner barrier, particlarly in the case of the light Th nuclei.

Fission of ^{238}U has been interpreted[21] as passage over an axially deformed inner barrier and a mass-asymmetric (pear-shape), axially symmetric outer barrier. But recent investigations[21] suggest the possibility of two distinct outer barriers, one mass asymmetric and axially symmetric, the other

TABLE 1

A comparison of the theoretical and experimental fission barrier parameters for a double-humped barrier

	E_A (MeV)		E_B (MeV)		E_{II} (MeV)
	Calculated[19]	Experimental[20]	Calculated[19]	Experimental[20]	Calc.[19]
^{238}U	6.1	5.9	6.5	6.1	2.7
^{232}Th	4.8	< 5.5	7.3	6.1	2.8

Fig. 2: Schematic representation of a double-humped potential barrier (solid line) and a LDM single-humped barrier (dashed line). Intrinsic excitations in the first and second wells at deformation β_I and β_{II} are designated class I and class II states respectively.

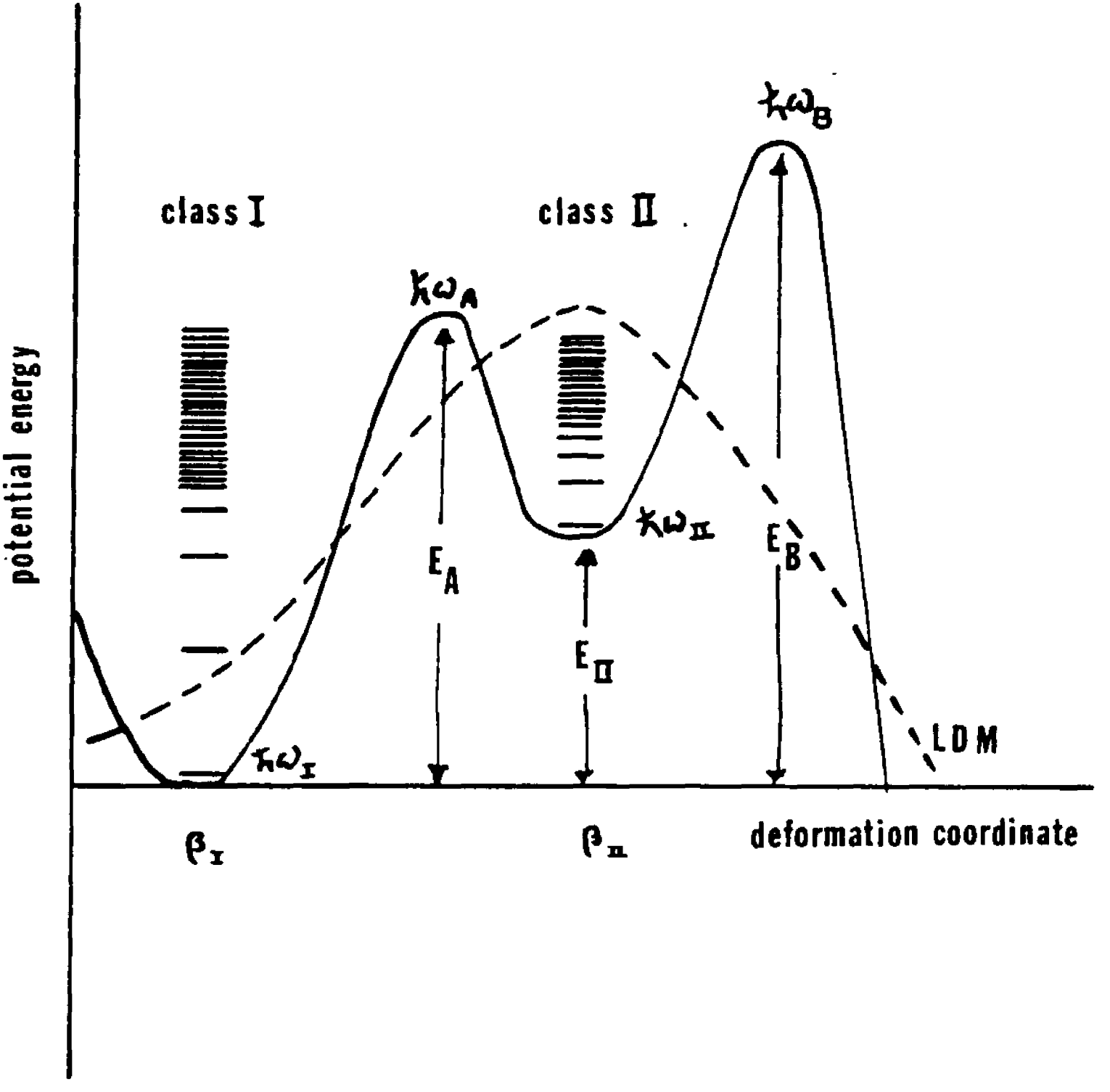
potential energy
class I
class II
$\hbar\omega_A$
$\hbar\omega_B$
$\hbar\omega_{II}$
$\hbar\omega_I$
E_A
E_{II}
E_B
LDM
β_I
β_{II}
deformation coordinate

mass symmetric and axially asymmetric. In the case of Th, Moller and Nix[22] have found that the outer barrier is split into two individual peaks separated by a "third minimum". This three-hump fission barrier explains, in principle, the sharp states at higher excitation energy, which has been called the "thorium anomaly"[23,24].

The existence of a double-humped barrier in many nuclei has been confirmed by numerous experiments[3,5,20]. The theoretical developements have been discussed in several reviews[25,26]. Among the most dramatic manifestations of the effects of the double-humped barriers are fission isomerism, a phenomenon whereby a heavy nucleus can exist in a relatively long-lived excited state before it decays by fission, and the appearance of several types of structure in the fission cross section as a function of the excitation energy. The latter topic is directly related to the photofission studies described in this work and will be discussed in some detail.

At lower excitation energies (below the barrier height), the existence of a double-humped potential barrier results in two categories of states. The states in the first well are denoted class I and the states in the second well class II. These states represent rotational, vibrational, and particle excitations. Because the vibrational motion is along the β deformation, the total Hamiltonian of the system H can be decomposed[27] to give an explicit term H_β as shown below.

$$H = H_\beta + \sum_i H_i + \sum_{i<j} H'_{ij} + \sum_i H''_{i\beta} \qquad (2)$$

All other degrees of freedom, corresponding either to vibrational motion other than β, to the rotation of the nucleus, or to particle excitation, are included in $H_i + \sum_{i<j} H_{ij}'$ for a given β deformation. The inter-

action between the degree of freedom i and β is described by $H''_{i\beta}$.

The eigenfunctions X_λ (with eigenvalues E_λ) of the Hamiltonian $H - H''$ are given by

$$X_\lambda = \sum_{\nu,\mu} C^{\lambda}_{\nu\mu} \Phi_\nu x_\mu \qquad (3)$$

where Φ_ν and x_μ are the eigenfunctions of H_β and $H_i + \sum_{i<j} H'_{ij}$ respectively. The class I and II compound states are defined accordingly:

$$\text{Class I} \quad X^{I}_{\lambda_I} = \sum C^{\lambda_I}_{\nu_I\mu} \Phi_{\nu_I} x_\mu$$

$$\text{Class II} \quad X^{II}_{\lambda_{II}} = \sum C^{\lambda_{II}}_{\nu_{II}\mu} \Phi_{\nu_{II}} x_\mu \qquad (4)$$

The compound nucleus states corresponding to the full Hamiltonian H are determined by adding H'', the coupling between class I and class II states.

There are two types of resonances in the formation of compound nucleus states leading to fission. The first corresponds to highly excited many-particles states of the compound nucleus, as shown in Fig. 2. These states, whether they are class I or II, have relatively small widths, and their level density ρ is computed from [25]

$$\rho(u) = C \exp(\sqrt{au}) \qquad (5)$$

where U is the effective excitation energy, and a is a parameter proportional to the density of the single particle states at the Fermi energy. Because U_I at the first well is higher than U_{II} at the second well, and a_I and a_{II} are comparable, it is clear that the level density ρ_I is much higher

than ρ_{II}. Fission resonances will occur when the energy, spin and parity of class I states match those of the class II states leading to structure in the fission cross section which is shown schematically in Fig. 3. The possible spin states J_i are drawn as vertical lines for class I states in Fig. 3a. In Fig. 3b the dashed envelopes show the fission clusters with level width $\Gamma_{\lambda_{II}}$ and average level spacing D_{II}. Such intermediate structure has been observed in neutron induced fission.

The other type of resonance is related to the vibrational motion in the fission degree of freedom. The vibrational states are broad because of the dissipation of vibrational energy due to damping. A typical width of a vibrational state at low excitation energy is of the order of a few tens of keV. The higher the excitation energy the larger the width because of increased damping and at sufficiently high energy the spectrum becomes continuous. A schematic diagram showing the vibrational states in a double-humped barrier is given in Fig. 4a. Both class I and class II vibrational states are drawn as horizontal lines. The damping of these states is indicated by hatched lines. Because of the larger effective excitation energy in the first well, the class I vibrational states form a continuous spectrum when the class II states are still separated. A resonance will occur as long as a discrete vibrational state at the second well is reached. Otherwise the fission yield will increase smoothly with the excitation energy. This is shown in Fig. 4b where the yield vs excitation energy exhibits vibrational resonances with level width Γ_{vib}. Such structure has been observed in particle induced fission.

The structure appearing in the fission yield curve depends on the damping of the vibrational states in the second well. For even-even

Fig. 3: Coupling between class I and class II states leading to intermediate structure.

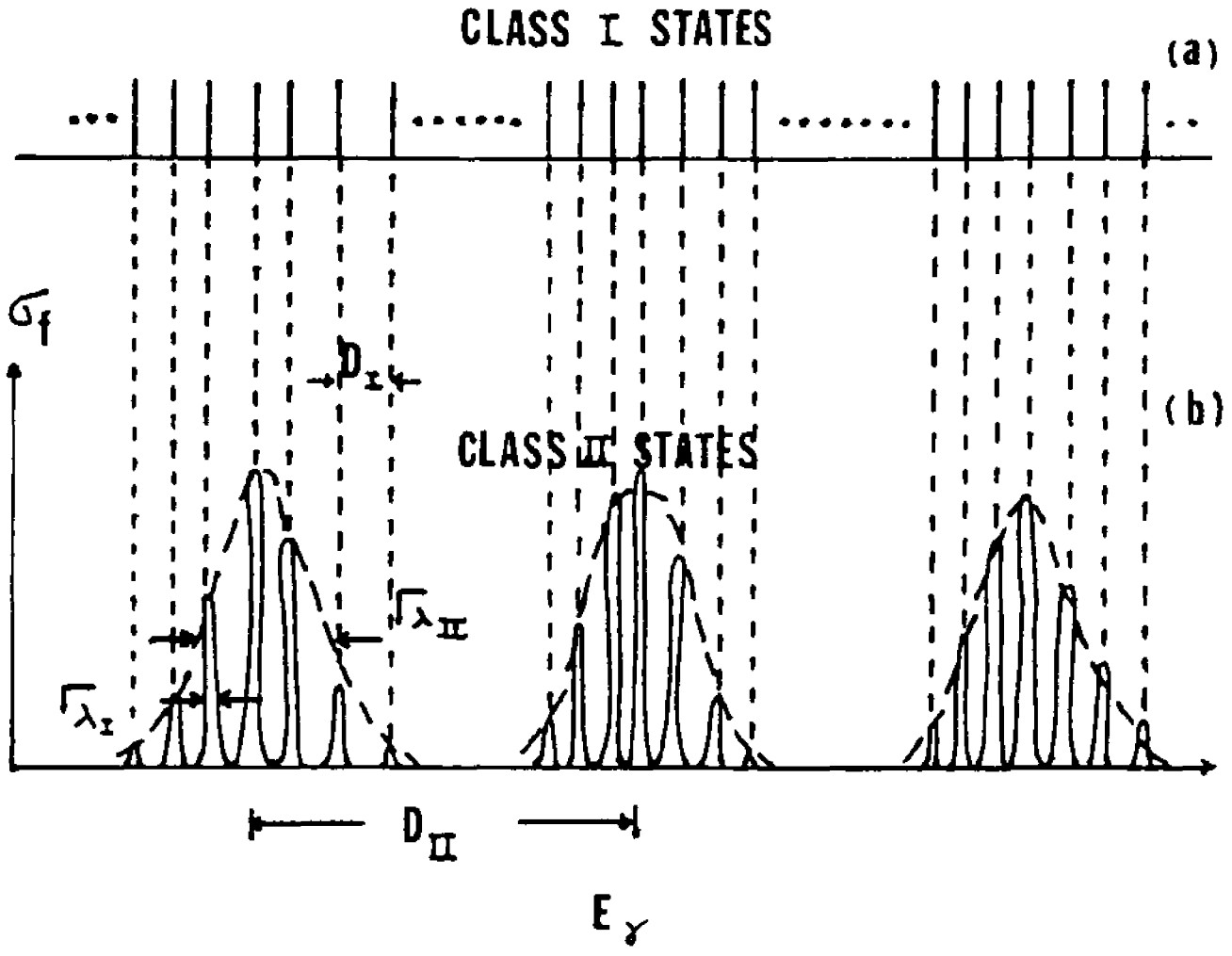
CLASS I STATES
(a)
σ_f
D_I
CLASS II STATES
(b)
$\Gamma_{\lambda II}$
$\Gamma_{\lambda I}$
D_{II}
E_γ

Fig. 4a: Schematical diagram of the vibrational states in a double-humped barrier.

b: Fission yield vs excitation energy exhibits vibrational resonances with level widths Γ_{vib}.

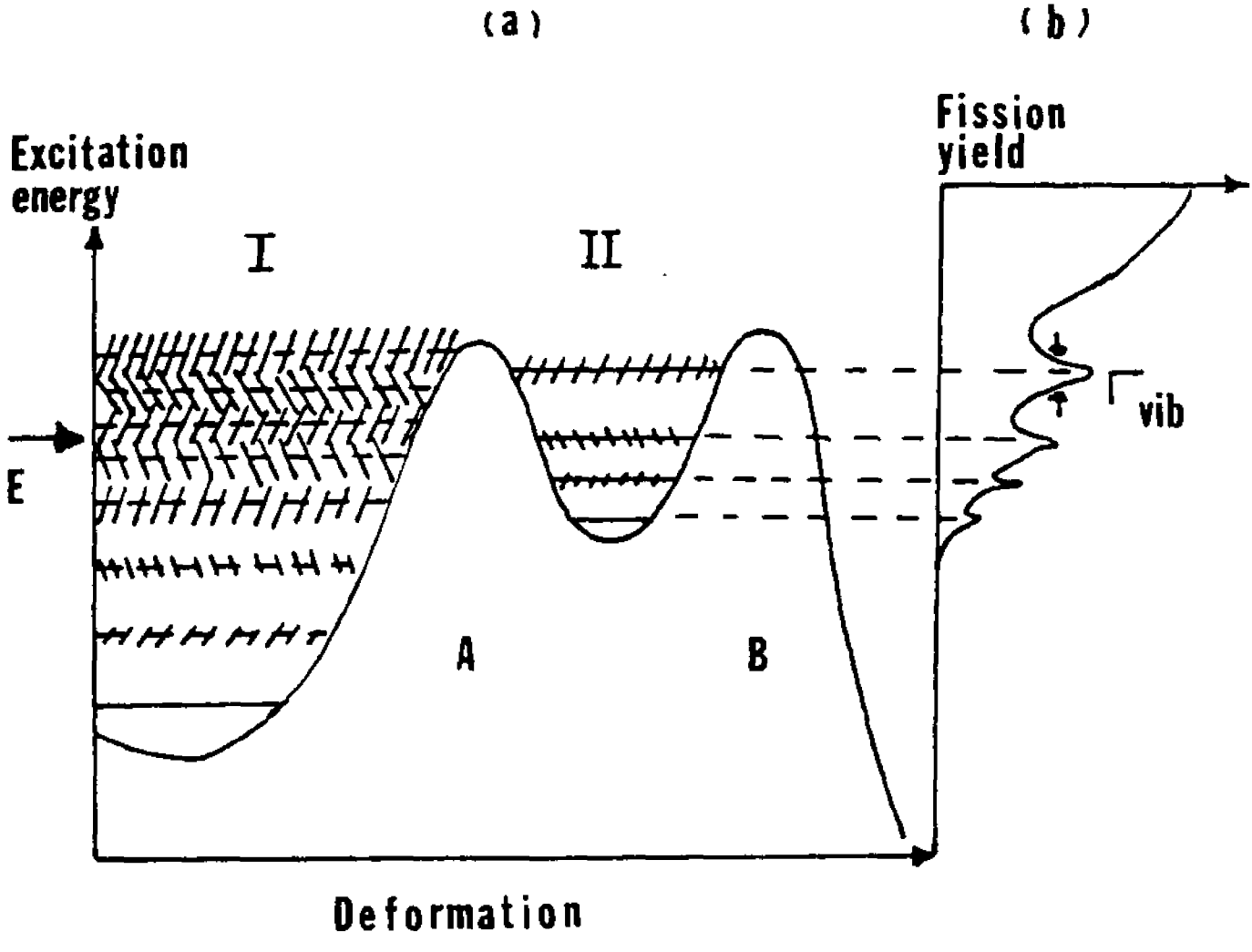
(a)
(b)
Excitation energy
Fission yield
I
II
E
A
B
vib
Deformation

actinide nuclei, pure vibrational states without damping are expected at low excitation energies. As the energy increases, the vibrational state is moderately damped to the surrounding states, and a resonance appears with a possible fine structure caused by the class II states. At an even higher excitation energy the vibrational state is fully damped, and structure in the yield represents a superposition of class I and class II states only. This is schematically shown in Fig. 5.

When the excitation energy is comparable to or higher than the fission barrier, it is known that the density of the compound states (vibrational, rotational,or particle excitations) is high. The wave functions of the compound states become very difficult to calculate, so that the fission properties of these states can not be predicted. A. Bohr[1], proposed the concept of fission exit channels, or so called transition states. It is assumed that near the fission threshold the excited nucleus is "cold" since a major portion of the excitation energy has gone into surface deformation. Hence this cold nucleus is expected to have quite simple collective excitations similar to the low lying states at ground state deformation. A schematic representation of the transition states is shown in Fig. 6. The level schemes at ground state and saddle point deformation are for an even-even nucleus.

Bohr has also pointed out that near the threshold, photofission of even-even nuclei has some especially simple features. The target nuclei have spin and parity $J^{\pi} = 0^{+}$. Photons are absorbed mainly through electric dipole (E1) and with a smaller probability quadrupole (E2) transitions yielding states with $J^{\pi} = 1^{-}$ and 2^{+} respectively. The transition states of an even-even nucleus therefore resemble the lowest 1^{-} and 2^{+} states present at the ground state deformation. The states,

Fig. 5: Types of structure in the fission yield as a function of excitation energy.

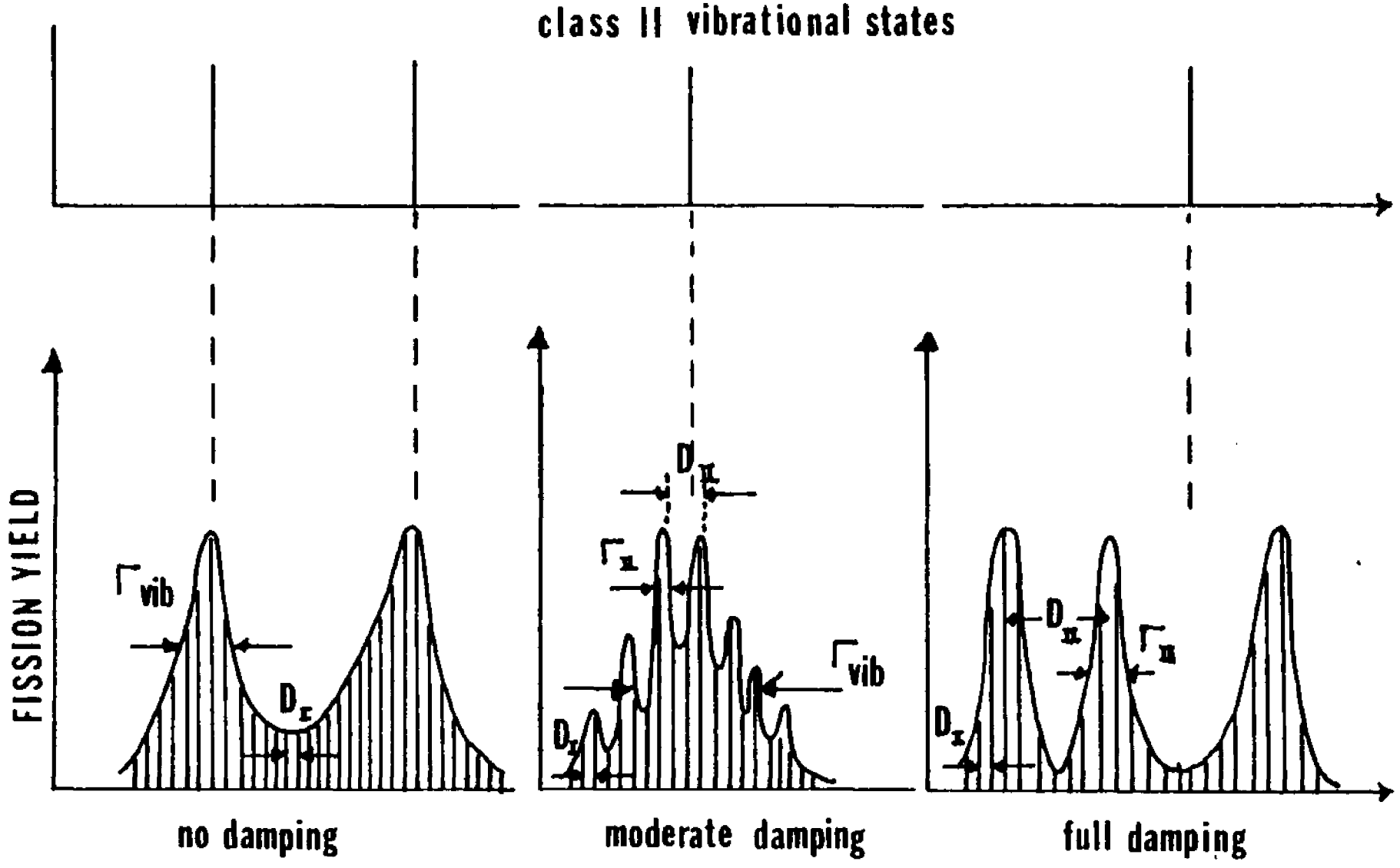
class II vibrational states
FISSION YIELD
Γvib
DΣ
DII
ΓII
Γvib
DΣ
DII
ΓII
DΣ
no damping
moderate damping
full damping
EXCITATION ENERGY

Fig. 6: Fission transition states in an even-even nucleus. States of importance in photofission are designated with an asterisk.

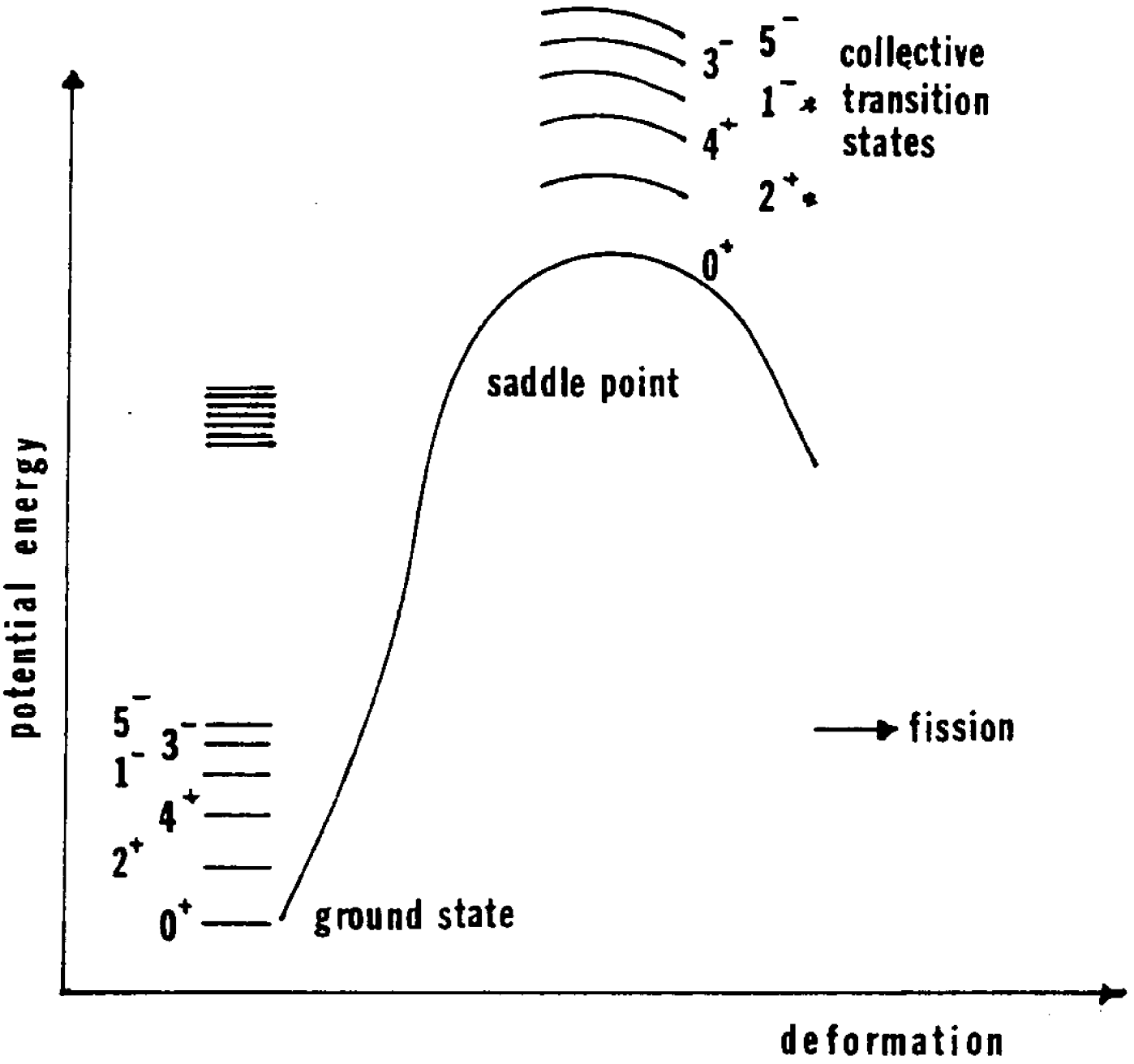
potential energy
deformation
5⁻
3⁻
1⁻
4⁺
2⁺
0⁺
ground state
saddle point
0⁺
2⁺*
4⁺
1⁻*
3⁻
5⁻
collective
transition
states
fission

which are important in photofission, are marked with an asterisk in Fig. 6.

To predict the angular distribution of the fission fragments, it is essential to make two assumptions. The first is that the fission fragments separate along the symmetry axis. The second is that the projection, K, of the total angular momentum J does not change once the transition state is reached, making K a good quantum number after this stage of the process. The latter assumption does not rule out the possibility of K mixing in going from the original compound nucleus to the transition state. The K value may change because the nucleus suffers many vibrations and changes in shape, and re-distributes its energy and angular momentum in many ways.

In the case of the double-humped fission barrier, the concept of transition states is rather complex, and it becomes of interest to know which barrier establishes the value of K. Some evidence[21] in ^{238}U, for example, indicates that at the inner barrier the deformation is axially asymmetric. This would cause K mixing at the first barrier. However, the second barrier is stiff against an axially asymmetric (gamma) deformation, and the K value is well established. Thus the angular distribution of the fission fragment is determined by the second barrier.

The angular distribution of fission fragments from a state with total angular momentum J, and its projection K on a space fixed axis, is derived from the rotational wave-function $d^{J}_{M,K}$. For electric dipole and quadrupole photo-excitations of even-even nuclei the angular distributions are given by the following equations

$$\omega^{J=1}_{k=0}(\theta) = \frac{3}{4}\sin^2\theta \qquad (6)$$

Fig. 7: Angular distribution of photofission fragments for dipole and quadrupole absorption in an even-even target nucleus.

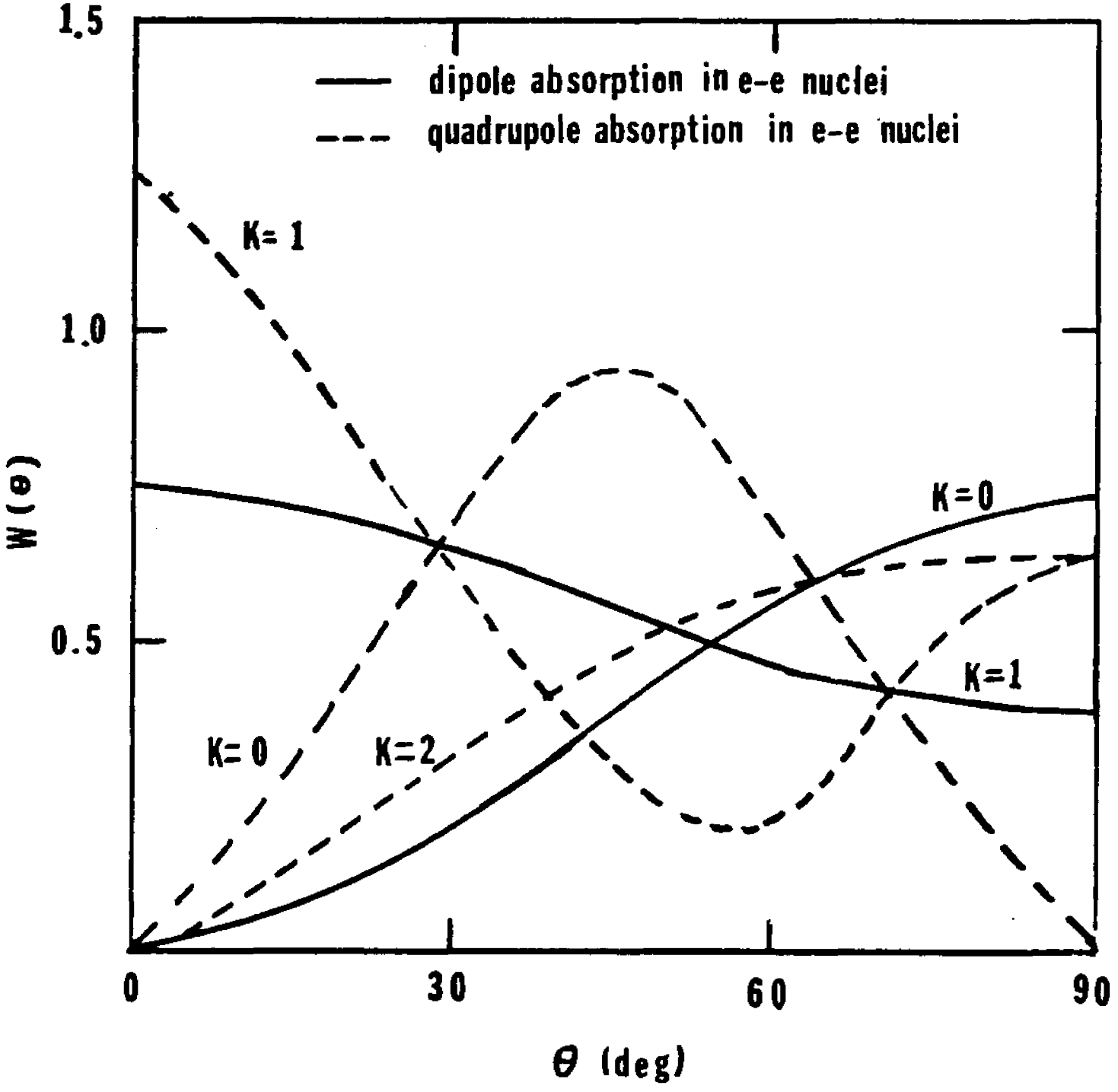
1.5
1.0
0.5
W(θ)
dipole absorption in e-e nuclei
quadrupole absorption in e-e nuclei
K= 1
K=0
K=1
K= 0
K=2
0
30
60
90
θ (deg)

$$\omega^{J=1}_{K=\pm1}(\theta) = \frac{3}{4} - \frac{3}{8}\sin^2\theta \qquad (7)$$

$$\omega^{J=2}_{K=0}(\theta) = \frac{15}{16}\sin^2 2\theta \qquad (8)$$

$$\omega^{J=2}_{K=\pm1}(\theta) = \frac{5}{8}(2 - \sin^2\theta - \sin^2 2\theta) \qquad (9)$$

$$\omega^{J=2}_{K=\pm2}(\theta) = \frac{5}{8}(\sin^2\theta + \frac{1}{4}\sin^2 2\theta) \qquad (10)$$

The angle θ is measured from the direction of the incident photons to the nuclear symmetry axis. All the distribution functions are normalized so that $\int_0^\pi \omega(\theta)\sin\theta\, d\theta = 1$, and are drawn by solid and dashed curves for dipole and quadrupole excitations respectively in Fig. 7.

The photofission cross section is given by:

$$\sigma_{\gamma f} = \sum_{J\pi} \sigma_\gamma(EJ\pi) \left\langle \frac{\Gamma_f(EJ\pi)}{\Gamma_t(EJ\pi)} \right\rangle \qquad (11)$$

where $$\Gamma_t(EJ\pi) = \Gamma_f(EJ\pi) + \Gamma_n(EJ\pi) + \Gamma_\gamma(EJ\pi) \qquad (12)$$

where σ_γ is the photonuclear absorption cross section in the compound nucleus at excitation energy E, total angular momentum J, and parity π; Γ_f, Γ_n, Γ_γ represent the widths for decay through the fission, neutron, and gamma-ray modes respectively. The emission of light charged particles is omitted because it is inhibited by Coulomb barriers.

The fission probability which is defined as the ratio of the photofission cross section to the photoabsorption cross section may be expressed as:

$$P_f(E) = \sum_{J\pi} \alpha(EJ\pi) \left\langle \frac{\Gamma_f(EJ\pi)}{\Gamma_t(EJ\pi)} \right\rangle \qquad (13)$$

where α (E,J, π) is the normalized probability for populating states with excitation energy E, spin J and parity π through photon absorption. For simplicity we assume that α is independent of energy

$$\alpha(E J\pi) \simeq \alpha(J\pi) = N_o \sigma_\gamma(J\pi) \qquad (14)$$

where N_o is a normalization constant determined by

$$\sum_{J\pi} \alpha(J\pi) = 1 \qquad (15)$$

Theoretical calculations of the fission probability which employ a statistical model with inclusion of several barrier parameters have been published by Back et al[9]. These calculations were originally for the purpose of interpreting the charged particle induced fission. Recently, Gavron et al have also adopted these calculations to fit (γ ,f) and (t,pf) data in the sub-threshold region as well as (γ ,f) data in the 7-11 MeV excitation region. The analysis of our photofission results will be carried out along similar lines and, therefore, the frame-work of these model calculations will be discussed briefly.

Due to the statistical distribution of individual Γ_f values about their mean, the fission probability can be rewritten approximately as:

$$P_f(E) = \sum_{J\pi} \alpha(J\pi) \frac{\langle \Gamma_f(E J\pi) \rangle}{\langle \Gamma_t(E J\pi) \rangle} S \qquad (16)$$

where S is the width fluctuation correction factor. Assuming a χ^2 distribution of the fission widths[28], these values have been calculated by Back et al in terms of the branching ratio of fission to total decay widths and the effective number of open fission channels.

The average fission width is composed of contributions from different

fission channels ν and is related to the barrier transmission coefficient T_f as follows:

$$\langle \Gamma_f(EJ\pi) \rangle = \frac{D_I}{2\pi} \sum_{\nu} T_f^{\nu}(EJ\pi) \qquad (17)$$

where D_I is the average spacing of levels in the compound nucleus. The fission transmission coefficient is related directly to the barrier parameters. For a one dimensional, single, inverted parabolic barrier of height E_f and curvature $\hbar\omega_f$, the transmission T_f can be written exactly as:[12]

$$T_f = \left(1 + \exp\left(\frac{2\pi}{\hbar\omega_f}(E_f - E)\right)\right)^{-1} \qquad (18)$$

This is a smooth function of energy which exhibits no resonances.

The transmission of a double-humped barrier comprised of smoothly joined parabolic sections has also been calculated by a number of groups[3,20,21]. Back et al[20], used the idea of splitting the fission transmission into two parts

$$T_f = T_d + T_i \qquad (19)$$

where T_d is the direct transmission from the incoming unit flux in the first well and T_i is the internal flux leading to fission in the second well. The latter part can be estimated as the absorbed flux T_{abs} multiplied by a branching ratio

$$T_i = T_{abs} \frac{P_A}{P_A + P_B} \qquad (20)$$

where P_A and P_B are the penetrability given in our case by eq. (18) through inner barrier A and outer barrier B respectively. T_{abs} and T_d

are obtained by solving the Schrodinger equation, with the total Hamiltonian containing a negative imaginary potential W_o to simulate the absorbed flux in the second well. In contrast to the single barrier, the transmission function will exhibit an enhanced penetration which is the result of the existence of the quasi-bound state in the second well of the potential. Thus the average fission width can be rewritten as:

$$\langle \Gamma_f(EJ\pi) \rangle = \frac{D_I}{2\pi} \left(N_d(EJ\pi) + N_{abs}(EJ\pi) \frac{N_B(EJ\pi)}{N_A(EJ\pi) + N_B(EJ\pi)} \right) \quad (21)$$

where
$$N_d = \sum_\nu T_d^\nu(EJ\pi) \ , \quad N_{abs} = \sum_\nu T_{abs}^\nu(EJ\pi)$$
$$N_A = \sum_\nu P_A^\nu(EJ\pi) \ , \quad N_B = \sum_\nu P_B^\nu(EJ\pi) \quad (22)$$

The average γ-decay width is calculated assuming that only E1 transitions are important and integrating over all possible final states j

$$\langle \Gamma_\gamma(EJ\pi) \rangle = C A^{2/3} D_I \sum_{j=|J-1|}^{J+1} \int_0^E \rho_I(\epsilon j - \pi) (E-\epsilon)^3 d\epsilon \quad (23)$$

where C is the normalization constant and ρ_I is the level density in the first well.

For energies above the neutron threshold, neutron decay starts to compete with fission so that the fission probability, after reaching a peak, will drop. The average width for neutron emission is calculated by summing transmission coefficients to known states in the A-1 residual nuclei.

$$\langle \Gamma_n(EJ\pi \rightarrow E-\epsilon I\pi') \rangle = \frac{D_I}{2\pi} \sum_{j=|J-I|}^{J+I} \sum_\nu T_{lj}(\epsilon_\nu) \quad (24)$$

where $T_{\ell j}(\epsilon_\nu)$ is the neutron transmission coefficient for a transition from a compound state at energy E, spin J, and parity π to a final state at energy $E-\epsilon_\nu$, spin I, and parity π'.

It can be seen clearly that the calculated fission probabilities depend on a number of barrier parameters, for example, barrier heights and barrier curvatures. These parameters can therefore be obtained by fitting the theoretically predicted fission probability to the experimental data. Although different parameters have a different influence on the fission probabilities, the four parameters E_A, E_B, $\hbar\omega_A$, and $\hbar\omega_B$ are mainly determined by the calculation.

(B) Fission experiments

In 1962 Polikanov et al[29] observed a fission isomer with a half life of 14 msec upon bombarding ^{238}U with ^{20}Ne ions. The fissioning nucleus was identified as ^{242}Am. Futher study revealed that this isomer has a rather low spin, and an excitation energy of $\sim$ 3 MeV. Within the framework of the existing theory it was hard to explain how this state could resist de-excitation by γ-emission for such a long life time. With the introduction of double-humped potential barrier, this and other later discovered fission isomers are identified as low lying states in the second well. The γ-decay from isomeric states to states in the first well is strongly inhibited by the presence of barrier A. The experimental verification[30] of this explanation of the existence of fission isomers came five years later when it was determined that the 4 nsec ^{240}Pu fission isomer has a quadrupole moment larger than the quadrupole moment of the ground state.

Evidence of intermediate structure was first observed in experimental studies of neutron-induced fission. For example, the measurements[31] of $^{240}Pu(n,f)$ clearly show large fission resonances clustered about neutron energies of 0.78, 1.4, 1.9, and 2.7 keV. The spacing of the clusters is $\langle D_{II} \rangle$ = 650 eV, roughly 50 times that of class I states which is $\langle D_I \rangle \simeq$ 12.5 eV. This structure can be explained by the coupling of compound class II states in the second well into nearby compound nucleus states in the first well. Similar structure was subsequently found in the (n,f) cross sections of other nuclei.

Broad resonances in the cross section of neutron-induced fission have been found[24] in the $^{230}Th(n,f)$ reaction. The resonance at 715 keV, about 30 keV wide, is attributed to a vibrational level in the second

well of the double-humped potential barrier.

The direct-reaction $^{239}Pu(d,pf)^{240}Pu$ provided[32] further evidence of a vibrational resonance state in the second well. The high resolution measurements resolve a 5 MeV peak into a number of sharp peaks. The whole structure was interpreted as being caused by a class II vibrational state damped into the intrinsic states in the second well.

Direct-reactions[20,33-34] which excite a nucleus to energies near the fission threshold have been used extensively to study the fission process. The method has two distinct advantages over neutron-induced fission. First, the region of excitation energy below the neutron binding energy can be studied. This is very useful, particularly for even-even nuclei, because the neutron binding energy is usually above the fission barrier for these nuclei. Second, a wider range of fissioning nuclei can be reached using the available targets and reactions such as (t,pf), (d,pf), (t,f), (^{3}He,df), (^{3}He,f) etc. Analysis of the fission data is complex because many angular momentum states are excited. A statistical model is used to extract barrier parameters averaged over many possible states. Barrier information associated with specific fission channels is therefore very difficult to obtain.

In contrast to the direct-reactions, photofission measurements are simpler to interpret because photons are absorbed predominantly with E1 and, with a considerably smaller probability, E2 multipolarities resulting in excited states of a very limited range of angular momenta. However, photofission reactions, in fact all photo-nuclear reactions, have been hampered by the very limited number of sources of monochromatic gamma-rays of sufficient intensity and good energy resolution. The early photofission data were obtained using bremsstrahlung spectra. Since the bremsstrahlung spectrum is continuous and broad, such measurements are

difficult. Photofission cross sections are obtained by changing slightly the end-point energy of the spectrum and measuring the difference in the fission yield. Detailed structure within energy intervals of less than 200 keV is very difficult to study.

Despite the poor energy resolution bremsstrahlung has been successfully used to measure the angular distribution of fission fragments [2,35]. Futhermore, measurements of photofission cross sections at very low energies have been done with bremsstrahlung beams by several groups [36-38]. Their results indicate a "shelf" which is due to the increasing influence of isomeric fission, populated through gamma-decay of the states excited by the incident photons.

Many attempts have been made to produce photon beams of high intensity and good energy resolution. Compton-scattered gamma-rays from neutron-capture reactions [3,4] have been used. Their energy resolution is typically $\sim$ 5% and the energy can be varied continuously. Although the scattered gamma-rays peak at the maximum energy, an unfolding procedure is still necessary. A 1% photon energy resolution has been obtained by means of the tagging technique, in which a coincidence is required of a prompt event produced by the bremsstrahlung photon, and the electron which generated it. The photon energy interval is determined by selecting electrons in the appropriate energy range. Photons of similar resolution can be obtained by the technique of positron annihilation in flight [9,39].

Monoenergetic gamma-rays are produced in slow neutron-capture reactions. Their excellent resolution ($\sim$ few eV) is determined by the Doppler broadening of the gamma-ray line and their intensity can be very high. However, since these gamma-rays have fixed energies and the number of suitable lines is small, their application to photofission measurements is very limited.

Some early results of photofission cross section measurements in ^{238}U and ^{232}Th exhibited a hump near 6 MeV. Khan and knowles[3] used variable-in-energy Compton-scattered gamma-rays from the Ni(n, γ) reaction to study the detailed structure of this hump. They found peaks at 5.2, 5.7, 6.2, 7.1, and 7.8 MeV in ^{238}U, and 5.5 and 6.4 MeV in ^{232}Th. The most pronounced were the 6.2 MeV peak in ^{238}U, which was 200 keV wide, and the 6.4 MeV peak in ^{232}Th, 650 keV wide. Knowles' interpretation of these latter peaks as photofission resonances was shown not to have been warranted. It was demonstrated by Huizenga and Britt that they are due to neutron competition which causes a depression in the fission yield at the neutron binding energy. Similar results have been reported by Yester et al[4,40] who used the same method of generating the incident photons. Their absolute photofission cross sections differ however from those of Knowles by factors of 2 and 5 at 8 MeV for ^{238}U and ^{232}Th respectively.

Dickey and Axel measured the photofission cross sections for both ^{238}U and ^{232}Th from 5 to 8 MeV by using the tagged photons. Their results reveal the lowest 1^- fission barrier at 6.5 MeV for ^{238}U and 6.3 MeV for ^{232}Th. The peak at 6.2 MeV in ^{238}U is also present in their $\sigma_{\gamma f}$ curve. However this peak disappears in the photon interaction cross section, seeming to indicate that the decrease in photofission just above 6.2 MeV should be attributed to the neutron competition. More extensive studies which raised the excitation energy to 18 MeV have been done by Caldwell et al[9] using photons from positron annihilation. In addition to the structure appearing near the threshold region, his results show splitting peaks at the giant-resonance region. This characteristic splitting, also observed by Veyssiere[39], is understood as the opening of (γ,2n) competition at 11.4 MeV for both ^{238}U and ^{232}Th.

Measurements of photofission cross sections using photons from slow neutron-capture reactions have been done for ^{238}U and ^{232}Th by several groups[6-7]. Although their excellent resolution ($\sim$10 eV) which is smaller or comparable to the spacing of 1^- levels near the threshold region, is too good to reveal a fission resonance in view of the limited number of available lines, the results are useful for higher excitation energies. For example, the values of 37 ± 11 mb and 8.4 ± 3.5 mb for ^{238}U and ^{232}Th respectively at an excitation energy of 9 MeV are comparable within the margin of error to those of Veyssiere et al. On the other hand, one should be careful when identifing the peak at 6.73 MeV for both ^{238}U and ^{232}Th nuclei as a fission resonance because an individual class I state may have been excited.

Photofission cross sections have also been measured by using monoenergetic gamma-rays from the $^{19}F(p,\alpha\gamma)^{16}O$ reaction[41]. Results at 6.13 MeV as well as 7 MeV match Dickey' for ^{238}U and ^{232}Th. However, the results are higher than those of Knowles and Yester at the 7 MeV excitation energy.

Back et al[20] studied the fission probability via the (t,pf) direct-reaction leading to ^{238}U and ^{232}Th nuclei. Their results show a broad peak at 5.1 MeV plus a shoulder at 5.8 MeV for ^{238}U, and a weak resonance at 5.5 MeV for ^{232}Th. Both structures in ^{238}U were identified as belonging to the $K = 0^+$ fission channel. Dickey et al, on the other hand, found a broad resonance at 5.6 MeV and identified it as an excited vibrational state in the second well.

Measurements of the fission fragment angular distributions have been done with bremsstrahlung beams[42-43], and monoenergetic gamma-rays from (n,γ) reactions[44]. The experimental data are well represented, for combined dipole and quadrupole absorption, by the following equation:

$$\omega(\theta) = a + b\sin^2\theta + c\sin^2 2\theta \qquad (25)$$

For values of excitation energy E > 5.5 MeV, b/a decrease sharply with increasing energy for both ^{238}U and ^{232}Th. On the other hand, the values of c/b for ^{238}U and ^{232}Th stay practically at 0.04 and 0.025 respectively. In addition, the b/a values derived from the bremsstrahlung measurements in ^{238}U are reasonably consistent with those obtained from monoenergetic gamma-rays at low excitation energies. However, at higher energies, where K = 0 and K = 1 fission channels are equally open, the neutron-capture gamma-ray data show smaller values of b/a than those of bremsstrahlung. This has been explained[44] as due to accidental excitation of K = 1 states by the monochromatic gamma-rays from neutron capture.

(III) THE EXPERIMENT

(A) Introduction

Measurements of photofission cross sections have been carried out on a number of actinide nuclei. The main difficulty in such measurements is in obtaining gamma-rays with high intensity, variable energy, and good resolution. A number of methods have been employed to achieve this. These were discussed in chapter II. They provide energy variability combined with moderate intensity, but the resolution is generally not better than 100 keV. Photons of very good resolution ($\sim$ a few eV) have also been produced from neutron capture reactions. However, these photons have fixed energies and the number of suitable lines is not very large ($\sim$10 have been used). Thus the use of these photons to study the detailed structure in the photofission cross section is of limited value.

A way of producing gamma-rays with good energy resolution, variable energy and adequate intensity for photofission measurements is provided by the (p, γ) reaction. This method takes advantage of the Doppler shift of the energy of the gamma-rays emitted from the recoiling nuclei at a given proton resonance. In order to produce sufficiently intense photons, high proton beam currents are necessary. Such beams were provided by the Dynamitron accelerator at Brooklyn College.

Fission fragments were detected by polycarbonate Kimfol film, which has the advantage of large solid angle and high efficiency of detection of the fission fragments. Gamma-rays were monitored by a 60 c.c. Ge(Li) detector. The experimental apparatus and procedure will be described in detail in this chapter.

(B) The gamma-ray source

(1) Gamma-rays from the (p, γ) reaction

The energy of the photons emitted from a given resonance in the (p, γ) reaction at an angle θ to the proton beams is given by

$$E_\gamma = E_0 (1 + (V/c) \cos\theta) - E_0^2 / 2Mc^2 \qquad (26)$$

where E_0 is the transition energy, M is the mass and V is the velocity of the recoiling nucleus. The first term, which is angle dependent, gives the Doppler shift of the gamma-rays. The second term is a correction due to the recoiling nucleus emitting the gamma-ray. Usually this correction is very small. The energy range covered by the gamma-ray from resonances in $15 \lesssim A \lesssim 50$ nuclei with θ changes from $\theta = 0^\circ$ to $\theta = 180^\circ$ is typically 20 — 40 keV.

The energy dispersion of the gamma-rays is determined by:

$$dE_\gamma = - E_0 (V/c) \sin\theta \, d\theta \qquad (27)$$

A typical value of the dispersion is several hundred eV per degree. By changing the angle and distance from the proton target one can vary both the energy and the resolution within limits determined by the properties of the (p, γ) resonance.

There are, of course, many other ways [47,48] to produce the gamma-rays necessary to study the photofission cross section. A comparison of the intensity, resolution, and variability of the various methods is presented in Table 2. It is clear that the bremsstrahlung beams are continuous and broad, whereas the neutron capture gamma-ray are narrow and have a fixed energy. Photons from the (p, γ) reaction can provide an "intermediate" resolution of several hundred eV combined with energy variability.

TABLE 2

Methods used for generating γ-rays in the energy region 5 — 10 MeV.

Method	Effective photon intensity at target $eV^{-1}cm^{-2}sec^{-1}$	energy resolution $\Delta E_\gamma/E_\gamma(\%)$	Energy variablity
Bremsstrahlung	1 — 10	10	variable
Monochromator (Bremsstrahlung)	(0.05 — 1) 10^{-3}	1	variable
(n, γ) Compton scatterred	1	2	variable
(n, γ)	10^{6}	10^{-4}	Fixed
Positron annihilation	10^{-2}	1 — 4	Variable
(p, γ)	1 — 10	3×10^{-3}	variable

In order to be suitable as a gamma-ray source for photofission studies, a (p, γ) resonance must decay emitting exclusively or almost exclusively one gamma line with an energy greater than 5 MeV. All other gamma-rays coming from it must be of lower energy. The strength of this resonance must be large and its natural width less than several hundred eV. A list of easily produced gamma-rays from (p, γ) resonances in light nuclei ($A \leq 44$) has been compiled[49]. In surveying this list, eleven cases were chosen covering the range of 5.8 MeV to 12 MeV. These are given in Table 3. Most of the notation used in this table is self-explanatory; however, the following shall be noted: (1) the gamma-ray energy E_γ is calculated from the proton energy E_p and the reaction Q value at $\theta = 90^\circ$; (2) the range is determined by the Doppler shift from $\theta = 0^\circ$ to 90°; (3) FOM (figure of merit) is the number of photons per μC of proton beams on target; (4) the resonance strength S is defined as $S = (2J+1)\,\Gamma_p\,\Gamma_\gamma / \Gamma$.

Perhaps the most crucial factor in using the (p, γ) reaction as a source of gamma-rays is their intensity. The use of the Dynamitron accelerator, therefore, is crucial for the success of the experiment. This accelerator will be described in the next section.

(2) The accelerator

The Dynamitron accelerator is an RF driven, gas insulated, high voltage DC source, with excellent voltage stability and high beam current capabilities. The maximum proton current available is 2 ma. At the high voltage end of this accelerator, a duo-plasmatron ion source generates the charged particles. A terminal magnet sitting between the ion source and the main accelerator mass-analyzes the beam before acceleration. This technique reduces loading and allows the maximum beam current. The beam transport system includes turbo-molecular pumps, an energy analysing magnet

TABLE 3

Gamma-rays used in the photofission measurements

E-gamma (keV)	Range (keV)	FOM	Target	E_p (keV)	E_{x1} (keV)	Branching (%)	Strength (eV)	Width (eV)
5871	13	1930	25Mg	1701	7941	75	10	
6180	10	656	29Si	1302	6858	63	1.4	170
6879	14	2578	30Si	1878	9114	49	4.0	22
7378	13	3306	30Si	1398	8649	73	3.1	100
7954	18	3356	25Mg	1716	7955	77	17	
8245	12	1372	30Si	982	8247	66	1.3	100
8727	15	3914	30Si	1480	8729	80	3.4	100
8923	20	6714	23Na	1417	13047	95	38	90
9981	15	2146	35Cl	1519	9983	100	14	410
10761	17	6559	27Al	992	12542	75	31	100
11540	25	3330	27Al	1800	13321	94	15	200

system with NMR-readout and slit feed-back, a switching magnet, and several quadrupole focussing devices.

The accelerator has been calibrated using three reactions: (1) $^{7}Li(p,n)^{7}Be$ at the proton threshold energy of E_p = 1.882 MeV; (2) $^{27}Al(p,\gamma)^{28}Si$ at the proton resonance of E_p = 1.984 MeV; (3) $^{27}Al(p,\gamma)^{28}Si$ at E_p = 0.9918 MeV. A table is then generated, the results showing that the NMR frequency is changed by 1.7 kHz per keV at $E_p \simeq 1$ MeV. The proton beam resolution of this accelerator is important in obtaining the necessary gamma-ray yield. The observed value from a narrow (p, γ) resonance is about 2 keV. This can be seen in Fig. 10 where the excitation curve of $^{23}Na(p,\gamma)$ at E_p = 1.41 MeV is plotted. The sharp rise in the yield at 4145 kHz gives a measure of the beam resolution, whereas the plateau and the slow drop indicate the target thickness.

(3) Proton targets

All target materials used in the (p, γ) reactions were evaporated under vacuum and deposited on a 0.2 mm tantulum backing. The Ta foil was used because of its high melting point, low gamma-ray yield from Coulomb excitation, absence of any (p,n) reaction at the proton energy employed, and relatively high neutron binding energy. Except for ^{23}Na and ^{27}Al, separated isotopes were used to optimize the gamma-ray yields. The target must be thick enough to last at least 5 hours under an average beam current of 100 μa, but it cannot be too thick since this would cause overlap of adjacent resonances. Thicknesses on the order of 100 $\mu g/cm^2$ ($\sim$10 keV) were used in most of the cases. The gamma-ray background caused by the $^{19}F(p,\alpha\gamma)^{16}O$ reaction was the most serious problem at the early stages of this experiment. It was found that the fluorine contaminations were present in the Ta backing. They were also contained by the deposits on

Fig. 10: The excitation curve of $^{23}Na(p, \gamma)^{24}Mg$ at E_p = 1.417 MeV.

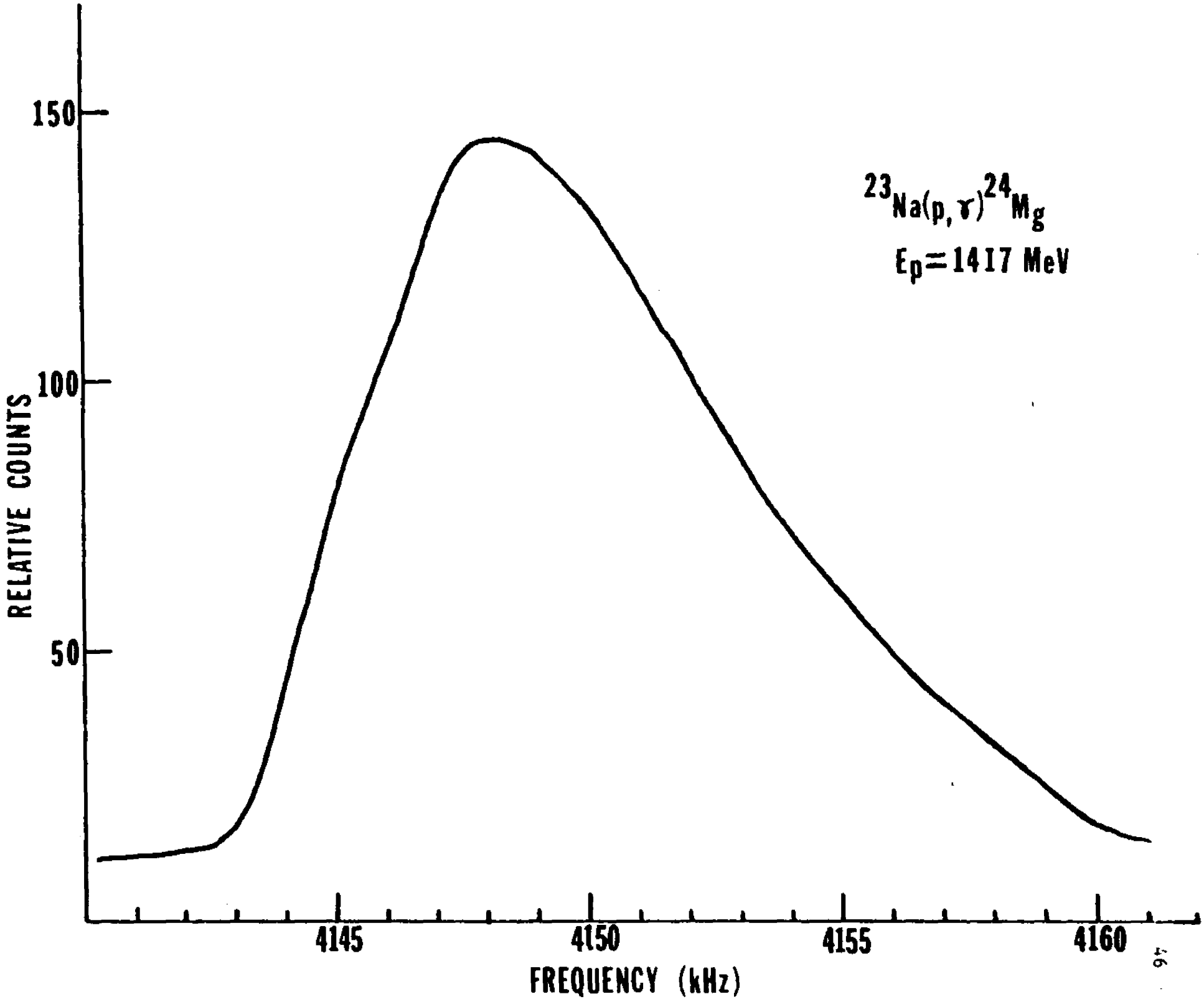
150
100
50
RELATIVE COUNTS
$^{23}Na(p,\gamma)^{24}Mg$
$E_p = 1417$ MeV
4145
4150
4155
4160
FREQUENCY (kHz)

target when it was bombarded by the high proton beams. The latter was due to insufficient high vacuum. The Ta contamination was kept low by electrically heating the backings to incandescence under vacuum for several minutes[50] and the vacuum was improved by mounting a diffusion pump with an LN_2 baffle attached to it and an LN_2 cold finger placed very close to the target chamber. These measures virtually eliminated the $^{19}F(p, \alpha\gamma)$ background from the gamma-ray spectra accumulated by the monitor during the photofission measurements.

In order to use the large beam current available from the Dynamitron, a target chamber which makes possible direct water cooling of the Ta backing was built, as shown in Fig. 11. Chilled water flowing under pressure of 40 PSI was used and therefore it was important to have a sturdy target backing capable of withstanding the pressure difference. A 0.2 mm thick molybdenum foil was also used as a target backing. However this material is too brittle after being heated and it was breaking repeatedly.

The size of the beam spot on the target could be varied with the help of two beam wobblers, drawn in Fig. 12. One of them was powered by an ordinary AC line, moving the beam horizontally at 60 cycles per second. The other was fed by a triangular wave, moving the beam vertically with about 700 cycles per second. As a result the beam spot had a rectangular shape of 6 mm x 9 mm. The target assembly could sustain a beam current of 170 μa at E_p = 1.7 MeV without losing the gamma-ray yield for at least 10 hours.

(4) The gamma-ray energy resolution

Perhaps the most interesting property of gamma-rays from a (p, γ) reaction is their resolution. As described earlier the gamma-ray energy is determined by

Fig. 11: Target assembly with direct water cooling of the Ta backing.

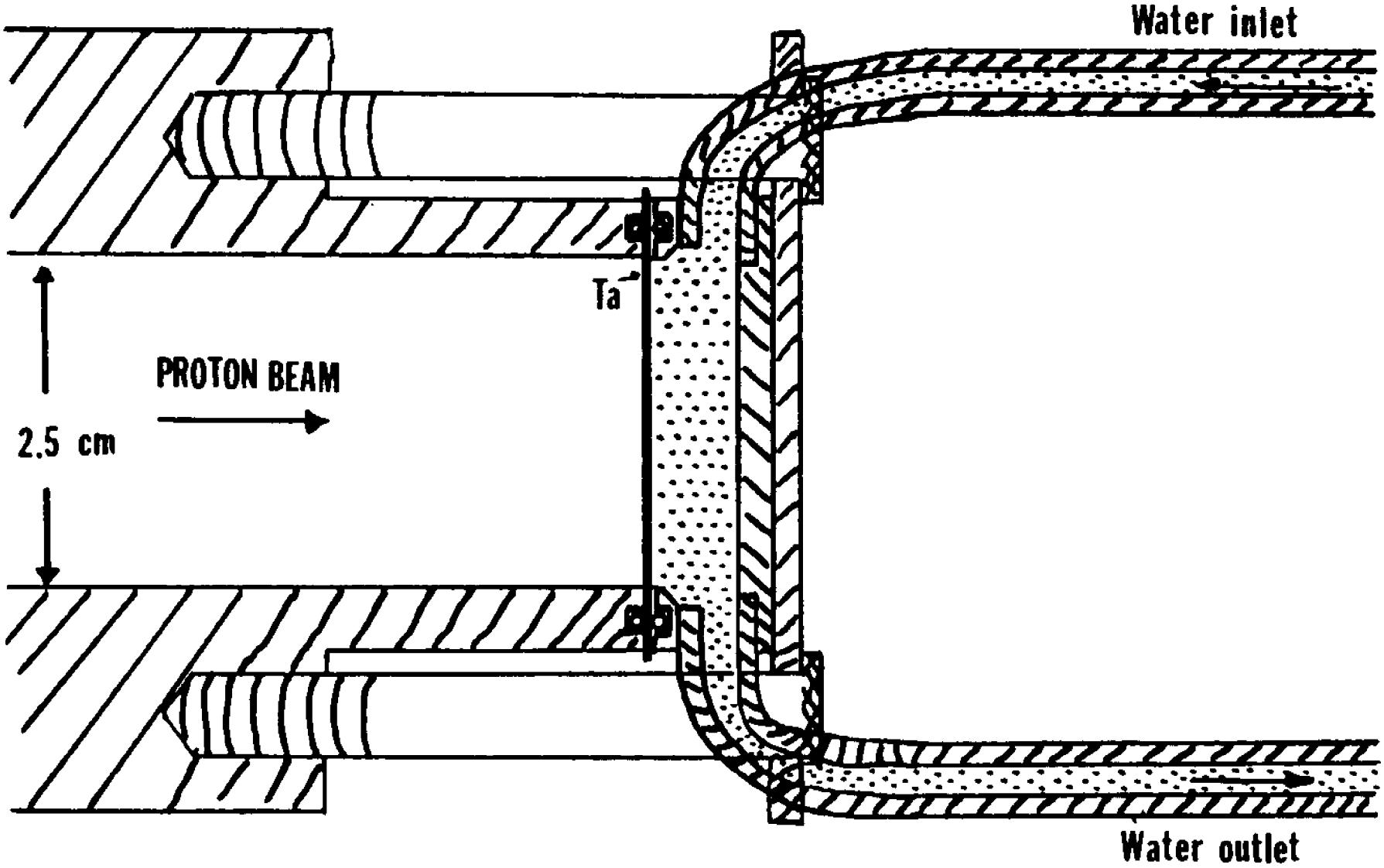
Water inlet
Ta
PROTON BEAM
2.5 cm
Water outlet
2.5 cm

Fig. 12: Beam wobbler assembly

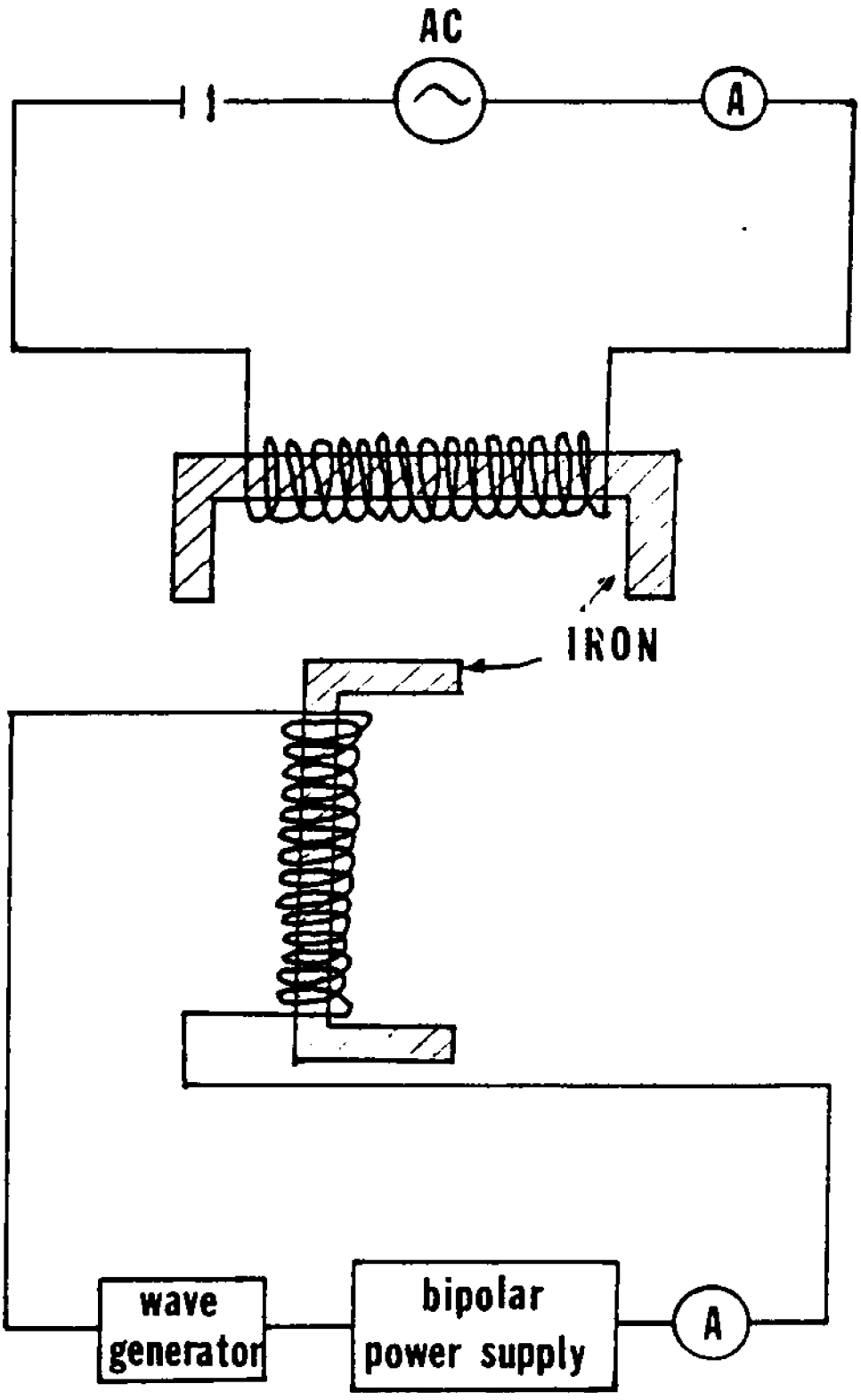
AC
A
IRON
wave generator
bipolar power supply
A

$$E_\gamma = E_o + \Delta E_D + E_R$$

where

$$\Delta E_D = E_o (V/c) \cos\theta \qquad (28)$$

$$E_R = -E_o/2MC^2 \qquad (29)$$

For a narrow (p, γ) resonance and a point beam spot the angle θ is well defined for a given point on the fission foil. Under the presently used scanning method (see page 84), the gamma-ray energy resolution is determined by the energy dispersion (eq. (27)). Typical values of 200 — 300 eV per degree can be easily obtained. However, the proton beam from the Dynamitron give a beam spot a few mm in diameter. Futhermore, this beam spot is enlarged by the two beam wobblers (fig. 12).

The extended size of the beam spot produced an uncertainty in the angle θ . In the present set-up the gamma-ray energy resolution is determined by the energy dispersion $dE_\gamma/d\theta$ and the Doppler shift ΔE_D which is also θ dependent.

In order to see the effect of each term, consider as an example the 1701 keV proton resonance in ^{25}Mg. The properties of the resonance are listed in Table 2. ΔE_D and $dE_\gamma/d\theta$ can be rewritten as

$$\Delta E_D = 13686.3 \cos\theta \quad eV \qquad (30)$$

$$\frac{dE_\gamma}{d\theta} = -238.7 \sin\theta \quad eV/degree$$

For a beam spot with dimension d along the y axis the differences in $(\Delta E_D)_{12}$ between positions 1 at d/2 and 2 at -d/2 on the y axis(Fig. 13)

Fig. 13: Part of the experimental set-up showing the proton target and the fission fragment detecting assembly.

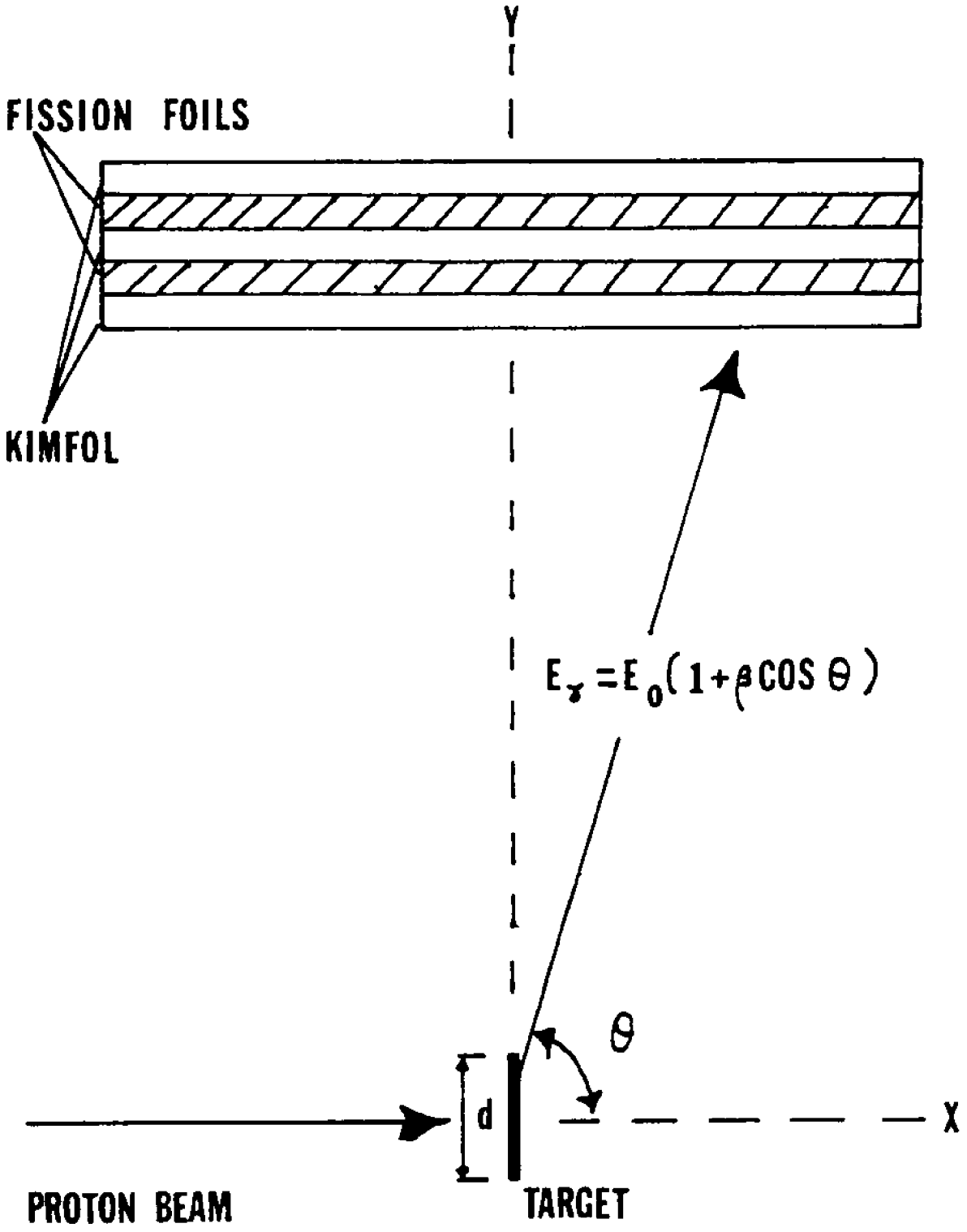
Y
FISSION FOILS
KIMFOL
$E_\gamma = E_0(1+\beta\cos\theta)$
θ
d
X
PROTON BEAM
TARGET

are tabulated for a number of points along the fission foils in Table 4. The distance from the foils to the middle of the target along the y axis is 5 cm. It is clear that the uncertainty in the Doppler shift $(\Delta E_D)_{12}$ increases with x. For a point on the proton target out of plane in Fig. 13 there is an additional small contribution which has been calculated for $z = \pm d/2$. The overal resolution R is calculated as a root mean square of $(\Delta E_D)_{12}$ and the energy dispersion used in scanning the spectra. It varies from 300 eV in the middle of the fission foils (x=0) to 900 eV at their edge (x=2.5 cm). The contribution of the natural widths of the proton resonances which we have used is negligible.

TABLE 4

Calculation of the energy resolution of the 5.871 MeV gamma rays from the $^{25}Mg(p,\gamma)$ reaction

x cm	d cm	$(\Delta E_D)_{12}$ eV	$(\Delta E_D)_z$ eV	R eV
0.5	0.6	162.4	2.4	287.7
	0.9	244.6	5.4	340.9
1.0	0.6	310.7	4.6	389.0
	0.9	467.9	10.4	533.2
1.5	0.6	434.1	6.5	490.6
	0.9	653.3	14.5	692.2
2.0	0.6	529.9	7.9	574.4
	0.9	792.4	17.6	822.9
2.5	0.6	588.4	8.78	625.9
	0.9	884.2	19.7	909.8

(C) Detection of fission fragments

(1) Introduction

The use of polycarbonate films as fission track detectors has become quite common in recent years. The idea is based on the fact that the passage of fission fragments through the film creates damage tracks. A recently published book of Fleischer, Price, and Walker entitled Nuclear Tracks in Solid[51] has reviewed the principles of operation and methods of handling these detectors; their various applications in nuclear science and earth and space science have also been described. Their high efficiency[52,53] and their insensitivity to light particles and gamma-rays makes them ideal for detecting fission fragments in situations where large solid angles are important.

When fission fragments impinge on a polycarbonate film, they produce damage tracks (typical size $\sim$ 50 A). These tracks are too small to be observed, but etching the film with a solution of NaOH or KOH will enlarge their size a thousandfold. The etching proceeds at a faster rate in places where the material is damaged. There exists a critical angle for the inclined tracks beyond which the tracks become obliterated by the bulk etching of the film. Etching conditions have been described[54-56] in the literature for ^{252}Cf fragments of undegraded energy. In our experiments thick fission foils have been used. The fragments emerging from deep layers of such foils have their energy heavily degraded. It was therefore necessary to determine the etching condition suitable for our situation.

(2) Film processing

Polycarbonate (Kimfol) films 8 μm thick were used as fission track detectors. Although thinner films have a higher efficiency for fragments coming from a thick target, this thickness was chosen because of ease of handling the films.

An aqueous solution of sodium hydroxide (NaOH) was used for developing the films. Hydrochloric acid of concentration $\sim$ 10% has been used successfully to rinse the film and stop the etching process.

Fifty mg/cm^2 thick ^{238}U foils have been employed as sources of fission fragments to find the optimal conditions for developing the polycarbonate films. The foils have been sandwiched between polycarbonate films. The effective thickness of the ^{238}U layers from which spontaneous fission fragments escape [53] is 4.3 mg/cm^2.

The fission counting rate per unit area of film obtained from the spontaneous fission of ^{238}U is plotted as a function of the etching time in Fig. 14 a. The temperature of the 6N NaOH solution was maintained at 60^{o}C. The counting rate saturates at 60 minutes. The error bars indicate only the statistical errors. Films which were not exposed to the ^{238}U foils were also etched under the same conditions to evaluate the possible background. This background starts to increase sharply at $\sim$ 70 minutes, as shown by the dashed curve in Fig. 14 a. Therefore 60 minutes was taken as the etching time in order to keep the background low.

Fig. 14 b, shows the fission counting rate vs etching time for fission fragments coming from a ^{252}Cf source. In contrast to Fig. 14 a, a plateau appears for etching time longer than 30 minutes. This is because the fragments of ^{252}Cf have a relatively narrow kinetic energy distribution. Thus all the tracks are revealed when the etching conditions reach a certain point.

Etching is also very sensitive to the temperature, as shown in Fig. 14 c. The results are obtained by treating the film with the 6N NaOH solution for 60 minutes. A 1.5% change in counting rate per degree celsius is found. Therefore the temperature had to be maintained at a constant value

Fig. 14: Determination of the optimized etching condition.

(a) Fission counting rate as a function of etching time for ^{238}U fragments.

(b) Fission counting rate as a function of etching time for ^{252}Cf source.

(c) Fission counting rate as a function of the etching temperature for ^{238}U fragments.

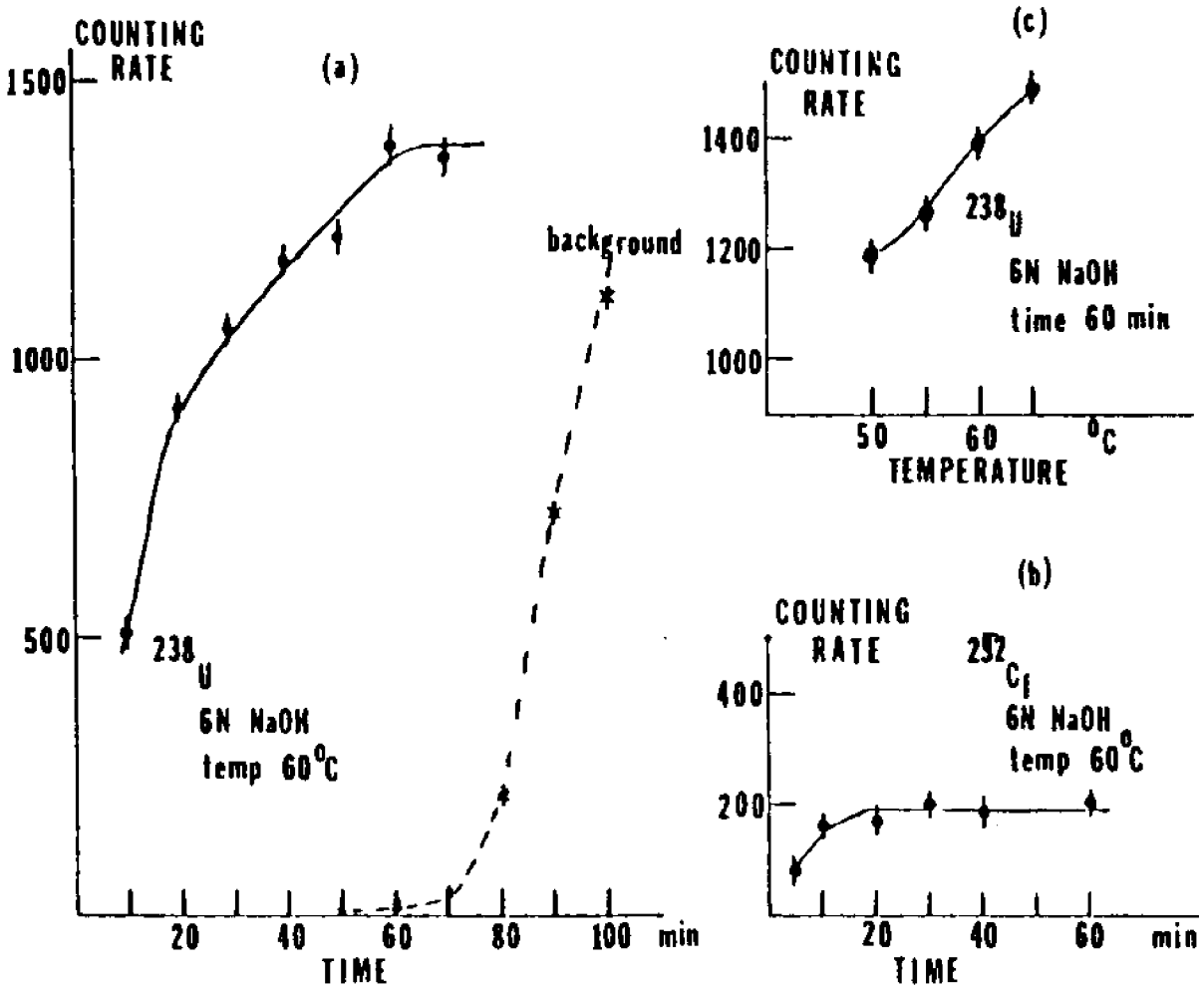
COUNTING RATE
(a)
1500
1000
500
background
238U
6N NaOH
temp 60°C
20
40
60
80
100
min
TIME
(c)
COUNTING RATE
1400
1200
1000
238U
6N NaOH
time 60 min
50
60
°C
TEMPERATURE
(b)
COUNTING RATE
252Cf
6N NaOH
temp 60°C
400
200
20
40
60
min
TIME

with an accuracy of $\pm 1^{o}C$. Although a higher temperature than 60°C would produce a faster etching effect, its use is limited by two factors: (1) temperatures $\gtrsim$ 75°C generate bubbles; (2) it becomes harder to keep the temperature constant when it is high. Therefore an etching temperature of 60°C was chosen for all the measurements.

The concentration of the etching solution is another factor. Experimental results show that a change from 6N to 5N, changes the counting rate by about 10%. A 6N NaOH solution was used because it is still easily handled and has been commonly used. The bulk etching-rate of the polycarbonate film in a NaOH solution was found by Peterson[57] and Paratzke et al[58] to depend significantly on the concentration of the products of the etching process. Because of this, the etching solution was changed every 50 films.

The tracks produced by etching are typically a few microns in diameter. Although this is large enough to be seen by an ordinary microscope, it is still too small to be visible with the naked eye. A number of techniques have been proposed[59,60] to scan these nuclear tracks. Of these, at the present time, the spark scanning technique is by far the simplest and most widely used[54]. The original idea of this method advanced by Lark[54], was to pass the film through a dc high voltage spark gap. A discharge is obtained when the track is within the gap which enlarges the size of the track. Recently, a multi-head scanning probe was developed by Patrick and Bowey[60]. This modification makes the scanning process faster.

The head of a multi-electrode sparking device used in the present experiment is shown in Fig. 15. Fifteen copper electrodes, 0.38 cm apart, were fitted in a lucite frame. Each electrode had a 2.8 mm in diameter flat disc at the tip. The gaps were formed between the electrodes and a 5.2 cm × 7 cm flat copper plate. Each electrode was connected independently to the

Fig. 15: The arrangement of multi-electrode sparking device.

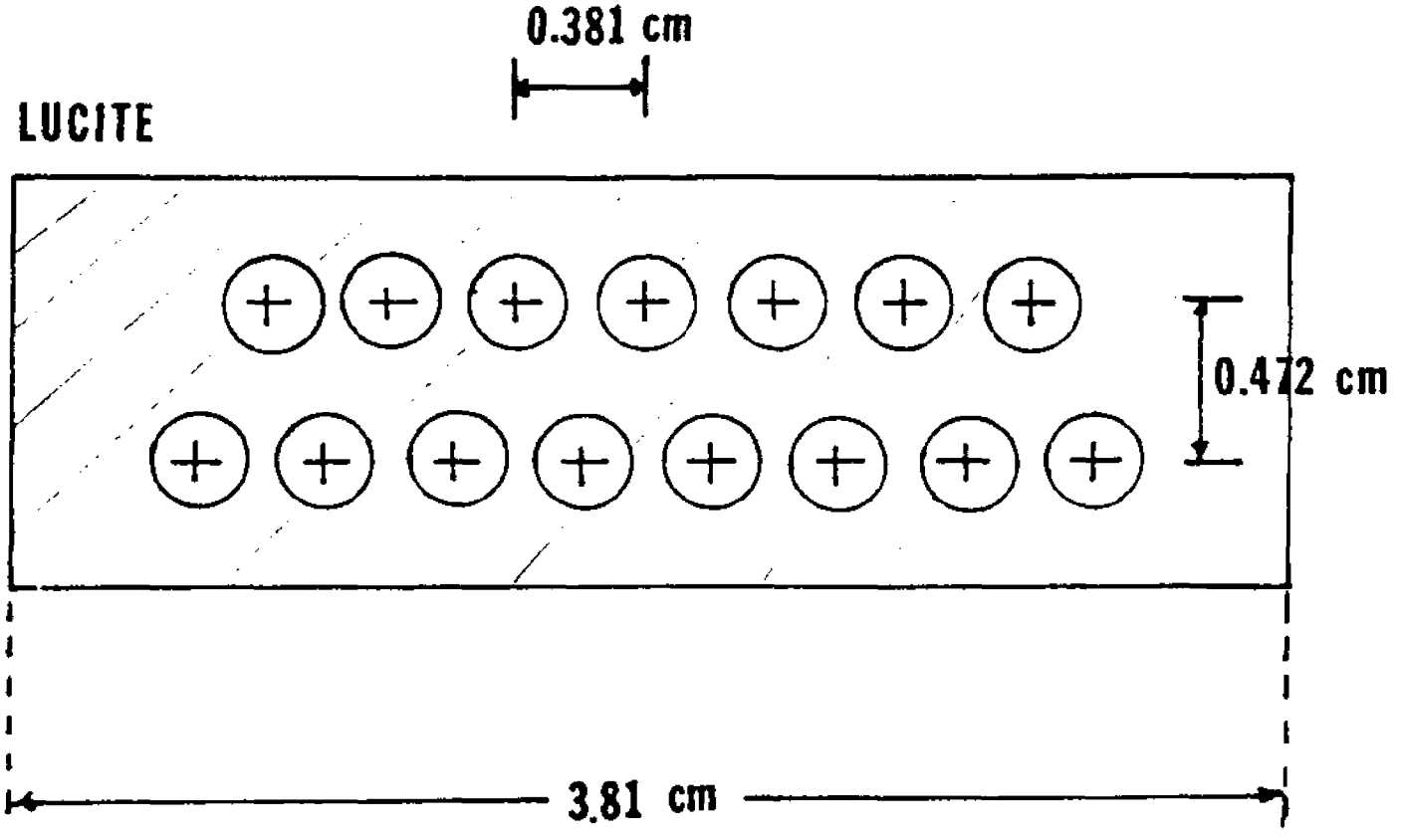
0.381 cm
LUCITE
0.472 cm
3.81 cm

high voltage power supply through a 2.7 MΩ resistor, and each had its own discharge capacitor of 100 pf, thus allowing simultaneous sparking. The focussing mechanism of a microscope was used to adjust the sparking gap between the base plate and the electrodes. The gap was kept at about 100 μm and the potential difference was maintained at 1600 volts. The choice of the potential is not very crucial. This can be seen from Fig. 16 a , where the fission counting rate vs the potential difference is plotted. The counting rate has a constant value within the range of 1400 — 2000 volts.

The tracks produced after etching in 6N NaOH at 60°C for 60 min. and sparking can be seen with the naked eye. They are about 0.1 mm in diameter and black rings around each hole make them easier to see. A developed film is shown in Fig. 16 b. Note that the reliability of this technique is restricted to a low track density, since each track occupies an area of about 0.4 mm^2. Thus it becomes very hard to count the tracks accurately when the tracks density is beyond 100 counts/cm^2.

(3) Absolute fission rate measurements

The absolute efficiency Ω of the polycarbonate film for detecting the fission fragments is simply the ratio of the number of observed tracks per unit area to the number of fission events that occur in the source per unit area. In the case of a thin source Ω is related directly to the critical angle, which is the minimum entering angle relative to the film at which fragments will produce tracks in the film. The smaller the critical angle the greater the efficiency of registration. For a thick source the fission fragments have a continuous energy distribution; the efficiency is then a complex function depending on the entering angle and the energy of the fission fragments. Since thick fission foils were used in the present experiment it was important to measure the absolute efficiency of the Kimfol

Fig. 16 a: Fission counting rate vs the potential difference applied to the spark gaps.

b: A developed film after etching and sparking. This film has been exposed to the 8.9 MeV gamma-rays from the 1.41 MeV proton resonance in the $^{23}Na(p, \gamma)$ reaction.

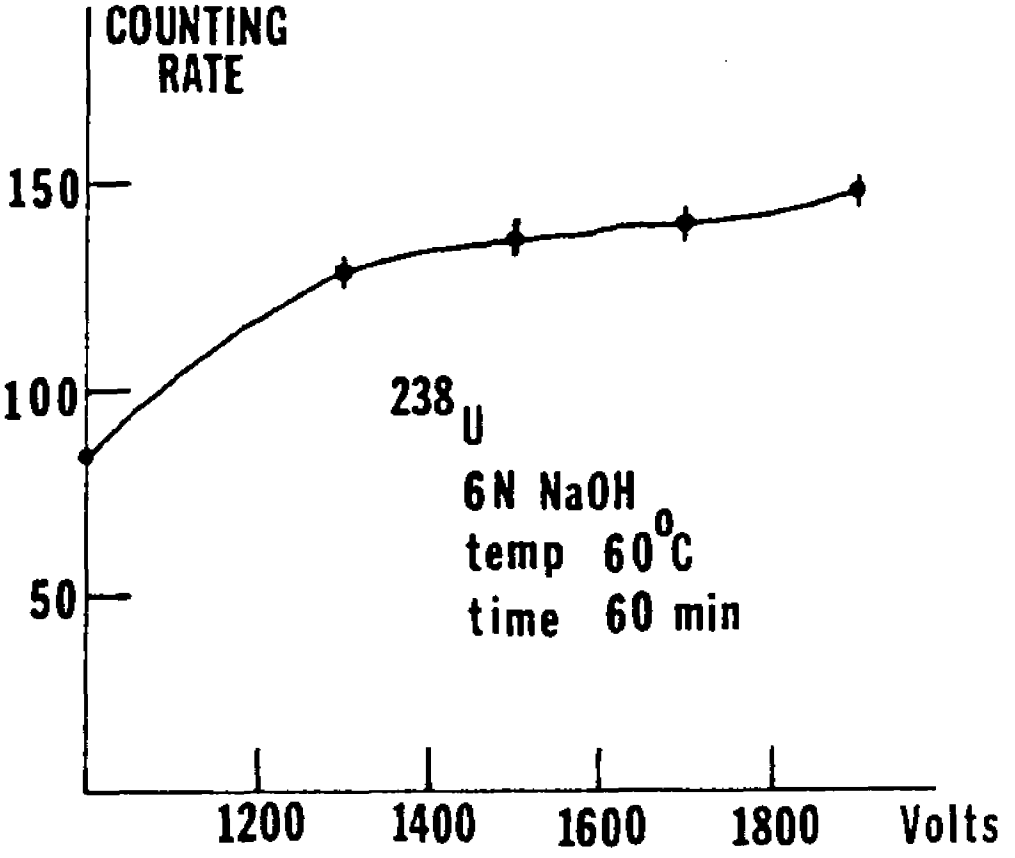
COUNTING
RATE
150
100
50
238 U
6N NaOH
temp 60°C
time 60 min
1200
1400
1600
1800
Volts

(a)

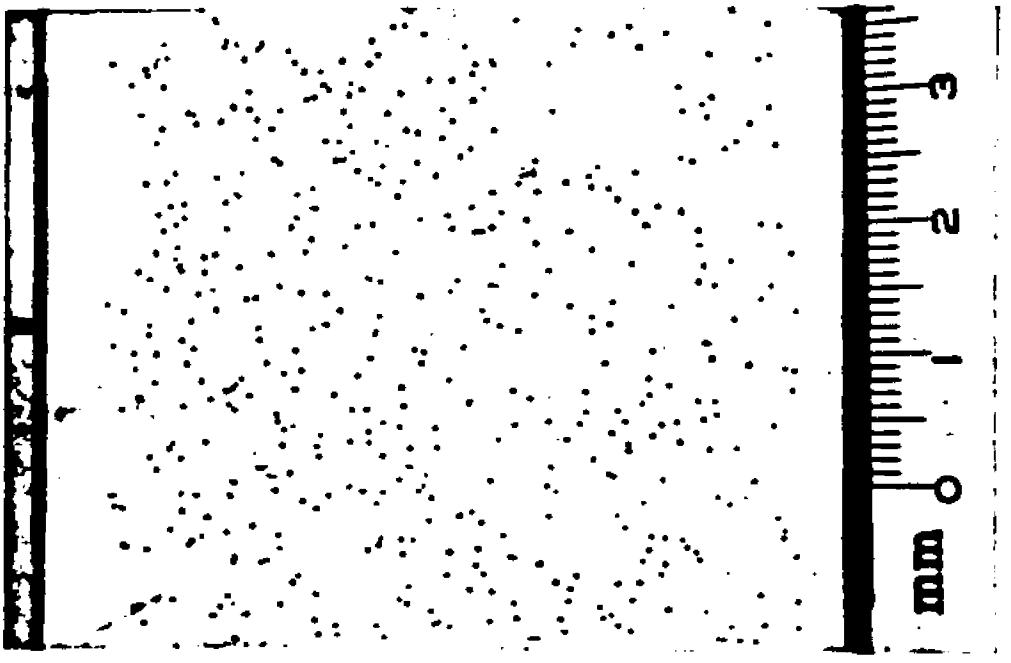
3
2
1
0
mm

(b)

film for fission fragments of degraded energy. These measurements were necessary to calculate the absolute photofission cross sections.

A ^{252}Cf source was used as an emitter of fission fragments. This source was covered with gold foils ranging from 0.5 mg/cm^2 to 10.91 mg/cm^2. A schematic diagram of the arrangement of the source and films is shown in Fig. 17. The ^{252}Cf source was 3 mm in diameter and was centered on a Pt backing 12.5 mm in diameter. The 8 μm Kimfol films were placed on a lucite frame above the ^{252}Cf source and the gold foils and exposed under vacuum to the fission fragments. The source could be lifted by a cylindrical spacer to change its distance from the films.

The films were processed in the same way as described in the previous section to reveal the fragment tracks. The number of tracks per unit solid angle was found as a function of the thickness of the gold foil and the angle which the fragments make relative to the normal to the film.

A surface barrier detector, 6 cm^2 in area and 6 micron thick, was used for absolute calibration of the ^{252}Cf source. The detector placed 7.6 cm away from the source was operated at the effective bias of $\sim$ 85 volts. An aluminum collimator defined a detection area of 2 cm^2. With this geometry, the average counting rate for both heavy and light fragments was about 1.2 counts/sec. The accumulated spectra which were stored in a multi-channel analyzer showed clearly the separation of the α particles from the fission fragments.

The fission counts were measured by the detector for a number of angles with respect to the normal to the Cf source to determine the angular distribution of the emitted fragments. The results indicated, as expected, that the source is isotropic. The activity of the source was found to be 0.213 ± 0.002 μCi. From this activity and the

Fig. 17: Schematic diagram of the arrangement of the source and films for the determination of the absolute efficiency of the Kimfol film.

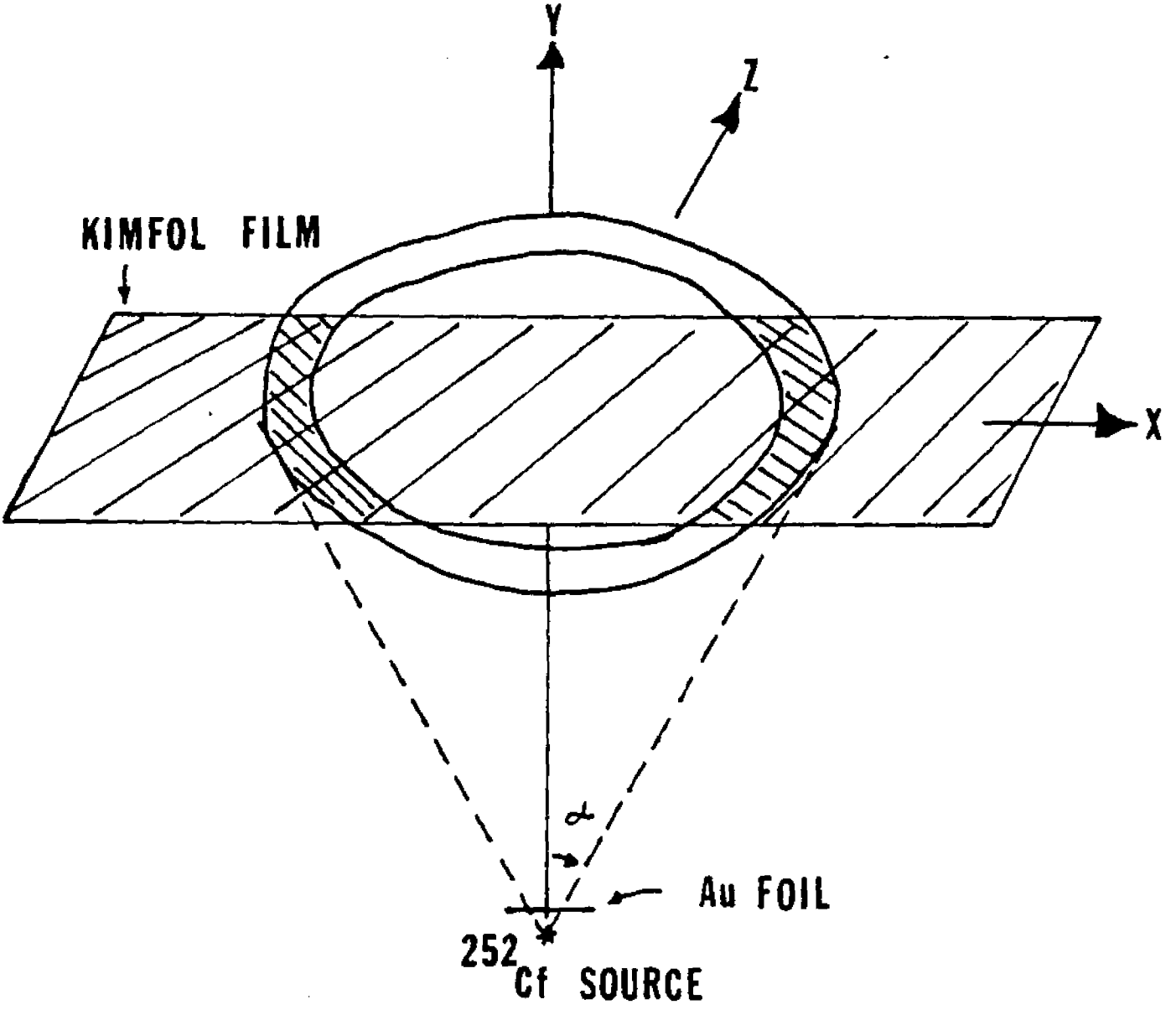
Y
Z
KIMFOL FILM
X
α
Au FOIL
252 Cf SOURCE

measured counting rate of the fission tracks one obtains an absolute efficiency of 100±3% for the Kimfol film as a detector of fission fragments of undegraded energy falling on the film at small angles with respect to the normal.

The efficiency $\Omega(j, \alpha)$ of the kimfol films for counting the ^{252}Cf fission fragments as a function of the thickness j of the Au foils through which the fragments have to pass on the way to the film and the angle α at which they are emitted is plotted isometrically in Fig. 18. It is clear that for thin layers of Au the efficiency is about 100% for fragments emitted in a cone of $\sim 120^{\circ}$. This angle decreases with increasing thickness of the Au foils and the overall efficiency drops. This can be seen in Fig. 19 where the fragment counts integrated over α are plotted vs the thickness of the Au foils. By extrapolating the data points, the range of the ^{252}Cf fission fragments in Au foils is found to be 10.6± 0.5 mg/cm^2. This value agrees closely with the value of 10.47±0.34 mg/cm^2 reported by Kahn et al[61].

In order to apply the efficiency curves to the photofission measurements in which thick fission foils of uranium and thorium are employed, we have to examine corrections resulting from the differences in energies of the fission fragments of ^{252}Cf, ^{238}U, and ^{232}Th and the differences in the stopping powers of gold, uranium, and thorium for these fragments. The passage of ^{252}Cf fragments through various materials including gold has been studied, however, no similar experimental information exists for ^{238}U and ^{232}Th. On the other hand the passage of fragments from $^{235}U(n,f)$ has been studied[61]. These fragments have average energies (85 MeV) which are very close to the calculated average energies[62] of the fission fragments of ^{238}U (84 MeV) and ^{232}Th (82 MeV). For this reason we have considered the fission fragments from the $^{235}U(n,f)$ reaction as simulating

Fig. 18: The efficiency $\Omega(j, \alpha)$ of the Kimfol film for counting the ^{252}Cf fission fragment as a function of the thickness j of the gold foils and the angle α .

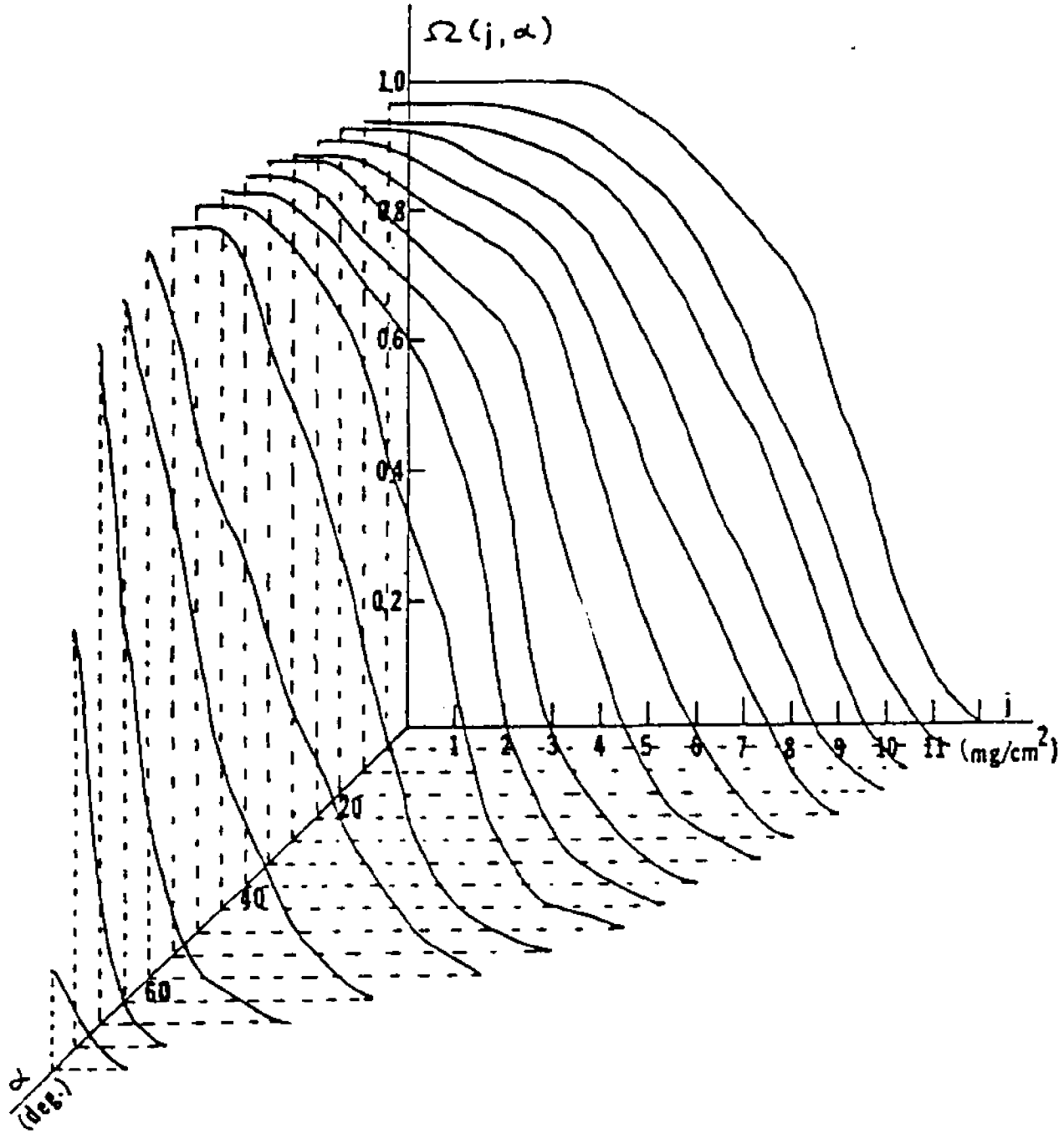
Ω(j, α)
1.0
0.8
0.6
0.4
0.2
j
1 2 3 4 5 6 7 8 9 10 11 (mg/cm²)
20
40
60
α
(deg.)

Fig. 19: The attenuation of the ^{252}Cf fission fragments by gold foils of various thicknesses.

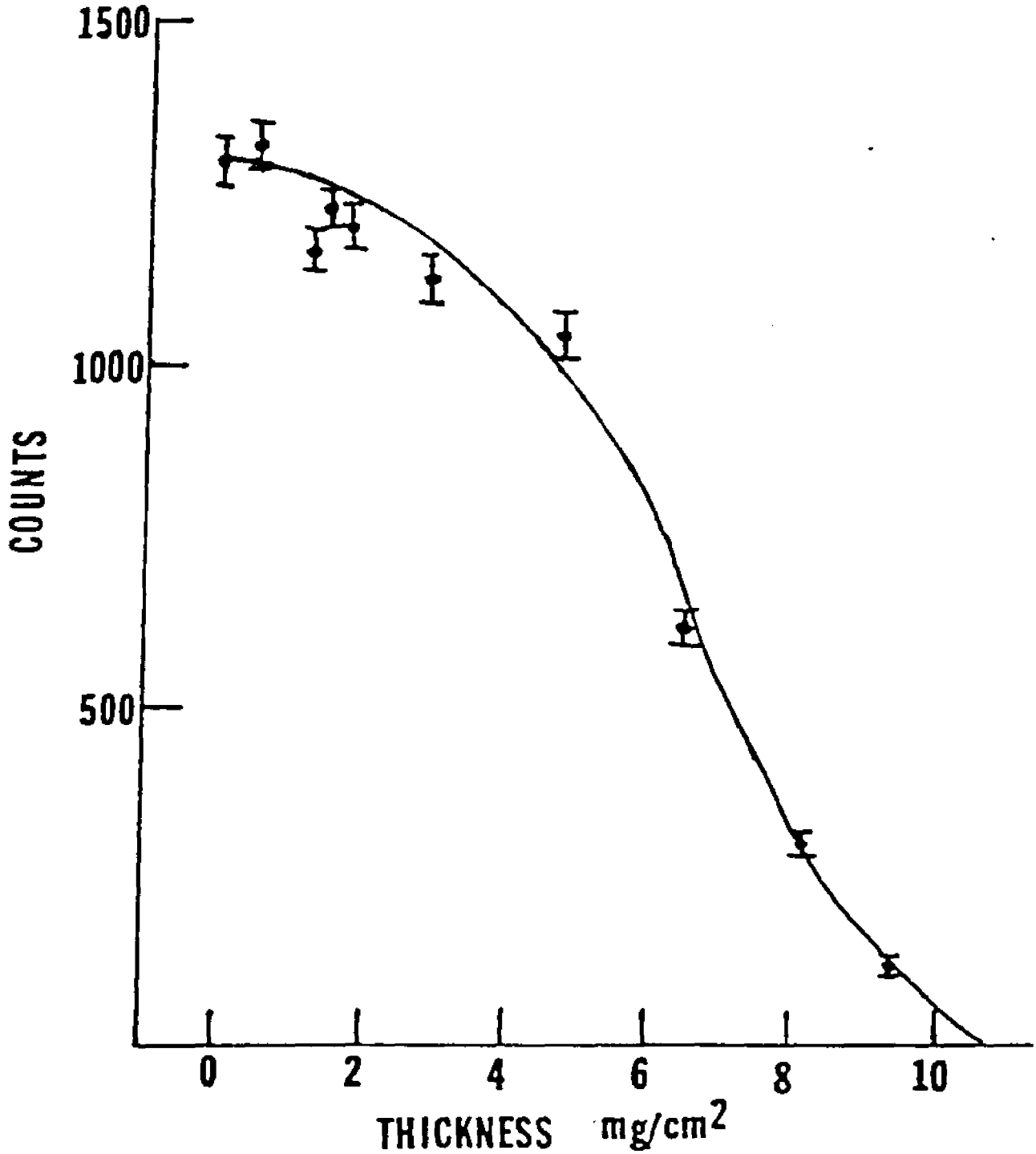
1500
1000
500
COUNTS
0
2
4
6
8
10
THICKNESS mg/cm2

the behavior of the fission fragments of ^{238}U and ^{232}Th.

To find the corrections to the efficiency curves, we have used the data of Kahn et al[61] to extrapolate the thickness corresponding to a given transmitted energy of ^{235}U fragments in Al, Ni, Ag, and Au to uranium. The average transmitted energy of the light and heavy fragments is plotted against the thickness of uranium in Fig. 20 (solid line). The dashed line is taken from Kahn et al for ^{252}Cf fragments in gold. Both curves have the same basic pattern i.e. the kinetic energy of the fission fragments is attenuated as they penetrate into the absorber.

Let us consider for example a thickness of 1 mg/cm^2 of uranium. The transmitted energy of ^{235}U fragments is 71 MeV. In order to yield a ^{252}Cf fission fragment with the same transmitted energy, the corresponding Au thickness is 1.4 mg/cm^2. If we assume that the Kimfol films have the same efficiency to reveal the fragment tracks of ^{252}Cf and ^{235}U at a given kinetic energy, we can take the efficiency for ^{252}Cf fragments that travelled at a given angle a thickness 1.4 mg/cm^2 in gold on their way to the film as equal to the efficiency for ^{235}U fragments that passed a thickness of 1 mg/cm^2 in uranium at the same angle. In this way the efficiency curves determined for ^{252}Cf fission fragments emerging from gold can be re-mapped to obtain the efficiency for ^{235}U fragments emerging from uranium.

To check whether the efficiency curve has been determined correctly we have calculated the spontaneous fission decay constant of ^{238}U from the spontaneous fission data. The spontaneous fission counting rate N_{SF} per unit area of foil having an effective number of fissioning nuclei $n\Delta y$ can be written in the form

Fig. 20: The average transmitted energy of the light and heavy fragments vs the absorber thickness. The solid line is obtained for $^{235}U(n,f)$ fragments transmitted through uranium, the dashed line is for ^{252}Cf fragments in gold.

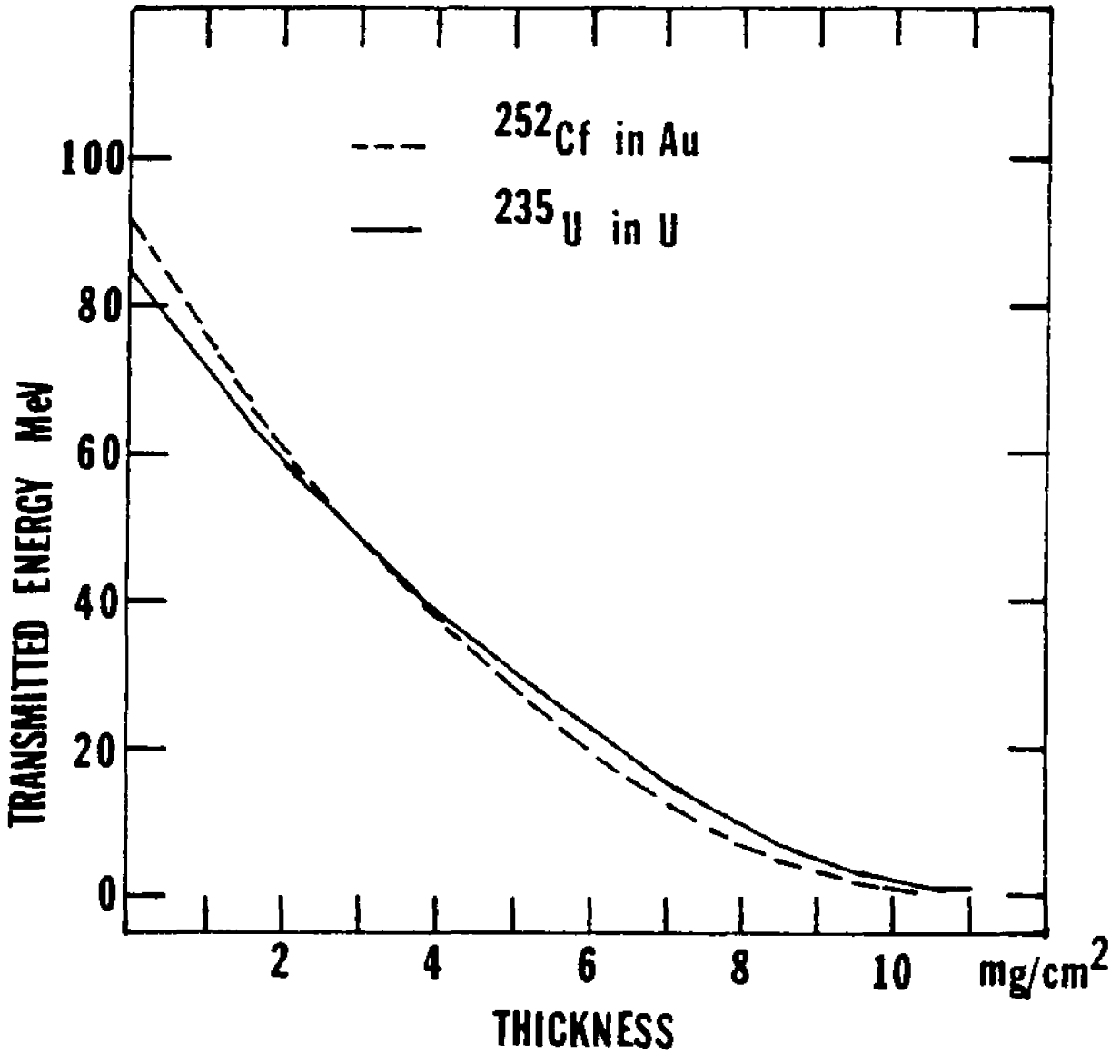
252Cf in Au
235U in U
100
80
60
40
20
0
TRANSMITTED ENERGY MeV
2
4
6
8
10
mg/cm2
THICKNESS

$$N_{SF} = \frac{2}{4\pi} \lambda_{SF} t \, n \, \Delta Y \sum_j \eta(j) \qquad (31)$$

where λ_{SF} and t, are the spontaneous fission decay constant and the exposure time respectively. Since the angular distribution of the fission fragments is isotropic, the efficiency $\eta(j)$ is given by

$$\eta(j) = \sum_{i,l} \Omega(j, \alpha_i) \sin\alpha_i \, \Delta\alpha_i \, \Delta\phi_l \qquad (32)$$

From the measured value of N_{SF} = 8.52±0.15 counts/cm^2/144 hrs we obtain

$$\lambda_{SF} = (6.4 \pm 0.3) \times 10^{-17} \quad yr^{-1} \qquad (33)$$

This decay constant, which is used in geophysical dating, has also been measured by other groups using various methods. Our result is close to the results[51] obtained by employing solid-state track detectors. In Table 5 we have listed the results of other measurements.

It is also of interest to find the effective thickness of the U foil from which fission fragments are detected by the Kimfol film. The effective thickness τ is defined as:

$$\tau = \frac{2\Delta Y}{4\pi} \sum_j \eta(j) \qquad (34)$$

We have found τ = 3.19 mg/cm^2. This value is smaller than τ = 4.3 mg/cm^2 reported by Gold et al[53] in which fission fragments were recorded by a pre-etched mica and counted with the help of a microscope. This technique is more sensitive than the one used by us and therefore a larger value of τ is expected.

TABLE 5

Measurements of the spontaneous fission decay constant of ^{238}U.

	Method	λ_{SF} ($\times 10^{-17}$ yrs^{-1})
Perfiler et al (1947) Zh. Eks. i. Teor. Fiz. 17,746	Fission chamber	5.3 $\pm$ 0.9
Segre (1952) Phys. Rev. 86,21	Fission chamber	8.7 $\pm$ 0.3
Fleischer and Price (1964) Phys. Rev. 133, B63	Track detector	6.85 $\pm$ 0.2
Rao and Kuroda (1966) Phys. Rev. 147,384	Radiochemical	7.8 $\pm$ 0.9
Roberts et al (1968) Phys. Rev. 174, 1482	Track detector	7.03 $\pm$ 0.11
Kleeman et al (1971) ACTA, 35, 637	Track detector	6.8 $\pm$ 0.6
Khan and Durrani (1973) Rad. Eff. 17,133	Track detector	6.32 $\pm$ 0.55
Emma et al (1975) Nucl. Inst. Meth. 128, 355	Track detector	7.2 $\pm$ 0.2
Hurford et al (1977) Nucl. Track Detect, #1, 41	Track detector	7.0 $\pm$ 0.78
Kase et al (1978) Nucl. Inst. Meth. 154, 334	Fission chamber	8.22 $\pm$ 0.2

(D) Fission foils

Self-supported thin fission foils used in the photofission measurements were prepared [63] by the rolling technique. After rolling, the foils were shipped inside a vacuum chamber and then covered by a 100 $\mu g/cm^2$ layer of gold evaporated under vacuum to protect them from oxidation.

All foils were 50 mg/cm^2 thick and 5 × 5 cm in area. The uranium foils contained 99.28% of ^{238}U, the thorium foils 99.9% of ^{232}Th. Measurements of spontaneous fission have been carried out for all uranium foils by sandwiching them between polycarbonate films. No spontaneous fission was detected from the thorium foils.

(E) Experimental set-up and procedures used in data acquisition

The schematic diagram of the experimental arrangement for measuring the photofission cross sections is shown in Fig. 13. Sandwiches of Kimfol films and fission foils were located on a cylindrical lucite surface the axis of which coincided with the proton beam. The radius of the cylindrical surface was 5 cm. The gamma-ray attenuation resulting from the pile-up of foils in the sandwiches was $\sim$ 2% for the foil furthest from the proton beam. The photons were monitored by a 60 c.c Ge(Li) detector placed 14.7 cm away from the target at an angle of 90^{o} to the proton beam.

In order to preserve the correspondence between the position of the photofission fragment tracks on the film and the energies of the photons, the fission foils and the Kimfol films must be in close contact. Futhermore, because data were collected with many sandwiches, good alignment of all sandwiches was essential. Under present experimental conditions, the overall accuracy of the alignment is estimated to be within 1 mm.

Pulser signals accumulated together with the gamma-ray spectrum were stored simultaneously in a scaler to determine the dead time corrections. A separate analyzer taking the same spectrum was used to check the gamma-ray yield from time to time without disturbing the storage of the data. The procedure is very useful in monitoring not only the deterioration of the target but also the possible build-up of ^{19}F contamination. The typical life time of a target was about 10 hours at 100 μa. Target with high melting points (i.e. Mg, Si) can withstand high beam currents for a longer time.

(F) Data analysis

(1) Efficiency of the Ge(Li) detector

For determination of the photofission cross sections, it was necessary to measure the absolute efficiency of the Ge(Li) monitor.

For gamma-ray energies up to 3 MeV, the relative efficiency was determined by using a 10.8 μCi ^{56}Co source. The activity of this source is deposited in the center of a plastic disc 1.89 cm in diameter and 0.3 cm thick. Ten gamma-ray lines were chosen[64] to cover the range from 0.8 to 3.2 MeV. This source was placed in the position of the proton target for the efficiency measurements.

For higher energies, the two lines method[65] was employed, with several (p, γ) resonances with well known simple decay schemes furnishing the lines. The efficiency ratio ϵ for two gamma-rays, γ_1 and γ_2 is related to the ratio of their peak areas Y and their relative intensity I in the source, as follows:

$$\frac{\epsilon(\gamma_1)}{\epsilon(\gamma_2)} = \frac{Y(\gamma_1)}{Y(\gamma_2)} \frac{I(\gamma_2)}{I(\gamma_1)} \qquad (35)$$

Some properties of the (p, γ) reactions used are listed in Table 6. The gamma-rays emitted following capture generally have a non-isotropic angular distribution that can be represented by

$$W(\theta) = A_0 + A_2 P_2(\cos\theta) + A_4 P_4(\cos\theta) \qquad (36)$$

where $P_i(\cos\theta)$ are the Legendre polynomials and θ is the angle between the emitted photons and the proton beam. The coefficients A_i are normalized

TABLE 6

(p, γ) reactions used in FEP efficiency measurement.

E_{γ_1} MeV	E_{γ_2} MeV	Reaction	Proton energy keV	$I(\gamma_2)/I(\gamma_1)$
11.583	1.369	$^{23}Na(p, \gamma)$	1318	0.948 ± 0.013
8.926	2.753	$^{23}Na(p, \gamma)$	1417	1.042 ± 0.013
8.434	4.237	$^{23}Na(p, \gamma)$	1020	0.737 ± 0.021
7.706	2.837	$^{27}Al(p, \gamma)$	767	0.999 ± 0.010
6.577	4.496	$^{27}Al(p, \gamma)$	1317	0.920 ± 0.045

to $A_o = 1$. Because of the small A_4 values the branching ratios were determined by Singh et al[66] at $\theta = 55^o$ where $P_2(\cos 55^o) = 0$. In order to fit into our experimental geometry, the intensity ratios $I(\gamma_1)/I(\gamma_2)$ were calculated for 90^o. The (p, γ) targets in the form of NaCl and pure aluminum were evaporated under vacuum on a 0.2 mm thick Ta backing. Pulser signals accumulated together with the Ge(Li) spectrum were used to determine the dead-time corrections. The relative efficiency for counting under the full energy peak (FEP) is plotted as a function of the gamma-ray energy in Fig. 21.

The absolute efficiency was determined by using a ^{60}Co source. Its activity was measured by the National Bureau of Standards as 2.79×10^5 dps (August 1966). The measured efficiency ϵ_{abs} at the 1.33 MeV peak was $\epsilon_{abs}(1.33) = 1.43 \times 10^{-4}$. The absolute efficiency $\epsilon_{abs}(E_\gamma)$ can be calculated from the FEP relative efficiency, $\epsilon_{rel}(E_\gamma)$ which is obtained from the graph, from the following expression:

$$\epsilon_{abs}(E_\gamma) = \frac{\epsilon_{abs}(1.33)}{\epsilon_{rel}(1.33)} \epsilon_{rel}(E_\gamma) \qquad (37)$$

The total gamma-ray intensity $I(E_\gamma)$ emitted from the target at a given (p, γ) resonance is related to the FEP counts $Y_o(E_\gamma)$ recorded by the Ge(Li) detector by

$$I(E_\gamma) = \frac{1}{\epsilon_{abs}(E_\gamma)} Y_o(E_\gamma) \qquad (38)$$

(2) Fission counts

As described previously, the fragments emitted from the fission foils were detected by the Kimfol films. These films were etched and sparked to reveal the tracks. The gamma-rays emitted from a (p, γ) reaction are Doppler-shifted. Therefore, by finding the counting rate of the tracks as

Fig. 21: The relative FEP efficiency of the Ge(Li) detector as a function of the gamma ray energy.

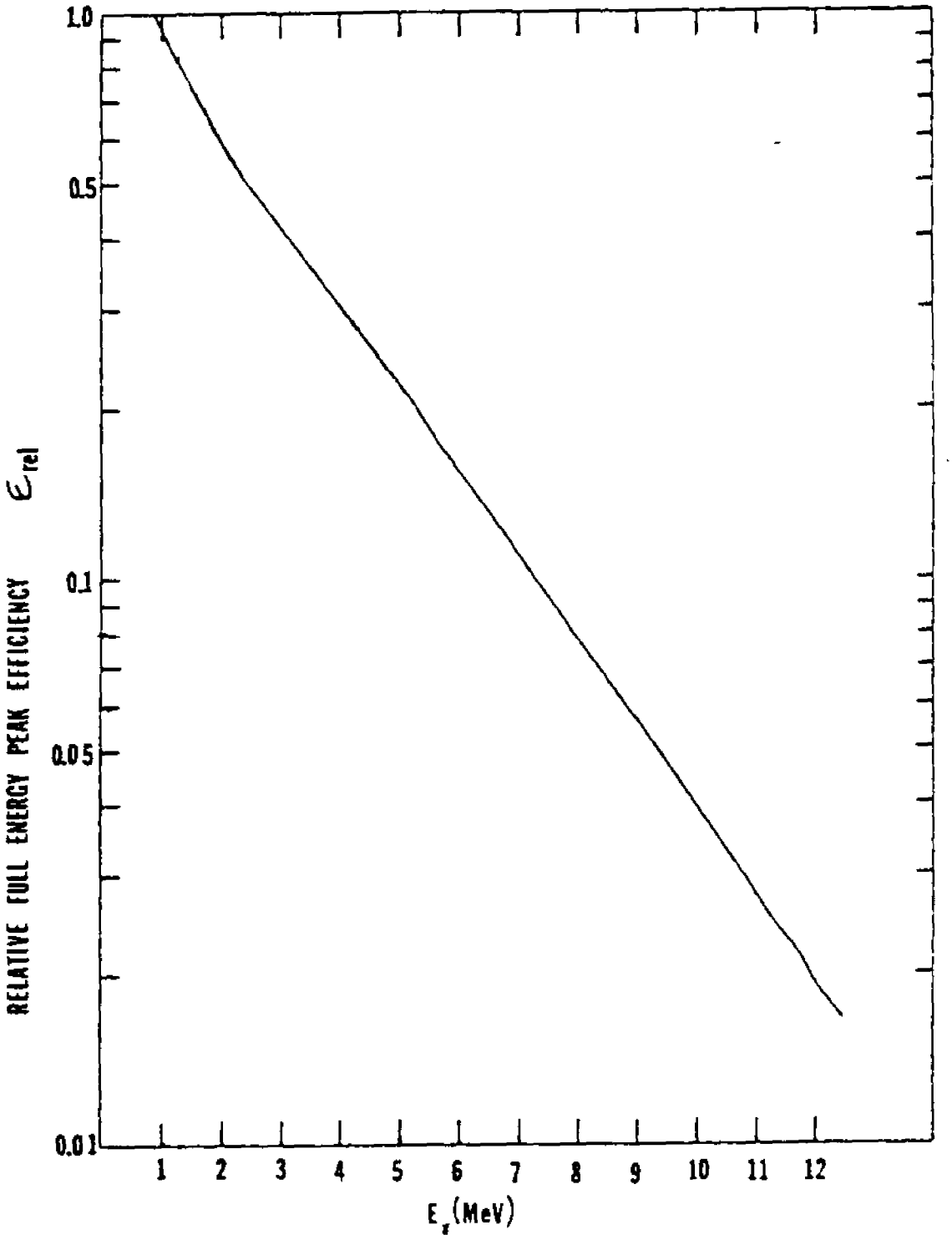
1.0
0.5
0.1
0.05
0.01
RELATIVE FULL ENERGY PEAK EFFICIENCY ϵ_{rel}
1
2
3
4
5
6
7
8
9
10
11
12
E_γ(MeV)

a function of their position along the axis of the proton beam the photofission cross sections as a function of the excitation energy can be determined.

For counting purposes the films were placed on a lucite plate whose surface was precisely divided into sections corresponding to equal energy intervals. This scale was different for each (p, γ) resonance. An example of a developed film superimposed on an energy scale is shown in Fig. 22. The fission fragments recorded in this film were produced by the 8.92 MeV photons from the 1417 keV resonance in the $^{23}Na(p, \gamma)$ reaction. The sections formed by the parallel lines correspond to energy intervals of 400 eV. For the 11 resonances used in these measurements three different sets of energy intervals were employed according to the photon energy E_γ: (1) 300 eV for $E_\gamma < 7$ MeV, (2) 400 eV for 7 MeV $< E_\gamma <$ 11 MeV, (3) 500 eV for $E_\gamma >$ 11 MeV.

The obtained fission counts are subject to corrections arising from various factors. The major correction in ^{238}U comes from spontaneous fission, which could amount to about 25 — 40% of the photofission counts, depending on the intensity of the gamma-rays. The spontaneous fission was also scanned in sections as described before. No spontaneous fission was observed in the case of thorium as expected.

(3) Determination of the cross sections

Because the fission foils used in all the measurements are thick, the fragments emerging from different depths in the foils have different kinetic energies as they enter the Kimfol films. Thus their detection efficiency is different. For this reason we have to consider separately the fission counts caused by fragments coming from different layers of the fission foil (Fig. 23). With this picture in mind the photofission cross section $\sigma_{\gamma f}(E_\gamma)$ is related to the fission counts as follows:

Fig. 22: A developed film superimposed on an energy scale for the 8.92 MeV photons from the 1417 keV resonance in the $^{23}Na(p, \gamma)$ reaction

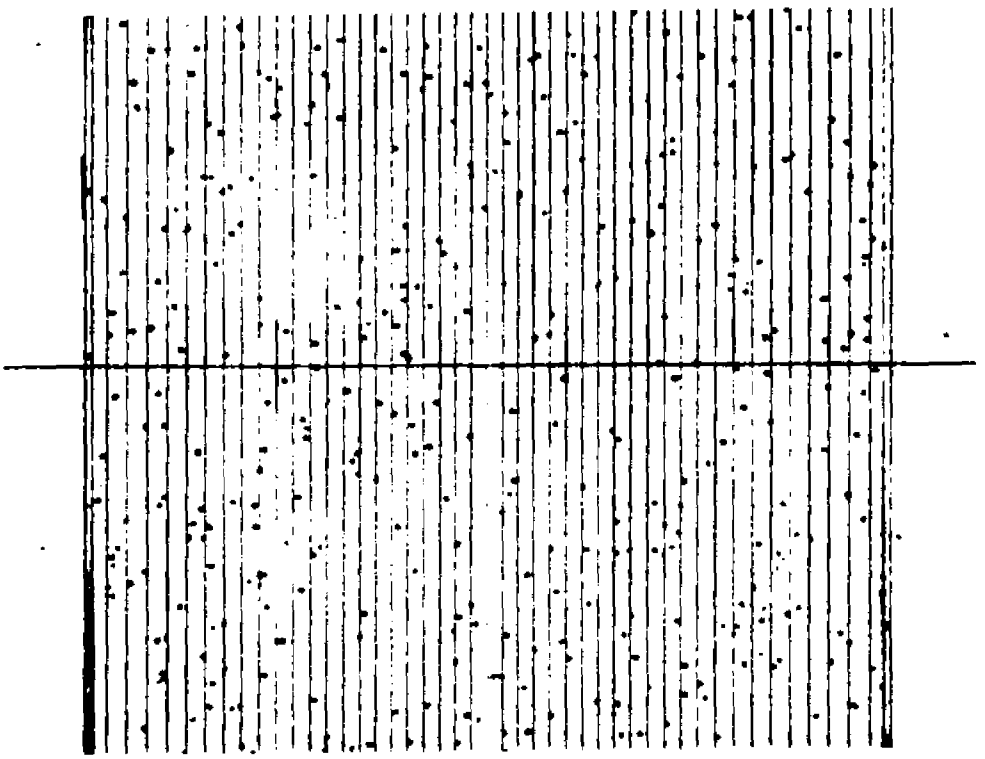

Fig. 23: Detection of photofission fragments produced by photons of energy $E_{\gamma}(\theta_k)$ in layer j of the fission foil.

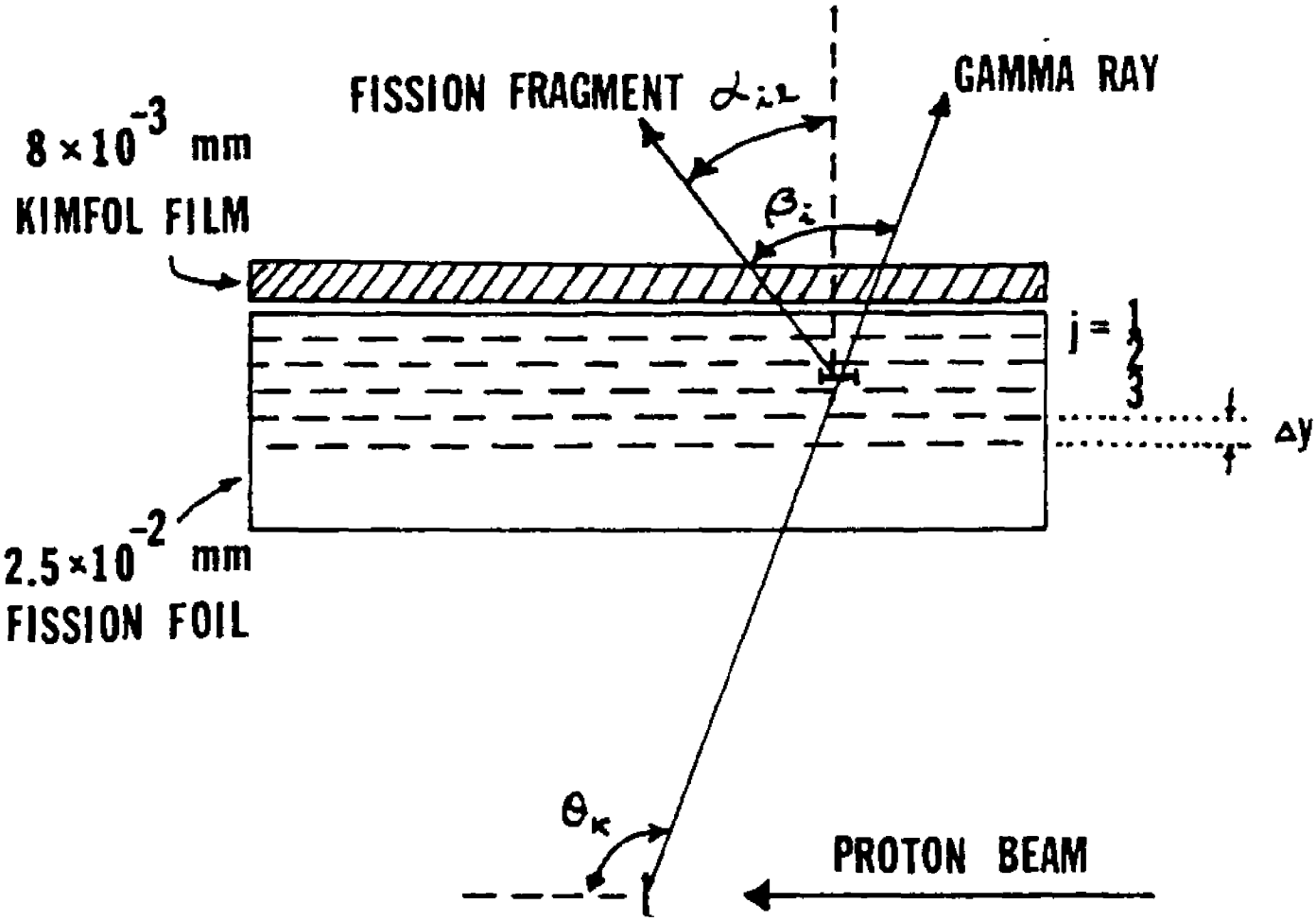
FISSION FRAGMENT α_{i2}
GAMMA RAY
8×10^{-3} mm
KIMFOL FILM
β_i
j = 1
2
3
Δy
2.5×10^{-2} mm
FISSION FOIL
θ_K
PROTON BEAM

$$N_f(E_\gamma) = 2\,C\,I(E_\gamma,\theta_k)\,\sigma_{\gamma f}(E_\gamma)\,n\Delta Y \sum \eta(j,\theta_k) \qquad (39)$$

where $N_f(E_\gamma)$ is the number of fissions occurring in the foils at a photon energy E_γ, C is a solid angle correction, $I(E_\gamma, \theta_k)$ is the number of photons of energy E_γ incident on the foil at angle θ_k, $n\Delta y$ is the effective number of fissioning nuclei, and $\eta(j, \theta_k)$ is the total detection efficiency of a fragment produced at layer j by a photon emitted at angle θ_k. The factor 2 appearing in front of eq. (39) accounts for the two fission fragments per fission event.

As described earier, the fission tracks are counted in sections having equal energy intervals. For a section of width $\Delta\ell(\theta_k)$ and length S the solid angle C is given by

$$C = \frac{S\,\Delta\ell(\theta_k)\,\cos(90^\circ - \theta_k)}{4\pi\,\gamma(\theta_k)^2} \qquad (40)$$

where $\gamma(\theta_k)$ is the distance from the proton target to the fission foil. For a given θ_k we have assumed a constant $\gamma(\theta_k)$ value and ignored the small differences for various j layers. The intensity of photons $I(E_\gamma, \theta_k)$ incident on the foil can be written as

$$I(E_\gamma, \theta_k) = I(E_\gamma)\,\omega(\theta_k)\,e^{-\mu x} \qquad (41)$$

where $W(\theta_k)$ is the gamma-ray angular distribution as defined in eq. (25). The intensity of photons emitted from the target $I(E_\gamma)$ was obtained with the help of the absolute efficiency curve for the Ge(Li) detector. The last term accounts for the gamma-ray attenuation on its way from the target chamber to layer j.

The efficiency $\eta(j, \theta_k)$ is given by

$$\eta(j,\theta_k) = \sum_{i,\ell} F(\beta_i)\,\Omega(j,\alpha_{i\ell})\,\sin\beta_i\,\Delta\beta_i\,\Delta\phi_\ell \qquad (42)$$

where $F(\beta_i)$ is the angular distribution of the fission fragments relative to the direction of the gamma-rays and $\Omega(j, \alpha_{i\ell})$ is the efficiency of the Kimfol film for detecting a fragment emitted from layer j at an angle $\alpha_{i\ell}$. For the angular distribution of the fission fragments $F(\beta_i)$, we have used eq. (25) in chapter II with the coefficients taken from Rabotnov et al[42]. The efficiency $\Omega(j, \alpha_{i\ell})$ is obtained experimentally as described in section C of this chapter. The four angles θ, β, α, and ϕ are related by

$$\cos\alpha_{i\ell} = \cos\beta_i \sin\theta_k - \cos\theta_k \sin\beta_i \sin\phi_\ell \qquad (43)$$

This can be seen from Fig.23. With the help of eqs. (40) through (43), we can obtain the photofission cross section $\sigma_{\gamma f}(E_\gamma)$ from eq. (39). A FORTRAN program has been written to do the calculation. The results and the discussion are presented in the next chapter.

IV RESULTS AND CONCLUSIONS

(A) Introduction

The photofission measurements have been carried out on ^{238}U and ^{232}Th over an energy range from 5.8 to 11.5 MeV. In the near threshold region an attempt was made to measure intermediate structure associated with the class II levels at various excitation energies. The typical resolution of the photon beams from a sharp (p, γ) resonance in our experimental set-up is a few hundred eV. The calculated class I level spacing at 6 MeV excitation is 11 eV[8]. Therefore, it was expected that the observed cross section will be averaged over the strongly fluctuating class I levels but show structure resulting from class II states, the average spacing[67] of which is expected to be 1.2 keV for ^{238}U and 5 keV for ^{232}Th at 6 MeV.

Absolute photofission cross sections have been measured by many groups using various methods. However, the results are only in qualitative agreement near threshold and differ markedly at higher energies. Additional measurements are therefore necessary.

In this chapter, we will first present the results of the photofission cross sections measurements. A detailed discussion and interpretation of the cross sections follows and suggestions for the extension of this work are presented.

The high intensity photon beams which we have been using to investigate photofission can also be employed for studying other photon induced processes. At the early stage of the photofission studies, we have used $^{19}F(p, \alpha\gamma)^{16}O$ to generate intense photon beams for the

purpose of testing the feasibility of the photofission measurements. At the same time, these photon beams were used to measure resonance scattering of gamma-rays from ^{208}Pb. The results of these measurements constitute the last part of this chapter.

(B). Photofission in ^{238}U and ^{232}Th

(1) Cross sections

The fission spectra $N_f(E_\gamma)$ at each proton resonance have been formed as described in the previous chapter. The spectra were corrected for background and contributions caused by the presence in the gamma-ray spectrum of weak lines with energies different from E_γ.

The background corrections were determined in off resonance runs and were found to be caused practically entirely by spontaneous fission in the case of ^{238}U. In the case of ^{232}Th these corrections were found to be negligible.

The photofission counts produced by the unwanted gamma-rays are small for all the resonances used in these studies. Their contribution to the photofission cross section can be estimated as follows: For a given (p, γ) resonance the total photofission counting rate N(tot) is caused by the chosen gamma-rays as well as the unwanted gamma-rays of energy E_{γ_i}.

$$N(tot) = const.\left(I_\gamma \sigma_{\gamma f}(E_\gamma) + \sum_i I_{\gamma_i} \sigma_{\gamma f}(E_{\gamma_i})\right) \qquad (44)$$

where I and $\sigma_{\gamma f}$ are the photon intensity and the photofission cross section respectively. The observed photofission cross section is calculated from N(tot)

$$\sigma_{\gamma f}^{obs}(E_\gamma) = N(tot)/const.\ I_\gamma \qquad (45)$$

$$= \sigma_{\gamma f}(E_\gamma) + \sum_i \frac{I_{\gamma_i}}{I_\gamma} \sigma_{\gamma f}(E_{\gamma_i}) \qquad (46)$$

Thus the actual photofission cross section $\sigma_{\gamma f}$ is obtained from

$$\sigma_{\gamma f}(E_\gamma) = \sigma_{\gamma f}^{obs}(E_\gamma) - \sum_i \frac{I_{\gamma_i}}{I_\gamma} \sigma_{\gamma f}(E_{\gamma_i}) \qquad (47)$$

In Table 7 we have listed the ratio of I_{γ_i}/I_γ for each resonance. The total correction to $\sigma_{\gamma f}^{obs}$ does not exceed 10% for any of the cases. The values of $\sigma_{\gamma f}(E_{\gamma_i})$ are taken from Caldwell et al[9].

The photofission cross sections of ^{238}U are plotted in Fig. 24 (a), (b), and (c) as a function of the gamma-ray energy for each resonance. The energy resolution is different for every spectrum, however its typical value varies from about 300 eV in the middle to 900 eV at the edge. The pronounced dip in the middle of each spectrum is the result of attenuation of the gamma-rays in the Ta backing of the proton target. The spectrum obtained at the 1701 keV proton resonance in ^{25}Mg exhibits indications of structure which may be due to the class II states in ^{238}U; however the statistical accuracy of the data is insufficient to claim this with confidence.

In contrast to the subbarrier region, the photofission spectra at higher energies are practicely flat and show no structure. The possible dips occurring at several energies e.g. in U at 8925 and 8927 keV could be somewhat surprising. If they are not due to statistics then a possible explanation would be that they correspond to sharp peaks in the (γ,n) cross section and are therefore due to neutron competition. They could also be caused by a concentration of 1^-, K = 0 and/or 2^+, K = 2 strength which is characterized by an angular distribution which favors emission of fragments in the direction perpendicular to the gamma-rays.

TABLE 7

Intensities of unwanted gamma rays

E_γ MeV	E_{γ_i} (I_{γ_i}/I_γ) MeV (%)
5.871	7.50 (5%), 6.13 (3.5%)
6.180	6.85 (3.4%)
6.879	7.336 (0.25%), 9.016 (0.25%)
7.373	6.402 (7%), 6.232 (0.1%)
7.354	5.884 (1.4%), 5.594 (6.2%)
8.245	6.975 (0.9%), 6.015 (4%)
8.727	6.497 (5.8%), 5.597 (3.5%)
8.923	11.673 (0.5%), 9.09 (1%), 7.81 (1.6%)
9.981	8.011 (1%), 6.13 (0.8%)
10.761	12.541 (0.02%), 7.931 (5.7%), 6.02 (4%)
11.540	13.32 (0.3%)

Fig. 24: Photofission cross sections $\sigma_{\gamma f}$ measured for ^{238}U as a function of excitation energy E_γ.

(a) 5.8 MeV $\leq E_\gamma \leq$ 6.9 MeV.

(b) 7.3 MeV $\leq E_\gamma \leq$ 8.8 MeV.

(c) 8.9 MeV $\leq E_\gamma \leq$ 11.6 MeV.

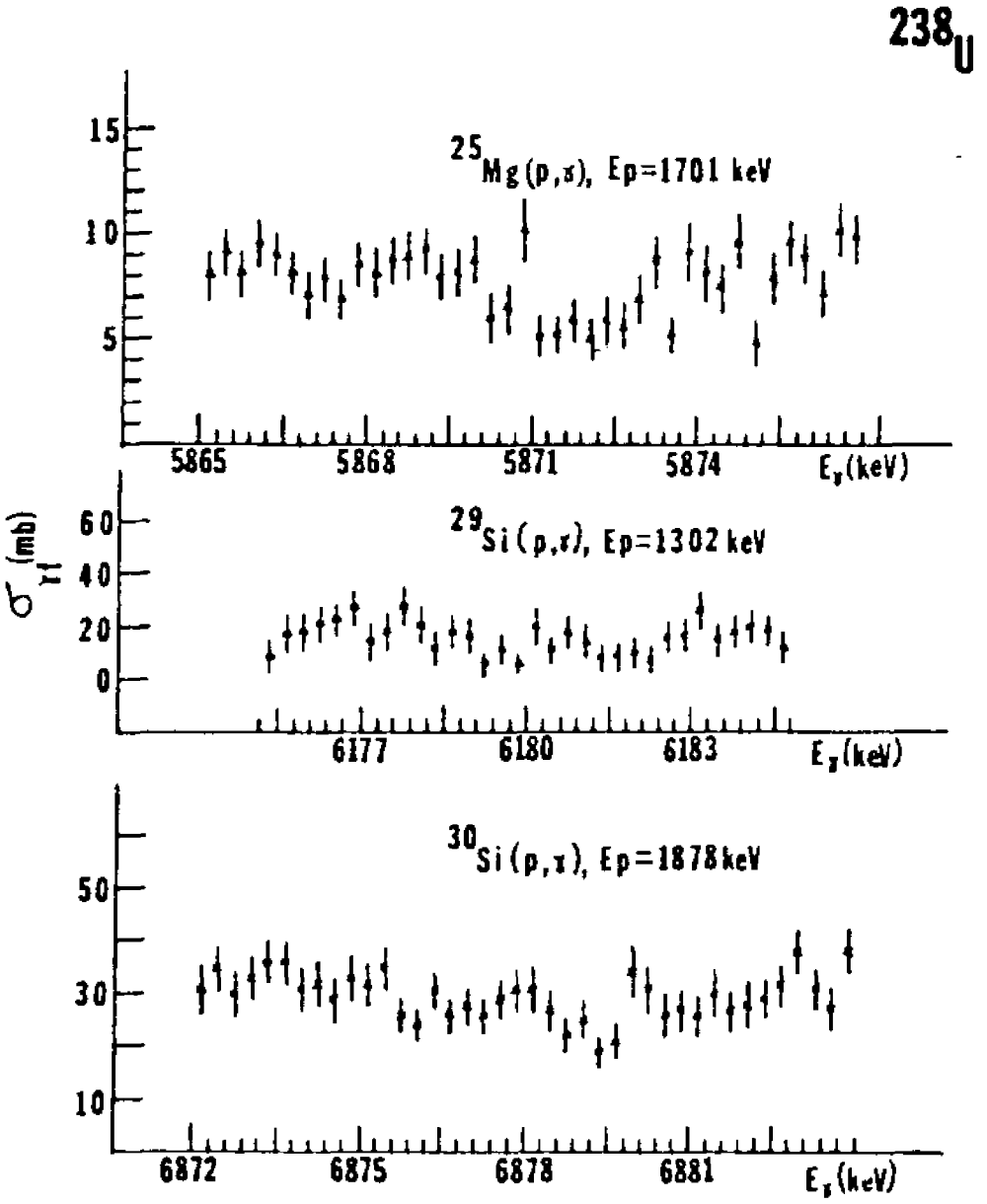
238U
25Mg(p,x), Ep=1701 keV
29Si(p,x), Ep=1302 keV
30Si(p,x), Ep=1878keV
σγ (mb)
Eγ(keV)
5865
5868
5871
5874
6177
6180
6183
6872
6875
6878
6881

(a)

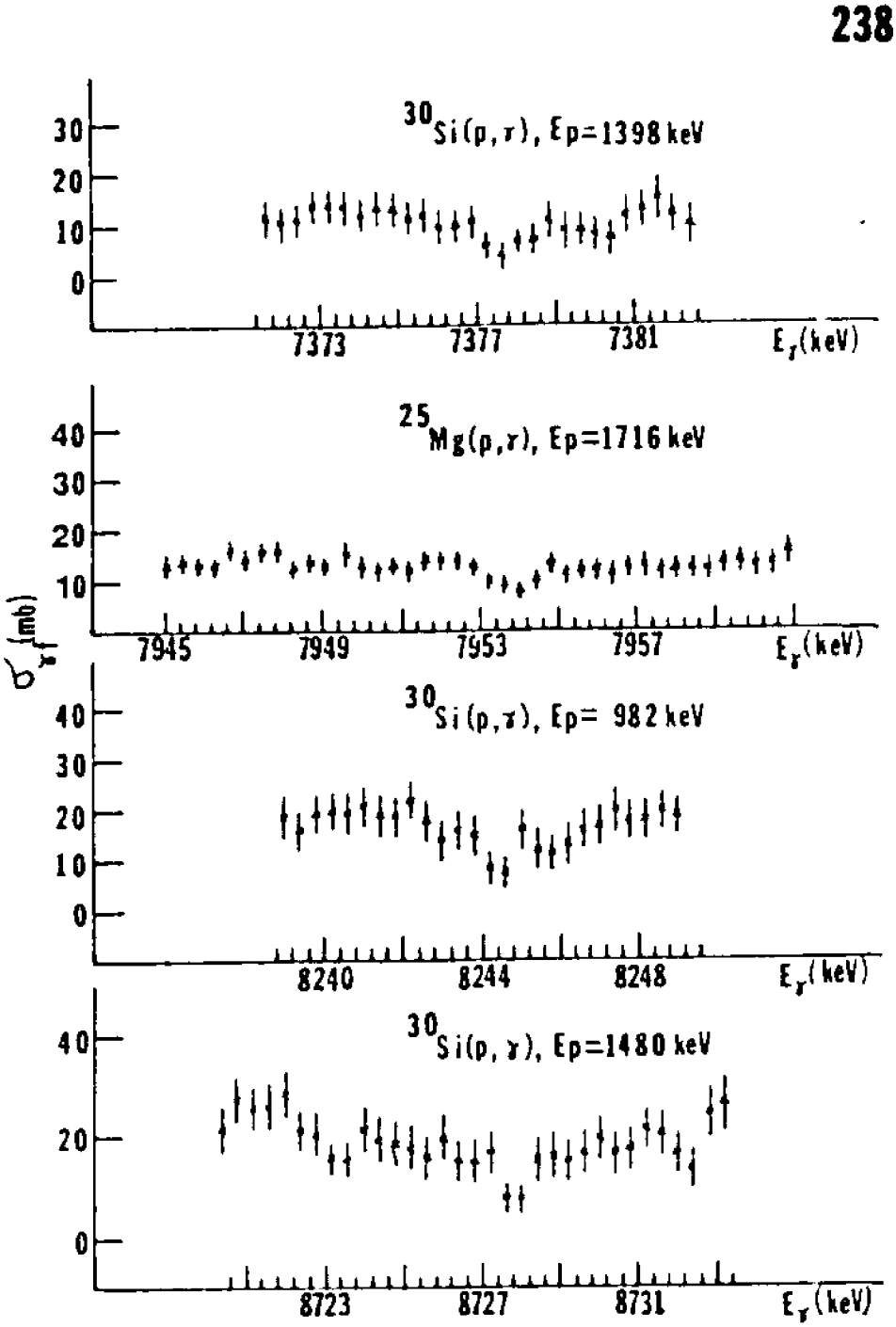
238U
30Si(p,γ), Ep=1398 keV
25Mg(p,γ), Ep=1716 keV
30Si(p,γ), Ep= 982 keV
30Si(p,γ), Ep=1480 keV
σγf (mb)
Eγ(keV)
7373
7377
7381
7945
7949
7953
7957
8240
8244
8248
8723
8727
8731

(b)

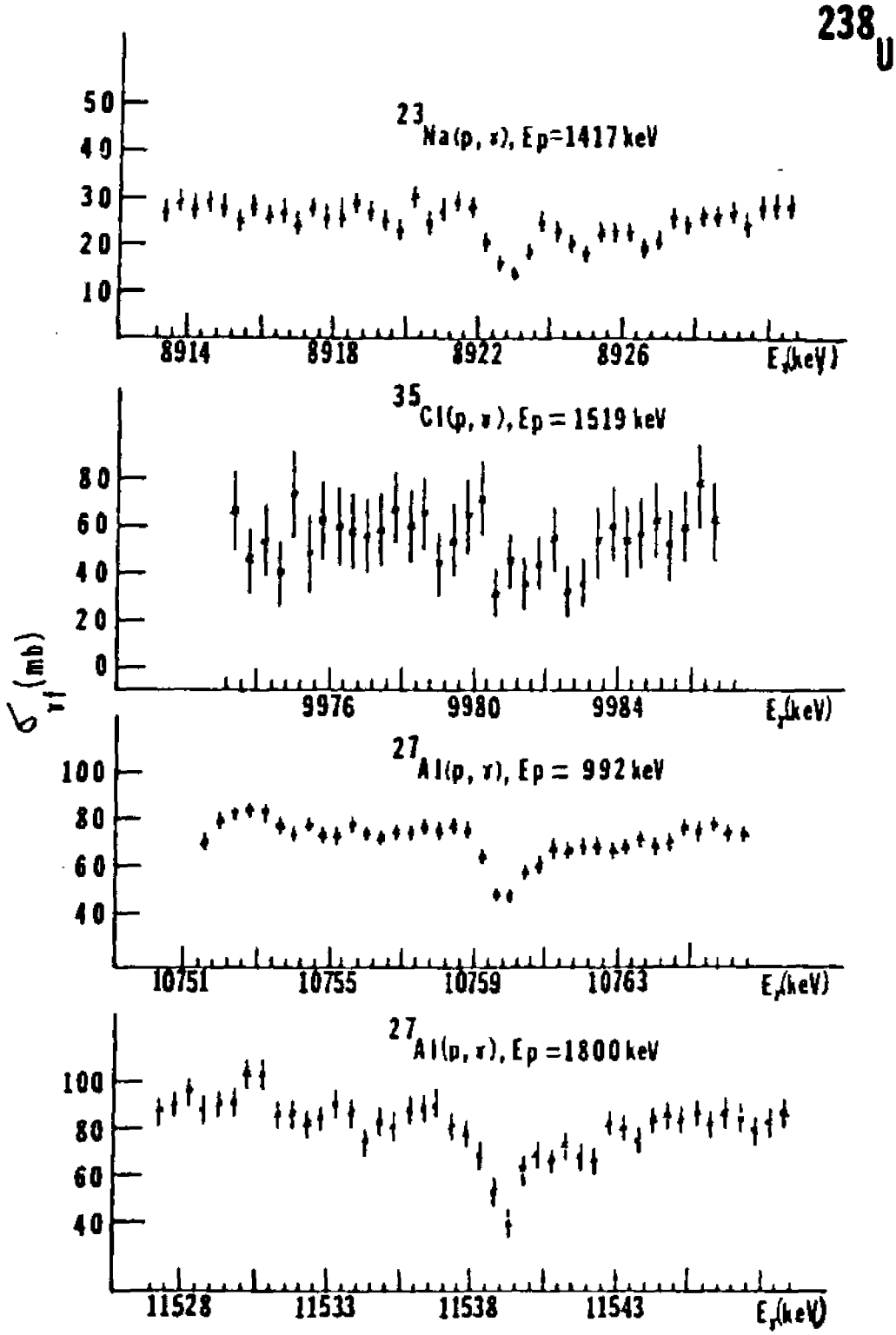
238U
23Na(p, γ), Ep=1417 keV
35Cl(p, γ), Ep = 1519 keV
27Al(p, γ), Ep = 992 keV
27Al(p, γ), Ep = 1800 keV
σγi (mb)
Eγ(keV)

(C)

The photofission cross sections averaged over the spectra obtained for each (p, γ) resonance with the part containing the dip excluded are listed in Table 8. The results of other experiments are given for comparison. Good agreement can be seen with the results of Caldwell et al[9] and Veyssiere et al[39] at $E_\gamma > 7$ MeV. At lower energies our values are higher than those of other groups. The closest to our results at 5.87 and 6.18 MeV are the values reported by Lindgren et al[35] and Dickey and Axel[5] respectively. It should be noted that in this energy region the energy resolution of the gamma-rays may significantly affect the values of the average photofission cross sections. The high value at 5.87 MeV may indicate a resonance at this energy in the second well of the barrier. The peak at 6.18 MeV is interpreted as due to the onset of neutron competition. Huizenga et al[41] determined the photofission cross section at 6.13 MeV using the $^{19}F(p, \alpha\gamma)^{16}O$ reaction as a source of gamma-rays. The value obtained was 13 ± 4 mb which is close to our result. The energy spread of the 6.13 MeV line is $\sim$15 eV.

The result at 6.87 MeV is surprisingly high and may indicate a concentration of strength characterized by an angular distribution of photofission fragments which favor a forward angle relative to the gamma-rays.

The ^{232}Th cross sections are plotted in Fig. 25 (a)—(c) for each of the (p, γ) resonances. Again the dip occurring in the middle is the result of attenuation of the gamma-rays in the Ta backing. In the 5.87 MeV spectrum two statistically significant peaks appear at 5866 and 5868 keV. Both peaks are 600 eV wide and are separated by about 2 keV. the calculated level spacing[67] of class II states at this energy is about 15 keV. A significant increase in the cross section is also observed at about

TABLE 8

$\sigma_{\gamma f}$(mb) for $^{238}U(\gamma, f)$

E MeV	Lindgren et al ref. 35	Dickey axel ref. 5	Veyssiere et al ref. 39	Mafra et al ref. 6	Yester et al ref. 40	Khan Knowles ref. 3	Manfredini et al ref. 7	Caldwell et al ref. 9	This work
5.868	6.4	$3.2^{+}_{-}0.5$			$3.0^{+}_{-}0.5$	$1.7^{+}_{-}0.4$		$4.5^{+}_{-}0.5$	$8.2^{+}_{-}0.2$
6.177	9.2	$11.4^{+}_{-}0.7$			$5.3^{+}_{-}0.6$	$6.05^{+}_{-}0.4$		$8.2^{+}_{-}0.5$	$16.2^{+}_{-}1.0$
6.875		$10.4^{+}_{-}0.6$		$1.9^{+}_{-}0.2$	$4.8^{+}_{-}0.6$	$6.5^{+}_{-}0.5$	$2.73^{+}_{-}0.32$	$10.4^{+}_{-}0.5$	$31.1^{+}_{-}0.7$
7.374		$10.1^{+}_{-}0.7$		$10.2^{+}_{-}1.1$	$8.0^{+}_{-}0.6$	$8.1^{+}_{-}0.5$	$12.0^{+}_{-}1.6$	$11.8^{+}_{-}1.0$	$11.7^{+}_{-}0.7$
7.949			$17^{+}_{-}2$	$14.3^{+}_{-}1.5$	$8.2^{+}_{-}0.5$	$16.5^{+}_{-}0.5$	$18.9^{+}_{-}6.7$	$16.9^{+}_{-}1.0$	$14.1^{+}_{-}0.2$
8.241			$22^{+}_{-}2$					$18.5^{+}_{-}1.0$	$18.5^{+}_{-}0.8$
8.724			$24^{+}_{-}2$					25	$20.7^{+}_{-}0.7$
8.918			$30^{+}_{-}2$	$37^{+}_{-}1.1$			$29^{+}_{-}1.8$	27	$26.6^{+}_{-}0.3$
9.976			$54.5^{+}_{-}5$					69	$58.4^{+}_{-}3.0$
10.755			$86^{+}_{-}7$					95	$76.5^{+}_{-}0.5$
11.533			$91^{+}_{-}7$					100	$88.3^{+}_{-}0.9$

Fig. 25: Photofission cross sections $\sigma_{\gamma f}$ measured for ^{232}Th as a function of excitation energy E_γ.

(a) 5.8 MeV $\lesssim E_\gamma \lesssim$ 6.9 MeV.

(b) 7.3 MeV $\lesssim E_\gamma \lesssim$ 8.8 MeV.

(c) 8.9 MeV $\lesssim E_\gamma \lesssim$ 11.6 MeV.

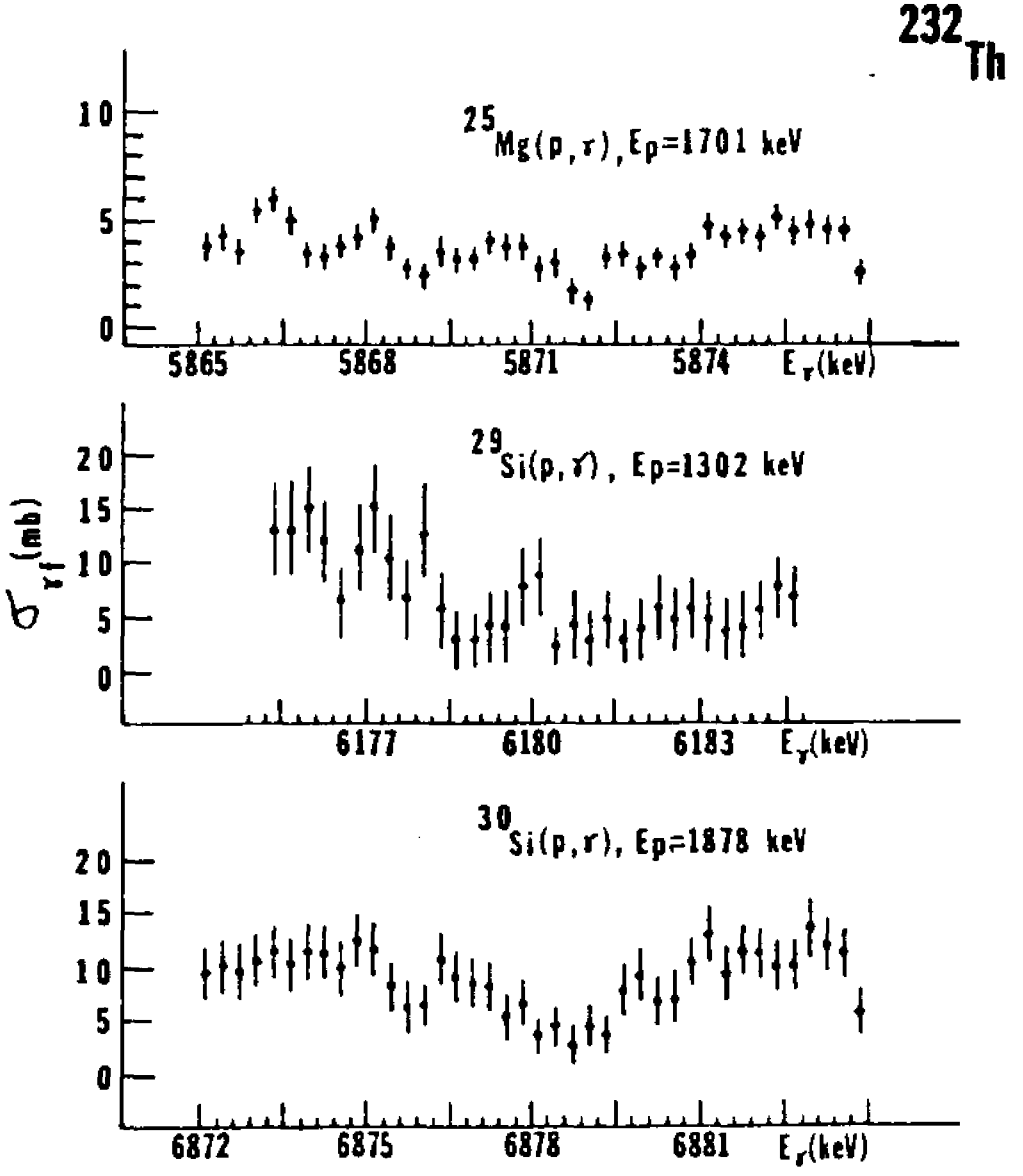
232Th
25Mg(p,γ), Ep=1701 keV
29Si(p,γ), Ep=1302 keV
30Si(p,γ), Ep=1878 keV
σγf (mb)
Eγ(keV)
5865
5868
5871
5874
6177
6180
6183
6872
6875
6878
6881

(a)

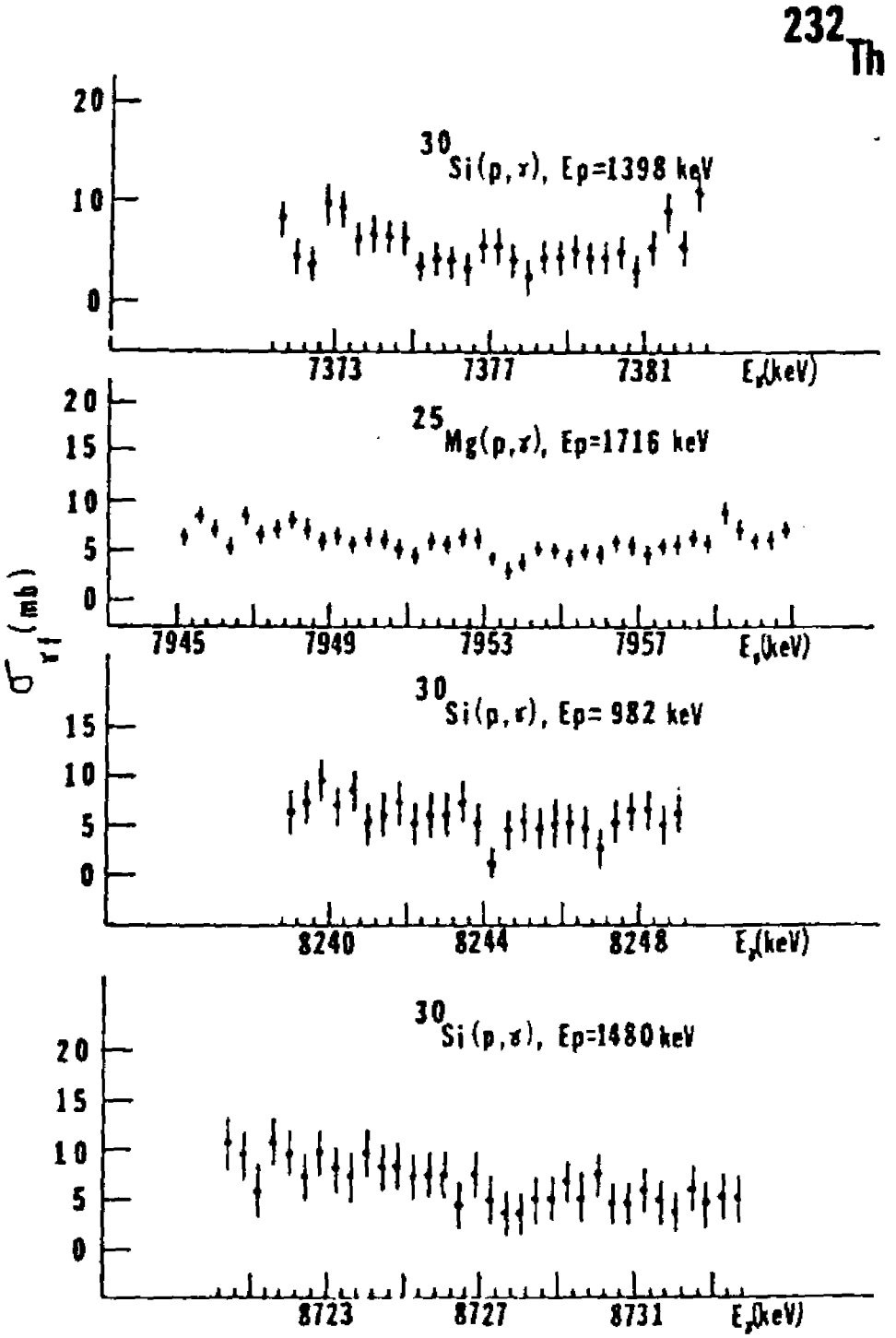
232Th
30Si(p,γ), Ep=1398 keV
25Mg(p,γ), Ep=1716 keV
30Si(p,γ), Ep= 982 keV
30Si(p,γ), Ep=1480 keV
σγf (mb)
Eγ(keV)

(b)

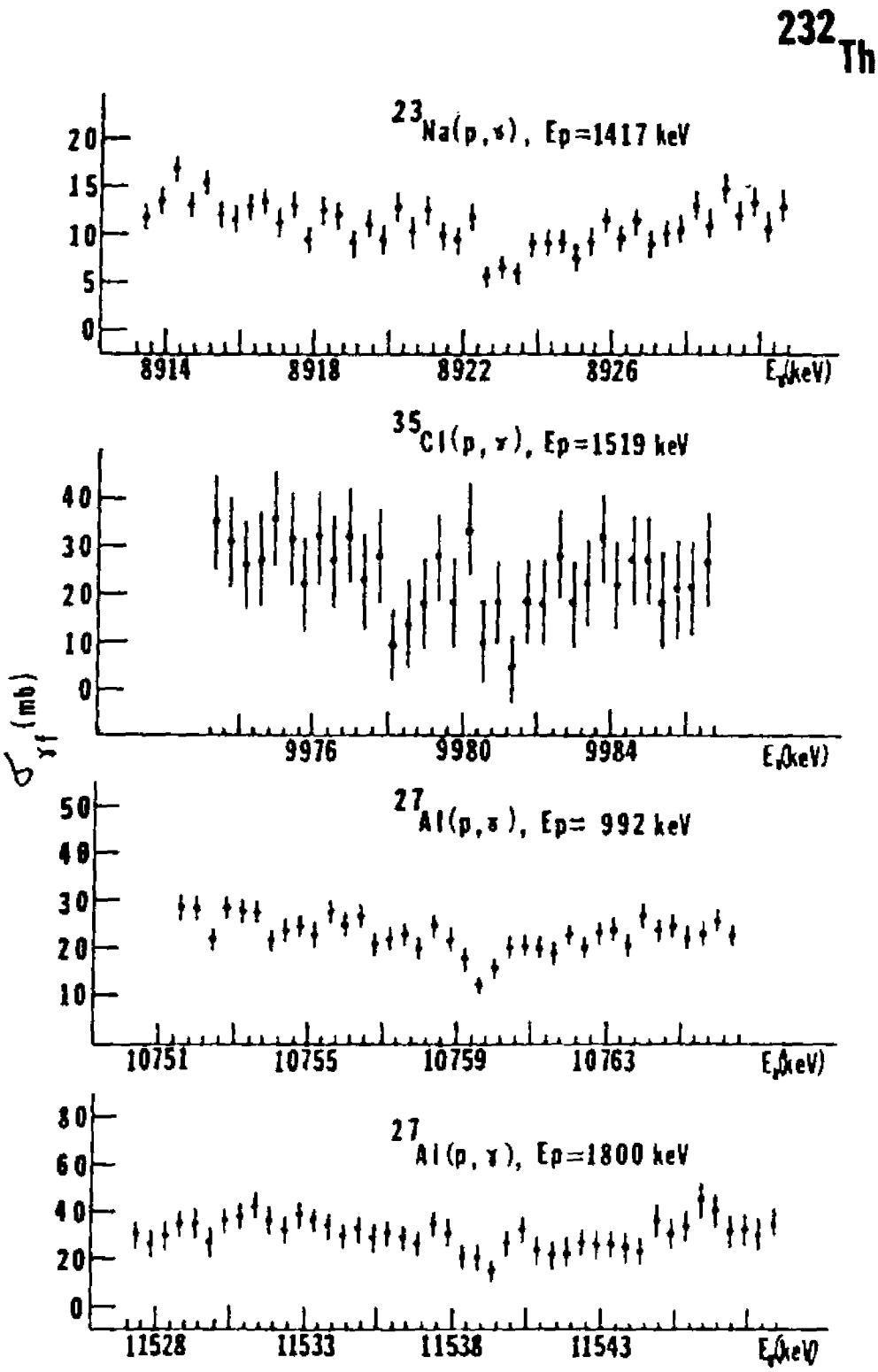
232Th
23Na(p,γ), Ep=1417 keV
35Cl(p,γ), Ep=1519 keV
27Al(p,γ), Ep= 992 keV
27Al(p,γ), Ep=1800 keV
σγf (mb)
Eγ(keV)

(C)

6177 keV covering a region of at least 3 keV. The other spectra exhibit no structure apart from statistical fluctuations. The average cross sections obtained from all (p, γ) resonances are listed in Table 9. Between 6 and 9 MeV, our results are in close agreement with those of Caldwell et al and Dickey and Axel. The results of Knowles et al[3] and Yester et al[4] are either too low or too high except at 7.3 MeV. The fact that at 5.87 MeV our cross section is higher than the others may, as in the case of ^{238}U, indicated the presence of a resonance at this excitation energy. At higher energies, the only available results are from Saclay and they are all smaller than ours except at 10.76 MeV. Again the cross sections of Huizenga et al of $\sigma_{\gamma f}$(6.13 MeV) = 9$\pm$3 mb and $\sigma_{\gamma f}$(7 MeV) = 9$\pm$3 mb are comparable to $\sigma_{\gamma f}$(6.18 MeV) = 8.7$\pm$0.7 mb and $\sigma_{\gamma f}$(7.37 MeV) = 5.6$\pm$0.4 mb respectively.

In conclusion, the photofission cross section near threshold is a non-monotonic function of energy. Our averaged photofission cross sections are in good agreement with those of Caldwell et al and Dickey et al as shown in Fig. 26 and 27 for ^{238}U and ^{232}Th respectively.

(2) Fission probability

In this section our measured photofission cross sections will be used to determine the fission probability. The results are fitted to the theoretical values given by the expression for P_f discussed in chapter II. Our aim is to obtain the fission barrier parameters. Of course, it is impossible to determine all the barrier parameters from our limited experimental data. The theoretical values of P_f are strongly affected by the variation of some of the parameters and quite insensitive to the change of others[20].

TABLE 9

$\sigma_{\gamma f}$ (mb) for ^{232}Th(γ,f)

E MeV	Dickey Axel ref. 5	Veyssiere et al ref. 39	Mafra et al ref. 6	Yester et al ref. 4	Khan Knowler ref. 3	Manfredini et al ref. 7	Caldwell et al ref. 9	This work
5.868	1.5±1.2			2.5±0.5	1.7±0.5		2.5±0.25	3.9±0.1
6.177	10.0±1.6			7.2±0.5	7.5±0.5		8.5±0.5	8.7±0.7
6.875	6.3±1.1		2.0±0.2	3.8±0.5	3.0±0.5	2.4±0.25	7.7±0.5	9.5±0.4
7.374	7.9±1.2		2.9± 0.4	4.5±0.5	7.2±1.0	3.25±0.56	6.7±0.5	5.6±0.4
7.949	9.5±2.7		5.1±1.4	2.7±0.6	13.0±1.0	6.9±2.5	6.9±0.5	6.6±0.1
8.241					15.0±1.0		7.8±0.5	6.8±0.5
8.724							10.3±0.7	8.0±0.5
8.918		7.0±2.0	8.4±3.5			5.8±0.9	10.7±0.7	12.0±0.3
9.976		14.0±2.5						26.0±1.9
10.755		18.0±3						24.4±0.4
11.533		23.0±3.0						33.4±0.8

Fig. 26: Comparison of the measured photofission cross sections of ^{238}U with those of Caldwell et al (solid line) and Dickey et al (dashed line).

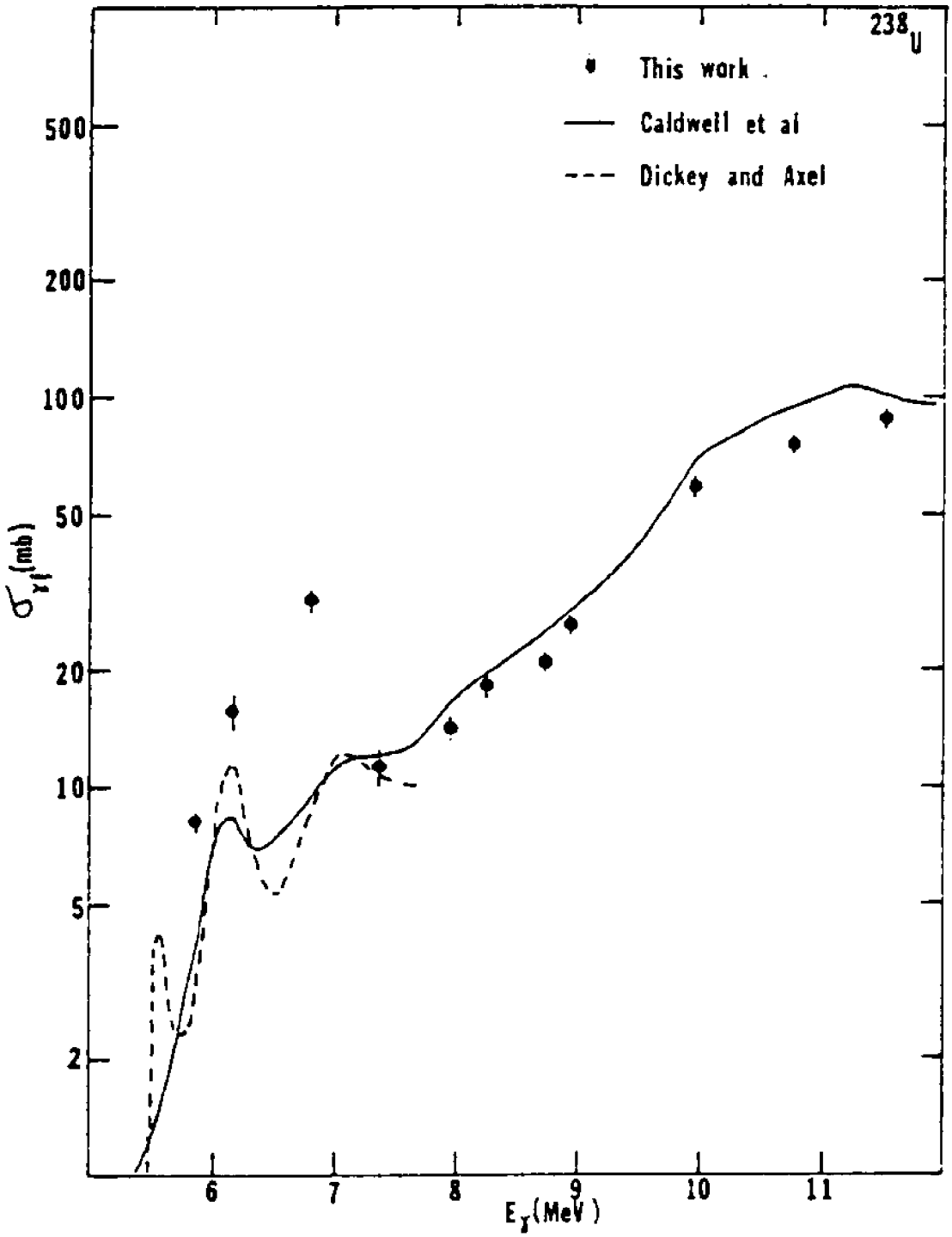
238U
This work
Caldwell et al
Dickey and Axel
500
200
100
50
20
10
5
2
$\sigma_{\gamma f}$(mb)
6
7
8
9
10
11
E_γ(MeV)

Fig. 27: Comparison of the measured fission cross sections of ^{232}Th with those of Caldwell et al (solid line), Dickey et al (dashed line), and Veyssiere et al (dotted line).

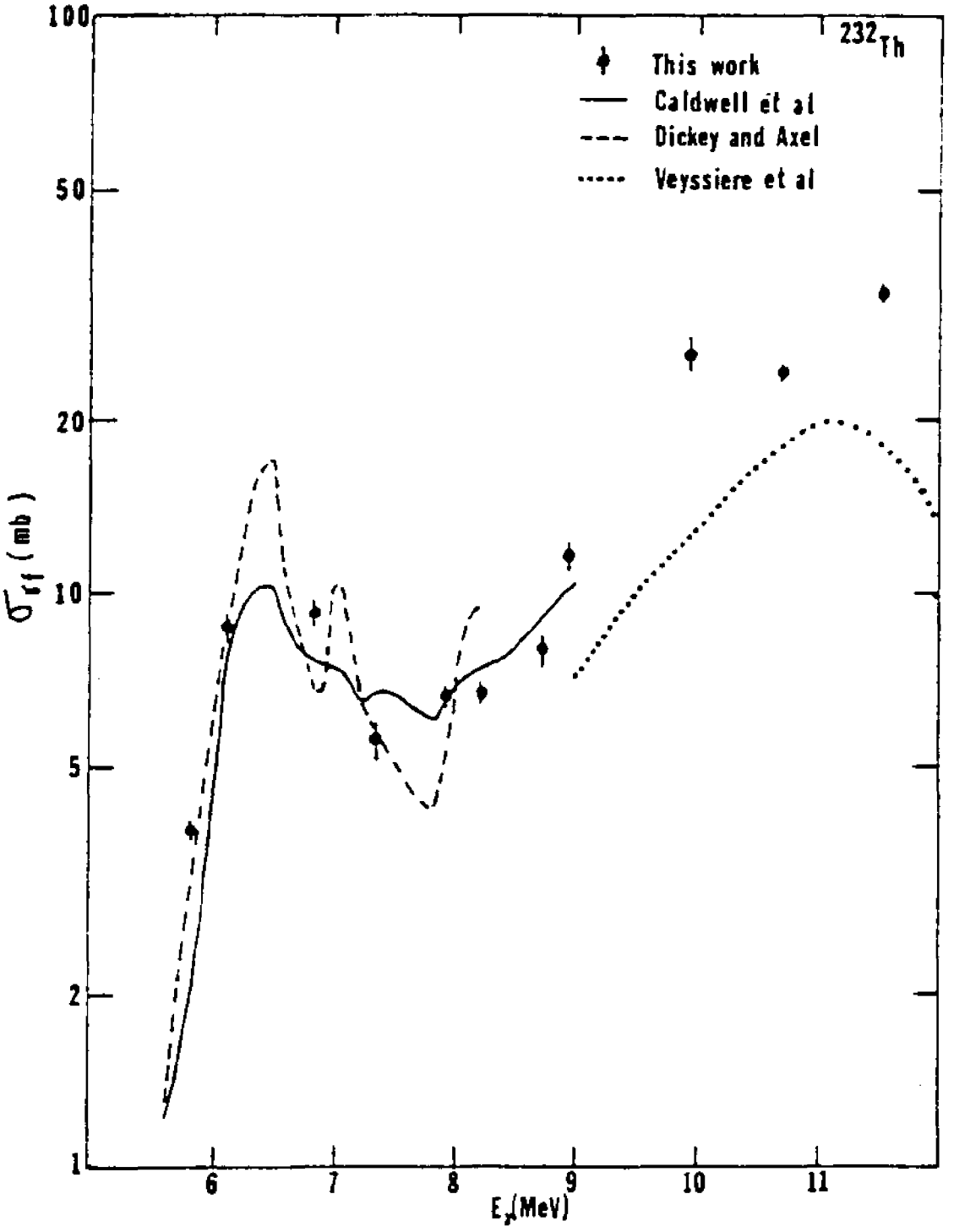
100
50
20
10
5
2
1
σ_{tf} (mb)
6
7
8
9
10
11
E_x(MeV)
^{232}Th
This work
Caldwell et al
Dickey and Axel
Veyssiere et al

Fission probability can be determined by dividing the fission cross section $\sigma_{\gamma f}$ by the total photoabsorption cross section σ_γ. The photoabsorption cross section σ_γ can be obtained by extrapolation from its value at the giant resonance. We have adopted the results of Veyssiere et al[39] in which $\sigma_\gamma = \sigma_{\gamma n} + \sigma_{\gamma f} + \sigma_{\gamma 2n}$ is fitted to the sum of two Lorentz lines

$$\sigma_\gamma = \sigma_1 \frac{(E\Gamma_1)^2}{(E^2-E_1^2)^2+(\Gamma_1 E)^2} + \sigma_2 \frac{(E\Gamma_2)^2}{(E^2-E_2^2)^2+(\Gamma_2 E)^2} \qquad (48)$$

The Lorentz line parameters $(E_1, \sigma_1, \Gamma_1; E_2, \sigma_2, \Gamma_2)$ are listed in ref.[39].

The theoretical expression for P_f is given by equation (16). For even-even nuclei, electric dipole (E1) excitation is dominant, although electric quadrupole (E2) excitation can also contribute. According to Huizenga et al[8] the quadrupole to dipole ratio $\sigma_\gamma(2^+)/\sigma_\gamma(1^-) = 0.02$ for gamma-rays of 7 MeV. Thus the population parameters are $\alpha = 0.98$ and 0.02 respectively for dipole 1^- and quadrupole 2^+ excitation.

The average fission width $\langle \Gamma_f \rangle$ is obtained from the sum of the fission transmission factors over all open fission channels and is given by equation (21). The N_d and N_{abs} are the direct transmitted and absorbed fluxes which are calculated exactly[68] under the assumption of the double-humped potential barrier. The increasing number of fission transition states above the pairing gap Δ allows us to replace the expression for N_A and N_B with integrals, for example,

$$N_A(EJ\pi) = \sum_\nu P_A^\nu(EJ\pi) + \int_\Delta^{E-E_A+2} \frac{\rho_A(\epsilon J\pi)\, d\epsilon}{1+\exp\left(\frac{2\pi}{\hbar\omega_A}(E_A+\epsilon-E)\right)} \qquad (49)$$

where $\rho_A(EJ\pi)$ is the density of transition states at the excitation energy ϵ above barrier A with spin J and parity π. In addition, the more

recent papers[21,69-72] from Los Alamos have shown that there exist two different paths to fission, corresponding to different nuclear shapes, at the second barrier in the Ra — U region. These two paths include one with a mass asymmetric shape and another, which has a higher potential energy, with a mass symmetric, axially asymmetric shape. The effect of this second outer barrier which we will designate barrier C is to provide more transition states so that

$$\langle \Gamma_f(EJ\pi)\rangle = \frac{D_I}{2\pi}\left(N_d(EJ\pi) + N_{abc}(EJ\pi) \frac{N_B(EJ\pi)+N_C(EJ\pi)}{N_A(EJ\pi)+N_B(EJ\pi)+N_C(EJ\pi)} \right) \qquad (50)$$

where N_C is the additional contribution from the second barrier.

The average widths for gamma and neutron emission are given by eqs. (23) and (24) respectively. To perform the calculation one has to determine the level density at the ground state deformation as well as the level densities at the barrier maxima (see eq. (49)). It has been pointed out by Bjornholm, Bohr, and Mottleson[73] that deviations of a nucleus from spherical symmetry cause an increase in the level density due to the presence of rotational bands built on each intrinsic state. Huizenga et al[74] have shown that with the inclusion of this collective enhancement , the axially symmetric nuclei have level density

$$\rho_{ax}(EJ) = f \frac{\omega(E)}{\sigma_{\perp}\sqrt{2\pi}} \sum_{K=-J}^{J} \exp\left[\frac{K^2}{2\sigma_{\perp}^2(E)} - \frac{J(J+1)-K^2}{2\sigma_{\perp}^2(E)} \right] \qquad (51)$$

where w(E) is the intrinsic state density calculated by Huizenga et al[74], $\sigma_{\perp}$ is the width of the K-distribution, $\sigma_{\perp}$ is the width of the spin J distribution taken to be $5.45\sqrt{\kappa}$[66], and f is an enhancement factor which is 2 for nuclei with no reflection symmetry and 1 otherwise[70].

When there is no axial symmetry, the level density becomes even higher and is given by[70]

$$\rho_{no}(E,J) = \frac{f}{N}\,\omega(E)\sum_{k=-J}^{J} \exp\left[\frac{k^2}{2\sigma_{\parallel}^2(E)} - \frac{J(J+1)-k^2}{2\sigma_{\perp}^2(E)}\right] \qquad (52)$$

where N = 1 for shape with no symmetry. If the nucleus has 180° rotational symmetry around a single axis, N is 2 and N is 4 for a nucleus which has symmetry of rotation by 180° around 3 perpendicular axes. The higher the point group rotational symmetry in a nucleus, the smaller the level density. By comparing eqs. (51) and (52) it is evident that an enhancement of $\sigma_{\parallel}\sqrt{8\pi} \simeq 25$ in the level densities is obtained in going from an axially symmetric shape to a shape with no symmetry.

Generally speaking, ten barrier parameters enter into the calculation of the fission probabilities, they are the barrier heights and barrier curvatures at the inner barrier A (E_A, $\hbar\omega_A$), the outer barrier B (E_B, $\hbar\omega_B$), the additional barrier C (E_C, $\hbar\omega_C$), the second well II (E_{II}, $\hbar\omega_{II}$), and the imaginary potential (W_o, ω). It is obvious that from the limited amount of data an unambiguous determination of all these parameters will be impossible. In order to simplify the complexity of the calculation other experimental information, for example data obtained in particle induced fission and data on fission isomers, will be used to determine several parameters. The analysis code which we are using has been discussed by Back et al[20]. The dependence of the fit on the parameters is reviewed briefly here.

The parameters E_{II} and $\hbar\omega_{II}$ determine the second potential well and they affect the position of the vibrational resonances in this well.

However the resonance positions will also be affected by other parameters, for example, the barrier heights and barrier curvatures. Therefore, a determination of E_{II} and $\hbar\omega_{II}$ by fitting to the resonance data is not unique. In our fitting, we have adopted $\hbar\omega_{II} = 0.9$ MeV following Back et al[20]. The values of E_{II} are evaluated from fission isomer data[75].

The imaginary potential is used, as described in chapter II, to simulate the damping of the vibrational states. The two parameters determining this potential which affect the fission probability mainly near these states have been taken from Back et al[20]. They are $W_o = 0$ and -0.05 MeV for U and Th respectively and $\omega = 0.05$ for both cases.

The four parameters E_A, $\hbar\omega_A$, E_B, $\hbar\omega_B$ affect strongly the theoretical fission probability in the region near threshold, particularly in cases where resonances are observed. The additional barrier given by the parameters E_C, $\hbar\omega_C$ is higher than barrier B and therefore its main contribution is to the fission probability at higher energies. In addition, the fission probability will be affected considerably as we add, remove, or even change the energy of the transition states. In the case of photofission of even-even nuclei, only $J^\pi = 1^-$ and 2^+ states are excited. Therefore the fitting process provides information on their transition states. We have taken the energies of the transition states reported by Dickey et al[5] as the first approximation and varied them slightly to obtain the best fits.

The introduction of barrier C which reflects the departure from axial symmetry of the nucleus leads to a collective enhancement of the level density at higher excitation energies, which in turn increases the fission probability. It was shown by Gavron et al[21] that only when the existence

of this barrier is taken into account can one reproduce theoretically the magnitude of the experimentally observed fission probability at higher energies in ^{238}U. The existence of the axially asymmetric second barrier is also supported by potential energy calculations for a number of heavy nuclei. In our analysis of fission probabilities of ^{238}U and ^{232}Th, we follow the approach of Gavron et al[21].

In Fig. 29 we show fits to the fission probability obtained from the $^{238}U(\gamma,f)$ data. In the region near threshold, we have initially taken the barrier parameters obtained from Back et al from their fits to the $^{236}U(t,pf)^{238}U$ data and then changed them slightly in order to fit the (γ,f) data taken from Dickey et al. These parameters of barrier A and B which are listed in Fig. 29 reproduce very well the peaks at 5.6 and 6.2 MeV. At higher energies they yield the fission probability shown by the dashed curve. This fission probability is not affected by a change of the fission barrier height within $\pm$0.5 MeV. In order to raise the calculated fission probability so that it agrees with the experimental data it is necessary to introduce the additional axially asymmetric barrier C. The result of the calculation is shown in Fig. 29 by the solid curve. The value of E_C was taken as assumed by Gavron et al. The fission probability increases by a factor of 3 at an excitation energy of 10 MeV. The data (the ■ are from the present work) agree reasonably well with the solid curve when $E \gtrsim 9$ MeV. In the region $\sim$ 7 MeV the experimental results are higher than the calculated values. Including the $K^{\pi} = 2^{+}$ transition state in the calculation produced a negligible effect. It should be noted that the photoabsorption cross section used in determining the experimental fission probability was extrapolated from the giant resonance. This extrapolation ignores possible structure at lower energies. There is experimental evidence[5,41] that the

Fig. 29: Comparison of the ^{238}U fission probability P_f with the results of the statistical model calculations.

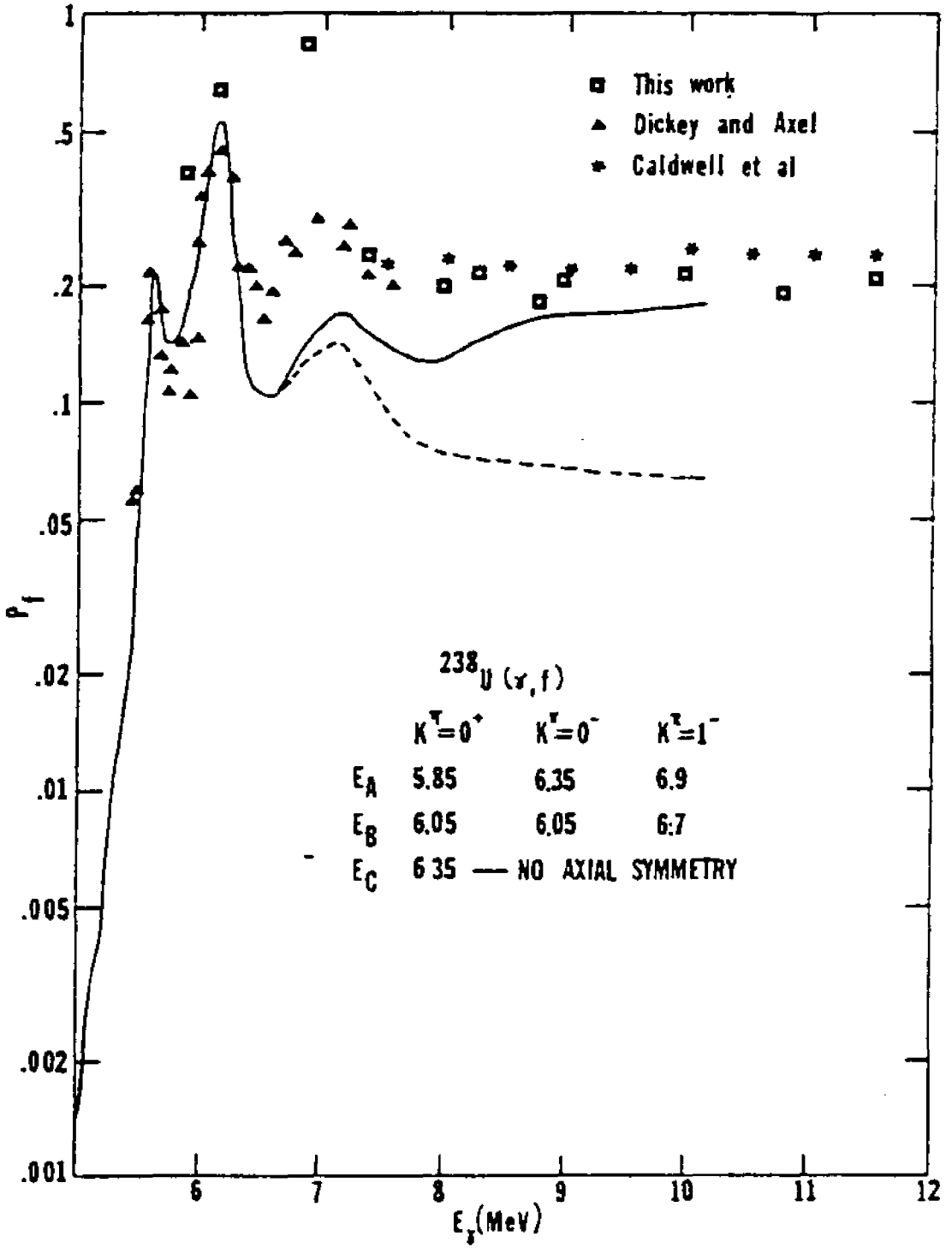
This work
Dickey and Axel
Caldwell et al
$^{238}U(\gamma,f)$
$K^{\pi}=0^{+}$ $K^{\pi}=0^{-}$ $K^{\pi}=1^{-}$
E_A 5.85 6.35 6.9
E_B 6.05 6.05 6.7
E_C 6.35 — NO AXIAL SYMMETRY
P_f
E_γ(MeV)
1
.5
.2
.1
.05
.02
.01
.005
.002
.001
6
7
8
9
10
11
12

photoabsorption cross section at 7 MeV is ~50% higher than the value obtained by extrapolation. This would explain the difference between the experimental fission probability and the calculated one around 7 MeV.

The fit to the ^{232}Th(γ,f) data is shown in Fig. 30. At energies above 7 MeV our results agree well with those of Caldwell et al. The results of Veyssiere et al are considerably lower. Since our data for thorium was obtained simultaneously with the data for uranium which is in good agreement with the data obtained by other groups. we think that the data of Veyssiere for ^{232}Th is incorrect, and therefore have not included it in Fig. 10. As in the case of ^{238}U the parameters characterizing barriers A and B are based on particle induced fission results and the low energy (γ,f) results of Dickey and Axel[3]. In the region near threshold, this set of barrier parameters produces a peak at 5.5 MeV and a small bump at ~ 6.2 MeV. The latter is consistent with our observed increase in cross section at 6177 keV as shown in Fig. 25 (a). On the basis of its width and excitation energy the observed peak could therefore correspond to a class II vibrational state in the second well. The solid curve and the dotted curve are obtained with additional outer barriers C, whereas the dashed curve is the result of a calculation without this additional barrier. In contrast to the ^{238}U case, the experimental results, at higher energies are higher than those given by the dashed curve only by a factor of 1.5. With an additional barrier C of the same symmetry as for ^{238}U the best fit to the data is obtained when one assumes E_C = 7.45 MeV. However the calculated probability shown by the dotted line is higher than the experimental one in the energy region around 8 MeV. A better fit is obtained when barrier C is assumed to have D_2 symmetry and E_C = 6.95 MeV as can be seen from the solid line. In order to determine with confidence

Fig. 30: Comparison of the ^{232}Th fission probability P_f with the results of the statistical model calculations.

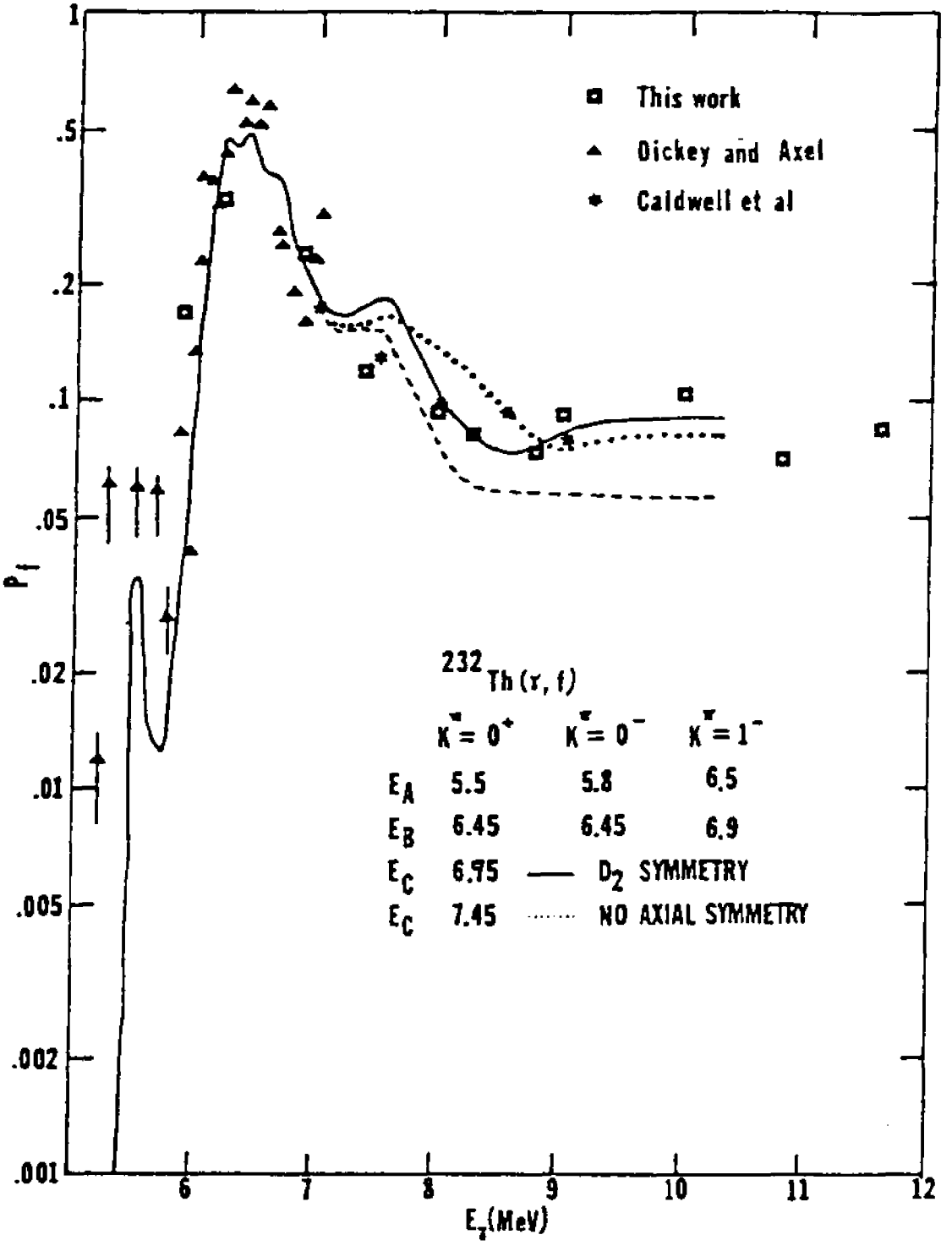
This work
Dickey and Axel
Caldwell et al
^{232}Th (γ, f)
K = 0⁺ K = 0⁻ K = 1⁻
E_A 5.5 5.8 6.5
E_B 6.45 6.45 6.9
E_C 6.75 — D2 SYMMETRY
E_C 7.45 ····· NO AXIAL SYMMETRY
P_f
E_γ(MeV)
1
.5
.2
.1
.05
.02
.01
.005
.002
.001
6
7
8
9
10
11
12

the symmetry and the height of barrier C considerably more extensive measurements of the photofission cross sections have to be done at higher energies. Reliable experimental data on the total photoabsorption cross sections below 9 MeV are also necessary. Finally it would be very useful to carry out potential energy calculations for ^{232}Th with the various types of deformations taken into account.

The close values of $E_A(0^+)$ and $E_B(0^+)$ are in contradiction to the theoretical calculation[19] which predicts that the inner barrier should be lower than the outer one by at least 3 MeV. However, as described in chapter II, Moller and Nix[22] have suggested the existence of a three-humped fission barrier in ^{232}Th, with the inner barrier being low and the outer two considerably higher. Only the outer two barriers contribute to the photofission cross section at energies near threshold. This argument is further supported by Bhandare[76] who calculated the fission penetrability under the assumption of a three-humped fission barrier, By comparing his results with the "deep" subbarrier photofission data of Bowman et al[37], Bhandare obtained the heights of the two outer barriers as E_A = 5.4 MeV and E_B = 6.4 MeV, in very good agreement with our value.

In conclusion, the experimental data presented here indicate that an axially asymmetric barrier C exists in ^{232}Th.

(3) Suggestions for further work

(1). Of the 11 spectra of fission fragments we have measured at energies between 5.8 to 11.5 MeV the longest exposure time $\sim$ 40 hrs was used in the run at 5.87 MeV. With 58 uranium and 28 thorium foils and an average proton beam current of 150 μa, the total number of fission

fragments recorded in an energy interval of 12 keV was $\sim$1500 for Th and $\sim$ 5000 for U after background subtraction. If we divide the 12 keV interval into 40 channels, the average number of counts per channel is therefore $\sim$ 120 for U and $\sim$ 40 for Th. The estimated accuracy for both cases is $\sim$ 17% and the measured photofission cross sections are 8.2 and 3.9 mb for ^{238}U and ^{232}Th respectively. In order to determine the cross sections down to $\sim$1 mb in both cases with the same accuracy (expected at excitation energies of about 5.2 MeV for ^{238}U and 5.5 MeV for ^{232}Th), we have to double the number of foils and run a proton beam current of $\sim$ 500 μa for two days. This is feasible so long as we can improve our beam handling capability and, futhermore, computerize the scanning process of the track detectors.

As described in chapter III, our present method to handle high beam currents is to spread the beam on target by using two mutually perpendicular wobblers. This introduces an uncertainty in the angle between the emitted gamma-ray and the proton beam, which lowers the gamma-ray energy resolution. To avoid this we have designed a target vibrator in which the target chamber is mounted at the end of a bellows and driven simultaneously by two vibrators in the vertical and horizontal directions at two different frequencies. As a result a well focussed beam scans the target area with no change in the position of the beam relative to the detectors. The use of the target vibrator will improve the gamma-ray energy resolution and, most important, will allow an increase in the intensity of the proton beam.

The scanning of the film is a very slow and tedious process. A typical scanning time for a 5 cm $\times$ 5 cm film having $\sim$ 200 holes is about 20 minutes. To speed up the scanning we are exploring the possibility of

using a Vidicon camera to scan the film and determine the X and Y coordinates of each hole. The information would be stored and processed by a computer. The expected scanning time of a single film is about 1 min. This is a considerable improvement which becomes crucial when the number of the fission foils is increased.

(ii). Obviously when structure reflecting excitation of individual states is observed knowledge of the angular distribution of the fission fragments is important for the determination of the cross section. This knowledge can be obtained by measuring the fission spectrum at two different angles θ of the fission foil relative to the gamma-ray. The dependence of the fission fragment counting rate on θ calculated for our detection system is plotted in Fig. 31 for the five transition states accessible through the gamma excitation. It can be seen that when a discrete state is observed, the ratio of the intensities measured at $\theta = 0^{\circ}$ and $\theta = 50^{\circ}$ is sufficient to determine its quantum numbers Such measurements can be done simultaneously at both angles

Fig. 31: The angular dependence of the fission fragments counting rate calculated for the presently used detection system and for states of different values of J^{π} and K.

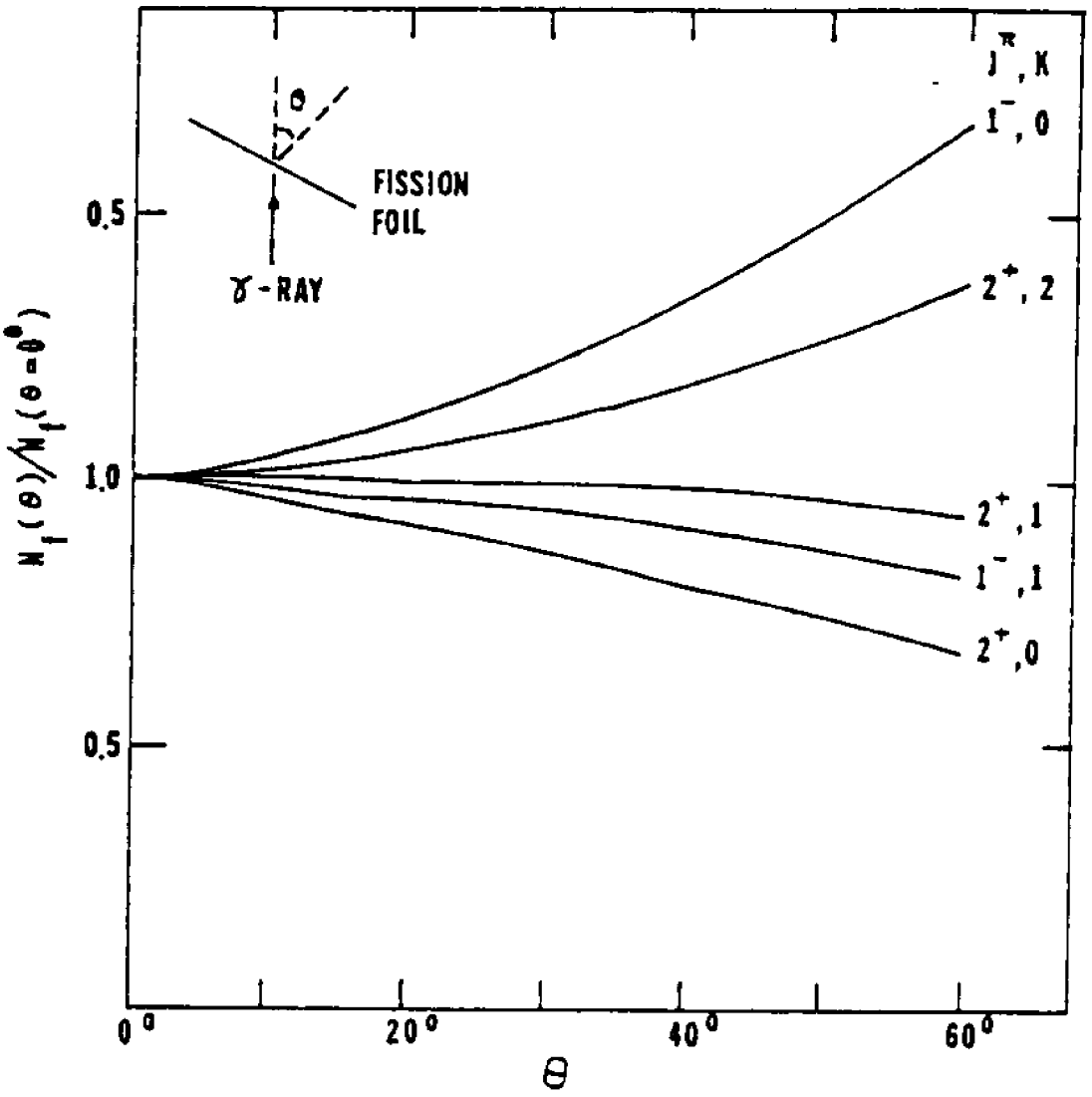
θ
FISSION FOIL
γ-RAY
J^π, K
1^-, 0
2^+, 2
2^+, 1
1^-, 1
2^+, 0
0.5
1.0
0.5
N_f(θ)/N_f(θ=θ°)
0°
20°
40°
60°
θ

(C) Photo-excitation of the 7.06 and 7.08 MeV dipole states in ^{208}Pb

The magnetic dipole strength distribution in ^{208}Pb has been the subject of extensive experimental and theoretical investigations. Recent measurements of angular distributions of gamma-rays following inelastic scattering of protons and deuterons, carried out by Freedman et al[77] indicated that the J = 1, 7.06 MeV state has positive parity and therefore constitutes a major component of this strength. However, investigations[78] of angular distributions of protons from the $^{207}Pb(d,p)$ reaction appear to yield a negative parity for this state. The nature of the 7.06 MeV state remains thus uncertain.

The width of the 7.06 MeV state has been measured a number of times by resonance fluorescence methods. The results of these measurements are summarized in Table 10. It can be seen that they are not in good agreement with each other.

The magnitude of the width of the 7.06 MeV state, if it is a magnetic dipole state, is important for determining the value of the spin dependent proton-neutron interaction[79]. In view of the large discrepancies between the existing results we decided to re-measure this width. Preliminary results of these measurements were reported elsewhere[80].

The 7.06 MeV state was excited in a resonance fluorescence experiment using the $^{19}F(p,\alpha\gamma)^{16}O$ reaction as a source of 7 MeV gamma-rays. The proton beam from the Dynamitron at Brooklyn College had an energy of E_p = 2.5 MeV. The average beam current was 30 μa. A 13 mg/cm^2 thick CaF_2 target evaporated on a water cooled Ta backing was used. A 10 cm × 10 cm × 1.025 cm lead scatterer was placed at an angle of 85° with respect to the proton beam as shown in Fig. 32. For the self-absorption measurement a 0.62 cm thick lead plate was located in the path of the

TABLE 10

Level widths obtained in this work and in previous experiments

E_x (MeV)	J	Γ_0 (eV)						
		This work	ref.83	ref.84	ref.85	ref.86	ref.87	ref.88
7.064	1	29 ± 3	18 ± 3	31 ± 3	29 ± 10		15	[a] 32 ± 2
7.084	1	16 ± 3		17 ± 2	14 ± 5	16^{+6}_{-4}	15	

[a] The two states were not resolved.

Fig. 32: Experimental set-up for the photo-excitation measurement in ^{208}Pb.

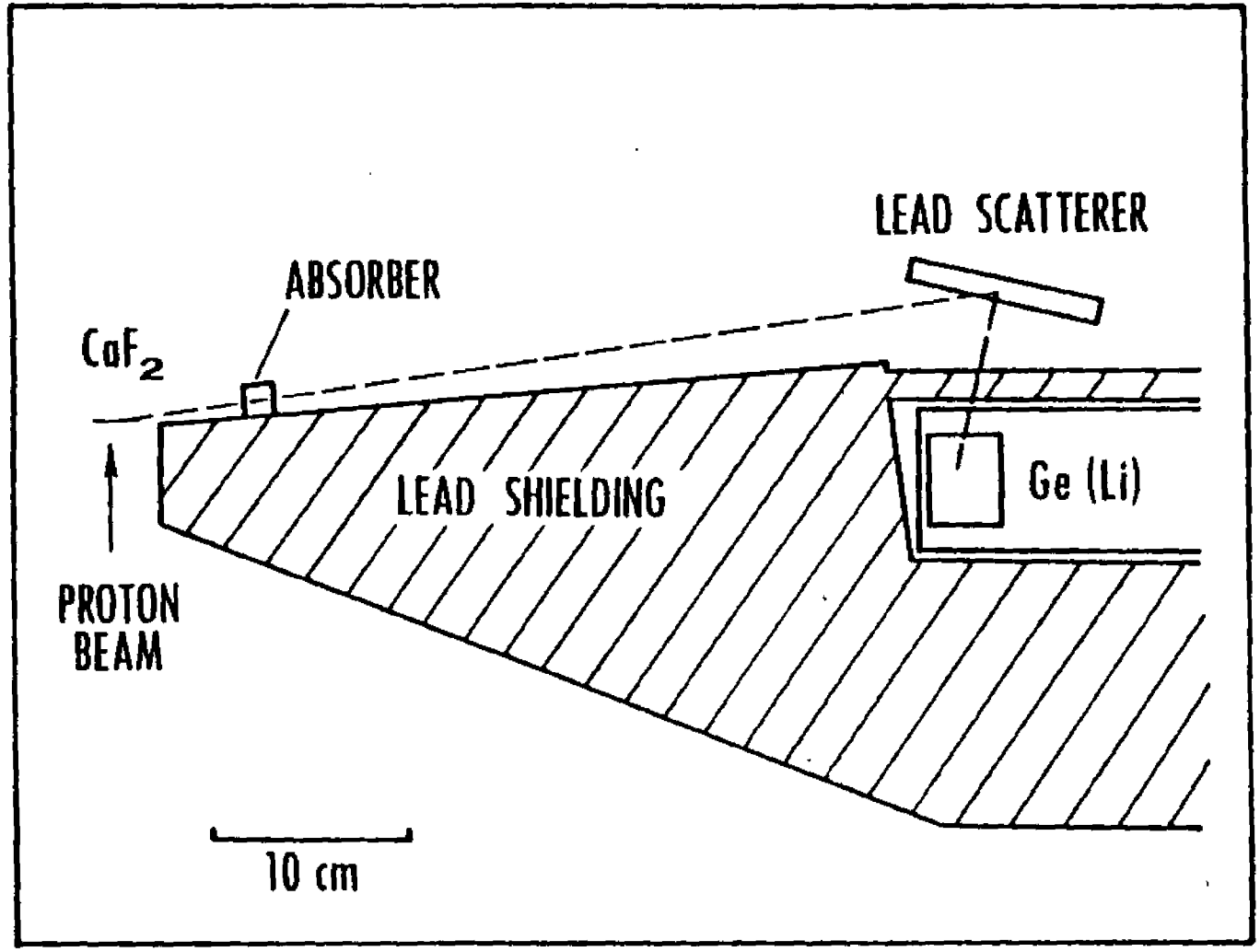
LEAD SCATTERER
ABSORBER
CaF_2
LEAD SHIELDING
Ge (Li)
PROTON BEAM
10 cm

incident photons. The scattered gamma-rays were detected by a 60 cm^3 Ge(Li) detector. A 7.6 cm x 7.6 cm NaI(Tl) detector, placed 1.6 m away from the target at an angle of 90^o to the proton beam served as a monitor. This detector was shielded in such a way that it could receive gamma-rays only from the CaF_2 target.

Pulser signals accumulated together with the Ge(Li) and NaI(Tl) spectra were used to determine the dead time corrections.

The resonance scattering method has been described before[81]. The intensity of resonantly scattered gamma-rays from a volume element at location ijk in the scatterer recorded by the detector can be written in the form

$$I_{ijk} = C f(\theta_{ijk}) N(E_\gamma) \epsilon_{ijk} \frac{\Gamma_o}{\Gamma} \int n_\gamma \sigma_{abs}(E) \exp[-n_\gamma \ell_{ijk} \sigma_{abs}(E)] \, dE \qquad (53)$$

where the constant C includes the geometrical factors and the corrections for electronic absorption; $f(\theta_{ijk})$ is the angular distribution of the scattered photons; $N(E_\gamma)$ is the number of photons per eV emitted from the target at the resonance energy E_γ ; ϵ_{ijk} is the efficiency of the detector; ℓ_{ijk} is the path length in the scatterer of the photon on the way to volume element ijk; n_r is the number of ^{208}Pb nuclei per unit volume; Γ and Γ_o are the total width and the partial width for the ground state transition respectively; σ_{abs} is the absorption cross section obtained by averaging the single level Breit-Wigner formula over thermal motion of nuclei in the scatterer. In its general form, used in the present work, σ_{abs} is given in terms of the Doppler integral[81].

The integration in the expression for I_{ijk} has to be carried out numerically. The intensity of scattered photons is obtained by summing

I_{ijk} over all volume elements. A 1 cm × 1 cm × 0.1 cm volume element of the scatterer was used for the numerical calculations.

The spectrum of resonantly scattered photons is shown in Fig. 33 (a). Both the 7.06 and 7.08 MeV lines are strongly excited. The background (not shown) was measured with the scatterer removed. It showed no structure in the region of the two lines. The Doppler-broadened spectrum of photons incident on the target is shown in Fig. 33 (b). This spectrum was taken with the proton beam current lowered and the detector located at the same average angle with respect to the proton beam as the scatterer. The direct spectrum and the spectra of resonantly scattered gamma rays were normalized to the monitor counts so that a determination of the absolute photon intensity and the detector efficiency were not necessary[82].

The calculated normalized intensity of the gamma-rays scattered from the 7.06 MeV state is plotted in Fig. 34 versus the ground state transition width Γ_0 for a number of values of Γ_0/Γ. The experimental value of the normalized intensity is also shown. The value of Γ_0/Γ can be determined in a self absorption experiment. The ratio of the intensity of scattered photons measured with the absorber in the path of the incident photons to that measured without the absorber depends on Γ_0/Γ when the natural width of the state is larger than the Doppler width. This ratio corrected for electronic absorption, was found to be 0.68 ± 0.1, which leads to $\Gamma_0/\Gamma = 0.9^{+0.1}_{-0.4}$. The value of Γ_0/Γ can also be determined by searching the spectrum of scattered photons for gamma-rays leading to lower lying states. This gives $\Gamma_0/\Gamma \geq 0.7$. In view of the large errors in Γ_0/Γ obtained from the self-absorption measurement a value of $\Gamma_0/\Gamma = 1$ was assumed in deducing the value of Γ_0 listed in Table 10.

Fig. 33: (a) Spectrum of scattered photons obtained at E_p = 2.5 MeV showing the full energy and the single and double escape peaks corresponding to the 7.06 and 7.08 MeV states.

(b) Spectrum of incident photon. The Doppler broadened 6.92 and 7.12 MeV lines are shown by the short horizontal lines.

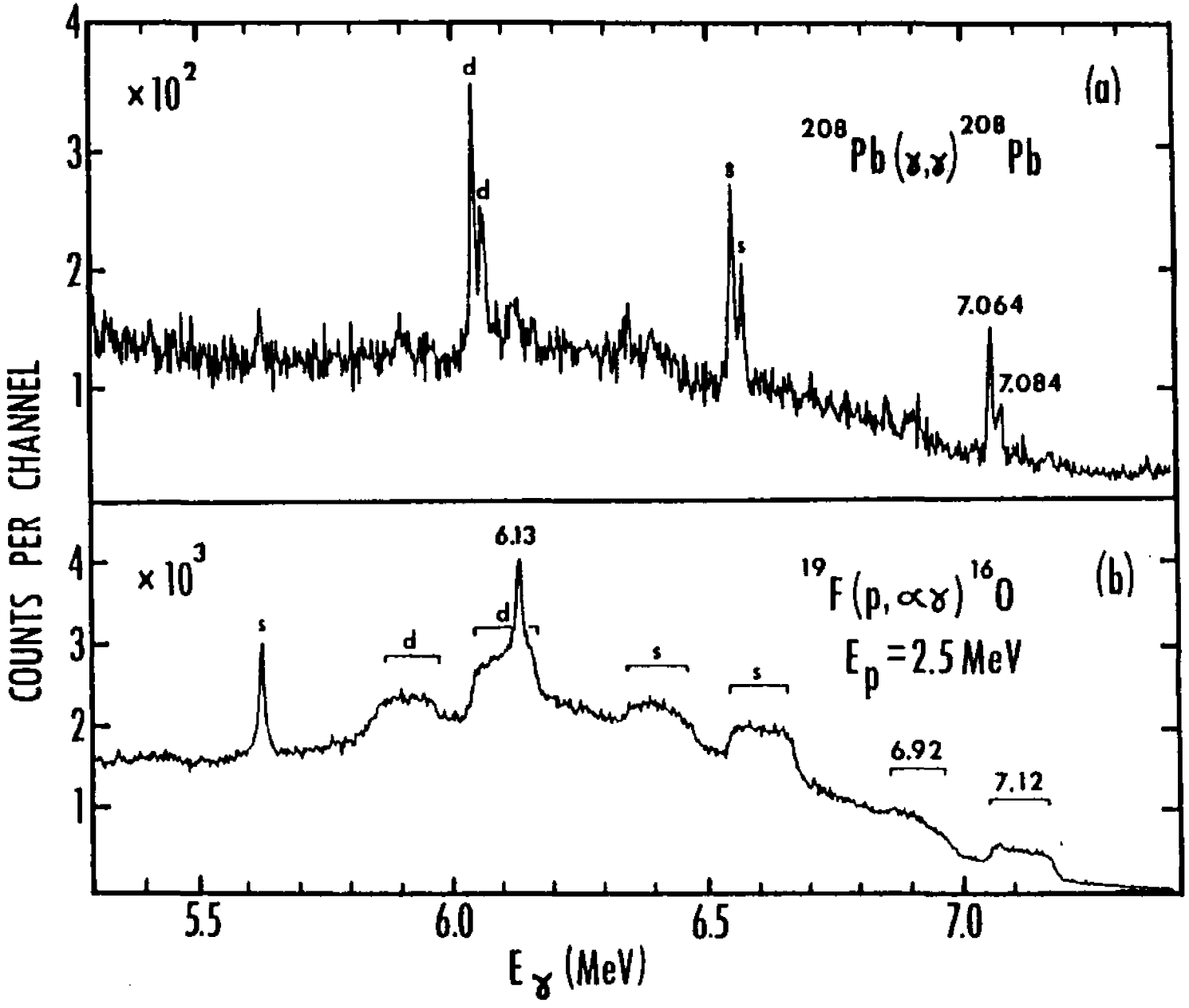
COUNTS PER CHANNEL
× 10²
d
d
s
s
7.064
7.084
(a)
208Pb(γ,γ)208Pb
× 10³
6.13
d
d
s
s
s
6.92
7.12
(b)
19F(p,αγ)16O
Ep = 2.5 MeV
Eγ (MeV)
5.5
6.0
6.5
7.0
1
2
3
4

Fig. 34: The intensity of scattered 7.06 MeV gamma-rays normalized to monitor counts. The horizontal lines shown the experimental value with errors; the other lines represent normalized intensities calculated as a function of Γ_o for a number of values of Γ_o/Γ .

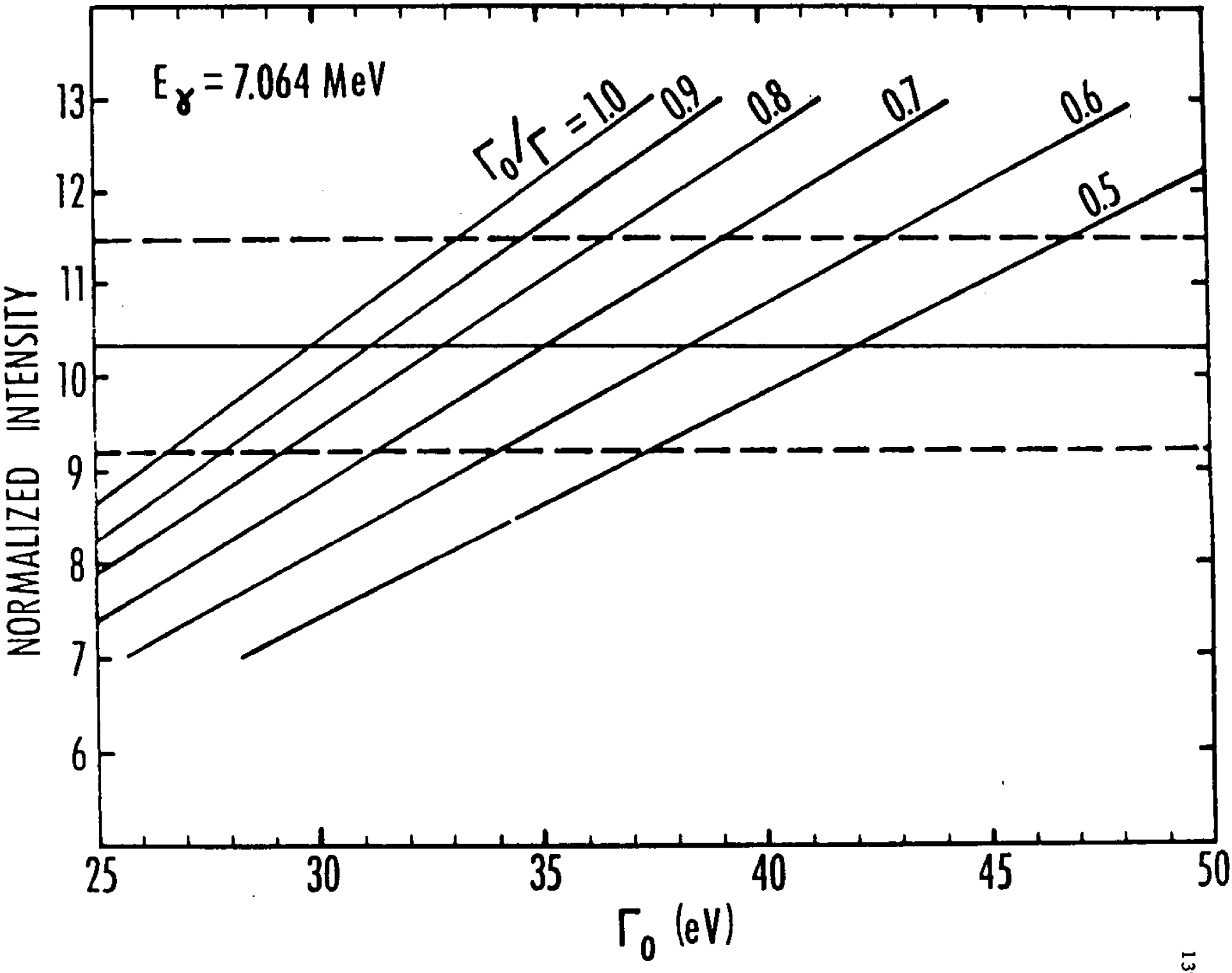
E_γ = 7.064 MeV
Γ_0/Γ = 1.0
0.9
0.8
0.7
0.6
0.5
NORMALIZED INTENSITY
13
12
11
10
9
8
7
6
25
30
35
40
45
50
Γ_0 (eV)

For the 7.08 MeV state the self absorption experiment gives $\Gamma_o/\Gamma = 0.8^{+0.2}_{-0.3}$ and a search for lower energy lines in the spectrum gives $\Gamma_o/\Gamma \geq 0.7$. Assuming a value of $\Gamma_o/\Gamma = 1$ we obtain the value of Γ_o given in Table 10.

The results of other measurements are listed in Table 10 for comparison. Our result for the 7.06 MeV state is in very good agreement with the values of Swann[84] and of Coope et al[85]. It differs markedly from the remaining results. The reason for this discrepancy is not clear. The difference between our result and that of the high resolution resonance absorption experiment[83] may indicate that the 7.06 MeV line observed in resonance scattering corresponds to the excitation of two or more closely spaced states. To check whether this is the case a resonance absorption experiment would have to be carried out over a wider energy range than the one covered in the experiment reported in ref. 83.

Because of the uncertainties concerning the 7.06 MeV state it is too early to make a comparison of the experimental results with the theoretical calculations. An attempt was made, in collaboration with C.P. Swann, to measure the polarization of the resonantly scattered gamma-rays in order to determine the parities of the excited states. However, because of the low counting efficiency of the polarimeter it proved unsuccessful.

BIBLIOGRAPHY

1. A. Bohr, Proc. Int. Conf. Peaceful Uses of Atomic Energy, 2,151 (1955).

2. N. S. Rabotnov, G. N. Sminenkin, A. S. Soldatov, L. N. Usachev, S. P. Kapitza, Y. M. Tsipenink, Sov. J. Nucl. Phys. 11,285(1970.

3. A.M. Khan, J.W. Knowles, Nucl. Phys. A179, 333(1972).

4. M.V. Yester, R.A. Anderl, R.C. Morrison, Nucl. Phys. A206,593 (1973)

5. P.A. Dickey, P. Axel, Phys. Rev. Lett. ,35, #8, 501(1975).

6. O.Y. Mafra, S. Kuniyoshi, J. Goldembery, Nucl. Phys. A186,110 (1972).

7. A. Manfredini, L. Fiore, C. Ramorino, H.G.de Carvolho, W. Wolfli, Nucl. Phys. A127, 687(1969).

8. J.R. Huizenga, H.C. Britt, Proc. Int. Conf. on Photonuclear Reactions and Applications, Vol. II, Asilomar, 833(1973).

9. J.T. Caldwell, Bull. Am. Phys. Soc. 20,1187(1975).

10. O. Hahn, F. Strassman, Naturwiss, 27,11(1939).

11. O. Hahn, F. Strassman, Naturwiss, 27,89(1939).

12. N. Bohr, J. Wheeler, Phys. Rev., 56,426(1939).

13. S. Cohn, W.J. Swiatecki, Ann. Phys., 22,406(1963).

14. V.M. Strutinsky, Nucl. Phys., A95,420(1967).

15. V.M. Strutinsky, nucl. Phys., A122,1(1968).

16. S.G. Nilsson, C.F. Tsang, A. Sobiczewski, Z. Szymanski, S. Wyeech, C. Gustafsson, I.L. Lamm, P. Noller, B. Nilsson, Nucl. Phys. A131,1(1969).

17. K. Lee, D.R. Inglis, Phys. Rev. 108,774(1957).

18. P. Vogel Phys. Lett., 25B,65(1967).

19. P. Moller, Nucl. Phys., A192,529(1972).

20. B.B. Back, O. Hansen, H.C. Britt, J.D. Garrett, Phys. Rev., C9, 1924(1974).

21. A. Gavron, H.C. Britt, P.D. Goldstone, J.B. Wilhelmy, Phys. Rev. Lett., 38,#25,1457(1977).

22. P. Moller, J.R. Nix, in Proceedings of the Third International Atomic Energy Symposium on Physics and Chemistry of Fission. Rochester, (1973 (I.A.E.A., Vienna,1974).

23. J. Blons, C. Mazur, D. Paya, Phys. Rev. Lett., 35,#26,1749(1975).

24. A. Michandon, Phys. Today, Jan.23(1978).

25. A. Michandon, Advance Nuclear Physics, 6,1(1973).

26. H.J. Specht, Phys. Scripta, Vol. 10A,21(1974).

27. J.E. Lynn, Physics and Chemistry of Fission, I.A.E.A., Vienna(1969).

28. B.B. Back, J.P. Bondorf, G.A. Otroschenko, J. Pederson, R. Rasmussen, in Proceeding of the 2nd International Atomic Energy Agency Symposium on Physics and Chemistry of Fission, Vienna, 1969.

29. S. Polikanov, K.A. Druin, V.A. Karnankhov, V.L. Mikheev, A.A. Pleve, N.K. Skobelev, V.G. Subbotrin, G.M. Ter-akopyan, V.A. Fomichev, Sov. Phys., JETP 15,1016(1962).

30. H.J. Specht, J. Weber, F. Konecny, D. Hennemann, Phys. Lett., 41B, 43(1972).

31. G.F. Auchampaugh, LW. Weston, Phys. Rev. C12,1850(1975).

32. H.J. Specht, J.S. Fraser, J.C.D. Milton, W.G. Davies, Physics and Chemistry of Fission, I.A.E.A. , Vienna, 363(1969).

33. B.B. Back, H.C. Britt, Ole Hansen, B. Leronx, J.D. Garrett, Phys. Rev., C10,#5,1948(1974).

34. P.D. Goldstone, F. Hopkins, R.E. Malmin, P. Paul, Phys. Rev., C18, 1706(1978).

35. L.J. Lindgren, A.Alm, A. Sandell, Nucl. Phys., A298,43(1978).

36. C.D. Bowman, I.G. Schroder, C.E. Dick, H.E. Jackson, Phys. Rev., C12, #3,863(1975).

37. C.D. Bowever, I.G. Schroder, K.C. Duvull, C.E. Dick, Phys. Rev., C17, #3,1086(1978).

38. G.Bellia, A.Del Zoppo, E. Migneco, Phys. Rev., C20, #3,1059(1979).

39. A. Veyssiere, H. Beil, R. Bergere, P. Carlos, A. Lepretre, K. Kernbath, Nucl. Phys., A199,45(1973).

40. R.A. Anderl, M.V. Yester, R.C. Morrison, Nucl. Phys., A212, 221(1975).

41. J.R. Huizenga, K. M. Clarke, J.E. Gindler, R. Vandenbosch, Nucl. Phys., 34, 439(1962).

42. I.E. Bocharova, V.G. Zolotukhin, S.P. Kapitza, G.N. Smirenkin, A.S. Soldatov, Yu.M. Tsipenyuk, Sov. Phys., JETP, Vol.22,235(1966).

43. A.N. Ignatyuk, N.S. Rabotnov, G.N. Smirenkin, A.S. Smrienkin, A.S. Soldatov, Y.M. Tsipenyuk, JETP, 34, 684(1972).

44. E.D. Dowdy, T.L. Krysmski, Nucl. Phys., A175, 501(1971).

45. S.E. Larsson, I. Ragnarsson, S.G. Nilsson, Phys. Lett., 38B, 269(1972).

46. S.E. Larsson, G. Leander, I. Ragnarsson, J.Randrup, Phys. Scr., 10A, 65(1974).

47. C. Schuhl, Proc. Int. Conf. on Photonuclear Reaction and Application, Asilmar, (ed. B.R. Berman, Lawrance, Livermore Laboratory, 1973) page 1249.

48. R. Bergere, International School of Electro and Photonuclear Reaction, Photonuclear Reactions I, Vol. 61 (ed. by S. Custo, C. Scharef), Springer-Verlay, (1977) chapter 2.

49. A.P.M. Van't Westende, H. Lancman, C.Van der Leun, Nucl. Inst. Meth., 151, 205(1978).

50. R.J. Sparks, Thesis, Ultrecht(1976).

51. R.L. Fleischer, P.B. Price, R.M. Walker, Nuclear Tracks in Solids, University of California Press (1975).

52. F.J. Congel, J.H. Roberts, D. Dreis, J. Kastner, B.G. Oltman, R. Gold, P.J. Armani, Nucl. Inst. Meth., 100, 247(1972).

53. R. Gold, R.J. Armani, J.H. Roberts, Nucl. Sci. Eng., 34, 13(1968).

54. N.L. Lark, Nucl. Inst. Meth., 69, 137(1969).

55. R.L. Fleischer, P.B. Price, R.M. Walker, E.L. Hubband, Phys. Rev., 133, A1443(1964).

56. H.A. Kahn, S.A. Durrani, Nucl. Inst. Meth., 98, 229(1972).

57. O.D. Peterson, Rev. Sci. Inst., 41, 1254(1970).

58. H.G. Paratzke, T.A. Gruhn, E.V. Denton, Nucl. Inst. Meth., 107, 597(1973).

59. N.G. Cross, L. Tommarsino, Proc. Intern. Topical Conf., 1, 73(1969).

60. B.H. Patrick, E.M. Bowey, Nucl. Inst. Meth., 120, 245(1974).

61. S. Hahn, V. Frogue, Phys. Rev., 163, #2, 290(1967).

62. R. Vandenbosch, J.R. Huizenga, Nuclear Fission, (Academic, New York, 1973), page 293.

63. Microfoils, P. O. Box 283, Argonne, Ill.

64. R.A. Meyer, Lawrance Livermore Laboratory, University of California, Livermore, M-100(1978).

65. B.P. Singh, H.C. Evans, Nucl. Inst. Meth., 97, 475(1971).

66. R. Verbey, Fysisch Laboratorium, Rijksuniversiteit, Utrech, V76-88(1976).

67. A. Gilbert, A.G.W. Cameron, Can. J. Phys., Vol. 43, 1446(1965).

68. J.D. Cramer, J.R. Nix, Phys. Rev., C2, #3, 1048(1970).

69. J. Weber, H.C. Britt, A.Gavron, E. Konecny, J.B. Wilhelmy, Phys. Rev., C13, #6, 2413(1976).

70. A. Gavron, H.C. Britt, E. Konecny, J. Weber, J.B. Wilhelmy, Phys. Rev. Lett., Vol. 34, #13, 827(1975).

71. H.C. Britt, A.Gavron, P.D. Goldstone, R. Schoemackers, J. Weber, J.B. Wilhelmy, Phys. Rev. Lett., Vol. 40, #15, 1010(1978).

72. A.Gavron, H.C. Britt, J.B. Wilhelmy, Phys. Rev., C13, #6, 2577(1976).

73. S. Bjornholm, A. Bohr, B.R. Mottelson, Proceedings of the Third International Atomic Energy Symposium on Physics and Chemistry of Fission, Rochester, Vol. I, 367(1973).

74. J.R. Huizenga, A.N. Behkami, R.W. Atcher, J.S. Sventek, H.C. Britt, H. Freiesleben, Nucl. Phys., A223, 589(1974).

75. H.C. Britt, M. Bolsterli, J.R. Norton, Phys. Rev., C7, 801(1973).

76. B.S. Bhandari, Phys. Rev., C19, #5, 1820(1979).

77. S.J. Freedman, C.A. Gagliardi, G.T. Garvey, M.A. Oothoudt, B. Svetitsky, Phys. Rev. Lett., 37, 1606(1976).

78. F.P. Calaprice, private communication.

79. J.S. Dehesa, J. Speth, A. Faessler, Phys. Rev. Lett., 38, 208(1977).

80. T.R. Yeh, H. Lancman, Bull. Am. Phys. Soc., 22, 643(1977).

81. F.R. Metzger, Progress in Nuclear Physics, Vol. 7, 54(1963).

82. H. Lancman, R.J. Sparks, C. Van der Leun, Nucl. Phys., A257, 29 (1976).

83. R.J. Sparks, H. Lancman, C. Van der Leun, Nucl. Phys., A259, 13 (1976).

84. C.P. Swann, Nucl. Phys., A201, 534(1974).

85. D.F. Coope, L.E. Cannel, M.K. Brussel, to be published in Phys. Rev. C.

86. W. Scholz, H. Bakhru, P. Colle, A. Li-Schulz, Phys. Rev. C9, 1568 (1974).

87. A.M. Khan, J.W. Knowles, Bull. Am. Phys. Soc., 19, 538(1967).

88. R. Laszewski, P. Axel, to be published.